AN MPPT CHARGE CONTROLLER FOR SOLAR POWERED PORTABLE DEVICES

2016-2017 WORCESTER POLYTECHNIC INSTITUTE MAJOR QUALIFYING PROJECT

Advisor: Fred J. Looft, ECE

Student Authors:
Joseph A. Agresta, ECE
jaagresta@wpi.edu

Nicole A. Mikolajczak, ECE
namikolajczak@wpi.edu

Updated: 4/26/2017

Table of Contents

Acknowledgements

We would like to thank our advisor Professor Fred J. Looft for guiding and mentoring us through our project. We would also like to thank Bill Appleyard and Xu Keshuai for their assistance and technical advice.

1. Introduction

With increasing markets for portable devices such as smartphones, field research equipment, and navigational devices, an easily transportable solar powered battery charger is an anticipated, off-grid energy supply option as seen in Figure 1. Most affordable solar chargers harvest solar power using photovoltaic (PV) solar panels with a simple buck (step-down) voltage regulator. Unfortunately, this type of solar charger has significant power loss during conversion due to underutilizing the maximum potential power output of the PV panel. This inefficiency occurs because a simple step down solar charger does not have a controller to determine the optimal output voltage and current levels to maximize PV panel efficiency. Also, buck only solar chargers typically operate at voltages that adhere to a buck voltage regulator's voltage requirements (in particular, PV input voltages have to be higher than the required load voltage) instead of compensating for the fluctuating panel output voltage levels produced by varying irradiance and temperature conditions on the PV panel when a PV panel optimal operating voltage can be either above or below the desired output load voltage. Consequently, if portable devices do not receive consistent maximum power output from solar panels, the result is premature battery failure or battery capacity loss from the absence of an appropriate "end-of-charge" voltage (or consistent current). Thus, current designs of solar chargers are poor investments for users because of the resulting costs of replacing batteries and wasted power. [14]

Figure 1. Portable Solar Charger

Fortunately, there are solar charge controller designs that have addressed the inefficiencies of solar chargers. These solar charge controller designs utilize Maximum Power Point Tracking (MPPT) to operate a solar charge controller at maximum panel power peak efficiency. MPPT is a method of adjusting the load presented to a PV panel to compensate for changes in temperature and irradiation of a PV panel to produce maximum output power to a load from the panel. Using sensors and an algorithm to compare the input solar power with the output power on the load, current and voltage settings for a DC-DC converter (voltage regulator) are adjusted to extract the maximum output power possible from the PV panel. Figure 2 illustrates how a charge controller using only a step-down (buck) DC-DC converter topology harvests only 50%-70% of the power from the PV panel, whereas, a system with an MPPT controller can provide about 90% of the PV panel's power.

Unfortunately, existing portable solar charge controller companies have yet to implement MPPT-centered designs affordably in their products. If a portable device was connected to an MPPT driven

solar charger, the battery would receive at least 90% of the panel's available power making an MPPT charge controller design a better investment than a PWM-driven solar charge controller. [14]

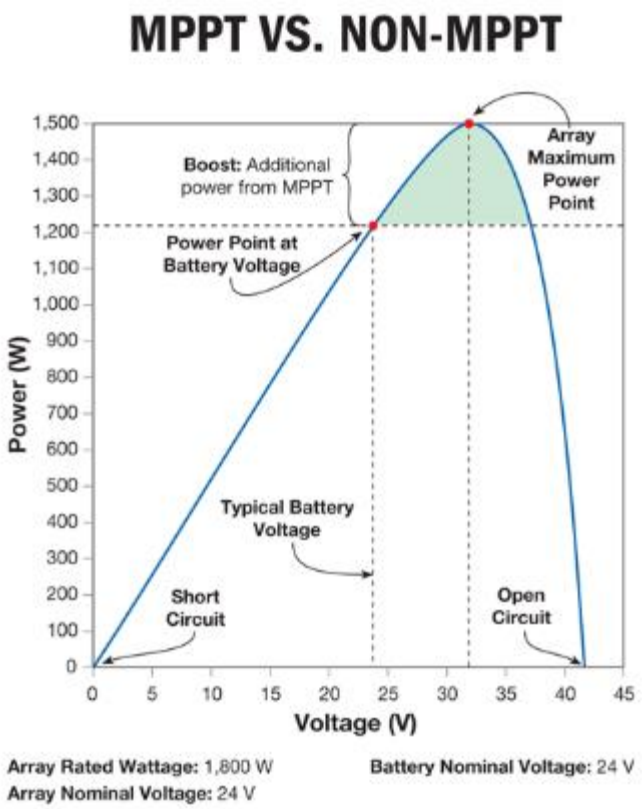

Figure 2. Power Comparison of MPPT vs. Non-MPPT Solar Charging [5]

The efficiency of an MPPT charge controller is dependent on both the MPPT algorithm and the type of voltage regulation implemented. The typical buck topology is unable to provide power efficiently because this typology can only work efficiently with input PV panel voltages that are higher than the desired output load voltage. Similar input voltage restrictions apply to a step-up (boost) converter because the input PV voltage can only be lower than the desired output load voltage. Because buck and boost controllers require a specific range of input voltages, these individual typologies do not enable the PV cell modules to produce maximum output power with a varying input voltage range. Since most portable, small capacity (10W) PV panels are subjected to varying amounts of sunlight (irradiance), the PV array can produce voltages higher or lower than the desired load voltage. In order for a solar charge controller to efficiently use a PV panel as a power supply for a portable device, the portable solar charge controller needs to be capable of regulating supply voltages that are both higher and lower than the desired load voltage. In addition, the portable charge controller should extract maximum power from the panel and meet the battery load requirements.

The purpose of our senior project was to design and prototype an MPPT charge controller for small capacity PV panels under varying temperature and irradiance conditions to charge portable devices. In this paper we discuss our research, simulation, design, and testing to develop an MPPT solar charge controller. Furthermore, we present out results and findings from testing our design.

2. Background Research

2.1 Introduction

This section aims to provide background research to describe the components necessary for the solar charger to function and how these components operate together to charge a battery. Figure 3 displays the four steps that occur within a solar charger. Each step is explored within this section in terms of fundamental components and operational processes for that topic.

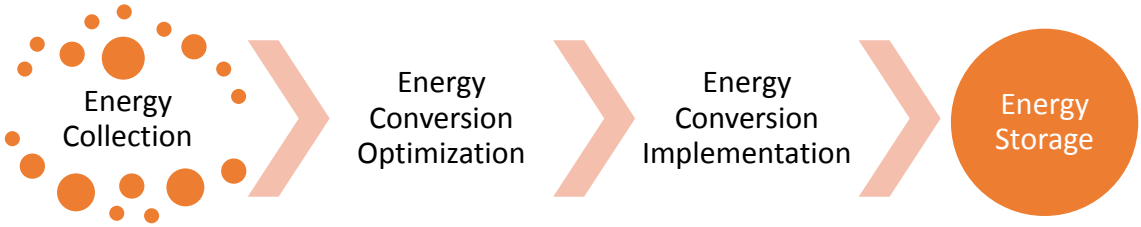

Figure 3. Energy Processes within a Solar Charger

2.2 Energy Collection

The first major step in a solar charger is energy collection. The energy harvested will be converted and used to charge a battery. Solar charge controllers use Photovoltaic (PV) panels to collect energy from the sun. Photovoltaic (PV) panels are made of PV cells, which are semiconductor devices that are designed to produce a current when exposed to light. To produce current, incident photons are absorbed within the PV cells by a semiconductor material (usually silicon) causing the excitation of valence electrons within the atoms of that material. By absorbing energy from photons, electrons are elevated in energy level from the valence band to the conduction band of an atom. Figure 4 shows how electron-hole pairs are formed if the incident photons provide enough energy for the electrons to surpass the band gap between the valence and conduction bands. [23]

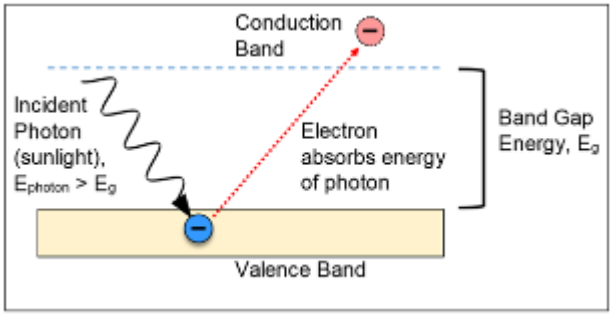

Figure 4.Excitation of Electrons across Band Gap

If the energy of an incident photon is greater than or equal to the band gap energy, an electron-hole pair is formed and the charge carriers are separated. The affected silicon atoms of a typical PV cell form a PN junction, which forces charge carriers to flow in one direction. In this way, the flow of electrons becomes available power as a form of current to charge a battery load. Figure 5 illustrates how current is supplied by PV cells once electron hole-pairs are combined. [23, 24]

A solar cell can be modeled as a light dependent current source in parallel with a diode PN junction as in Figure 6. To account for non-ideal conditions such as shading on the panel, the model also includes both a series resistance and a parallel shunt resistance. The PV circuit model illustrated in Figure 6 can be described with a photovoltaic current (I_{ph}), a PN junction diode current (I_d), a diode (D), the parallel shunt resistance (R_p), a series resistance(R_s), the load current (I_L), and the load voltage (V_L). Equation 1 expresses the load current as described by current analysis of the model. [24, 15]

$$I_L = I_{ph} - I_d - \frac{V+I_L \times R_S}{R_p} \quad (1)$$

From Equation 1, the photovoltaic current (I_{ph}) and the diode current (I_d.) depends on the solar cell irradiance and temperature. Thus, the power generated from the PV panel depends on the variation of irradiance and temperature upon the PV cell. Equation 2 expresses the PN junction characteristic of a PV cell as the diode current through Shockley's Diode Equation. [15]

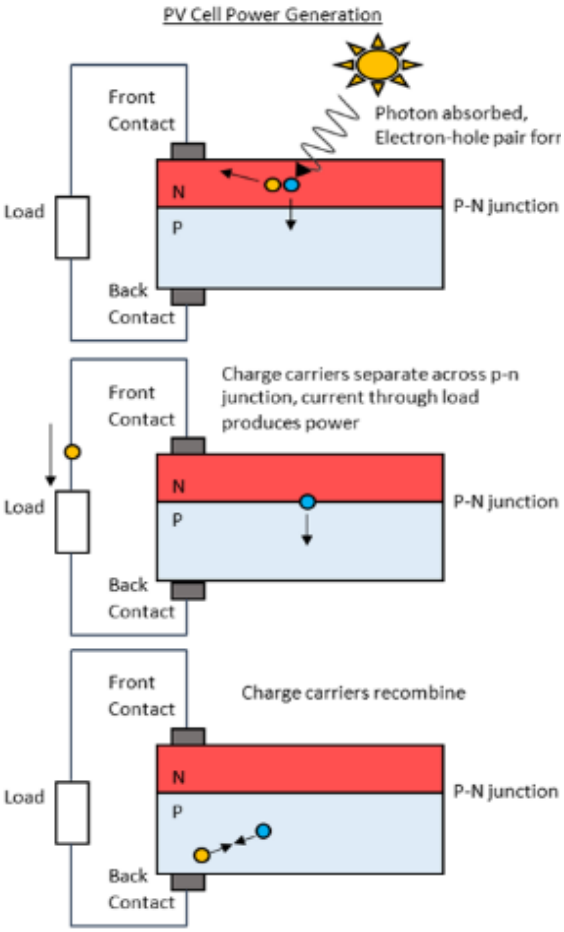

Figure 5 Generation of current in a PV Cell

$$I_d = I_o * [(e^{\frac{q(V+I_L R_S)}{nKT_C}} - 1] \quad (2)$$

In Equation 2, I_d, represents the diode current, I_o, the diode saturation current, q, the charge constant of an electron (1.602×10^{-19} C), V, the load output voltage, n, a form factor (usually a value of 1 or 2), K, the Boltzmann Constant (1.381×10^{-23} K), R_S, the PV cell series resistance, T_C, the junction temperature, and I_L, the load current. [24, 15]

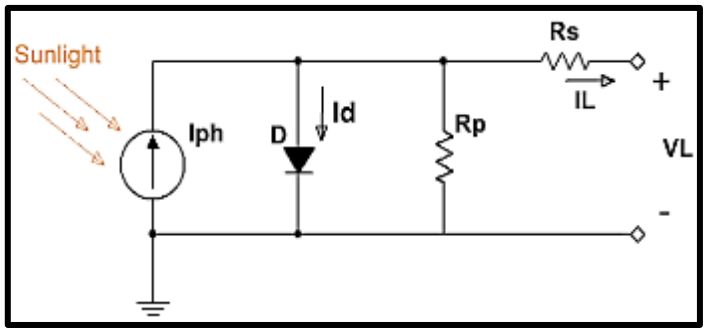

Figure 6 PV Cell Circuit Model Created in Multisim

Modeling PV cell efficiency depends on the influence of temperature and irradiance seen in Equation 1. With an increase in cell temperature, the output voltage of the PV cell decreases resulting in lower output power. If temperature is decreased relative to the reference temperature, the voltage increases, but

there is a slight decrease in current, and an overall increase in output power. [19] Equation 3 provides the solar cell power conversion efficiency in terms of solar irradiance:

$$\eta_C = \frac{P_{max}}{P_{in}} = \frac{I_{max} * V_{max}}{I(t) * A_c} \quad (3)$$

Where the maximum power current and voltage are represented as I_{max} and V_{max}, and solar intensity and the area of the solar cell are represented as $I(t)$ and A_c.

Equation 4 describes the relationship of cell temperature and solar cell conversion efficiency. By observing Equation 4, the relationship between ambient temperature and efficiency is linear with efficiency decreasing as temperature increases. [19]

$$\eta_C = \eta_{Tref} \left[1 - \beta_{ref}\left(T_c - T_{ref}\right) + \gamma log_{10} * I(t)\right] \quad (4)$$

In Equation 4, η_C is defined as the PV electrical efficiency at the PV cell temperature (T_C), η_{Tref} is the efficiency of the PV cell at the reference temperature, β_{ref} and T_{ref} are the solar temperature coefficient and the reference temperature, respectively. [19] In Equation 5, the temperature coefficient depends on the PV material, PV reference temperature, and at T_O the efficiency of the PV cell drops to zero.

$$\beta_{ref} = 1/(T_o - T_{ref}) \quad (5)$$

From the efficiency equations above, the dependency of the temperature and irradiance conditions on the PV cell affect both the overall power generation and power efficiency of the PV panel. Considering this dependency, to obtain the maximum power from a PV cell, an MPPT controller must be able to account for variations in both cell temperature and solar irradiance. Both factors will result in changes to the voltage and current characteristics of the solar cell, as well as overall efficiency.

2.3 Energy Conversion Optimization

Varying temperature and irradiance conditions influence the power voltage and power current ultimately produced by the PV panel. To efficiently utilize the maximum output power of the panel, a solar charger requires a step between the panel providing power and the DC-DC converter receiving power, or broadly, energy conversion optimization. In this process, Maximum Power Point Tracking (MPPT) is implemented within the solar charger to detect and determine the maximum power point voltage and current that can be provided by the PV panel. By adjusting the voltage and current set-points to maintain the maximum power point (MPP), maximum power output can be achieved under dynamically varying conditions of temperature, cell shading, and solar irradiance. By using MPPT, the charge controller can communicate to the DC-DC converter the amount of voltage it will receive and how it should handle it. The following section introduces how MPPT operates in a solar charger.

2.3.1 Maximum Power Point Tracking (MPPT)

Before explaining MPPT, it is important to understand the current and voltage (I-V) characteristics of the PV panel. Equation 6 shows that the product of voltage and current is power:

$$P = I * V \quad (6)$$

From Equation 6 we can understand that fluctuations in power also means changes in the current and voltage values. Since the power delivered by the panel is dependent on the irradiance, temperature, and shadowing conditions imposed upon it, the power voltage and power current are dependent on the dynamic changes from these conditions. [39] Thus, the panel can operate at a range of voltages and currents depending on the irradiance level and the load current of the circuit as previously explained. We can now define the maximum power point using the specific coordinates of the voltage value and current value associated with the maximum power output of the PV panel as seen in the PV panel's I-V curve illustrated in Figure 7. The point where the product of the load current and the output voltage is greatest is designated as the maximum power point (MPP). Figure 7 shows that the MPP is often located close to the knee of the PV I-V curve.

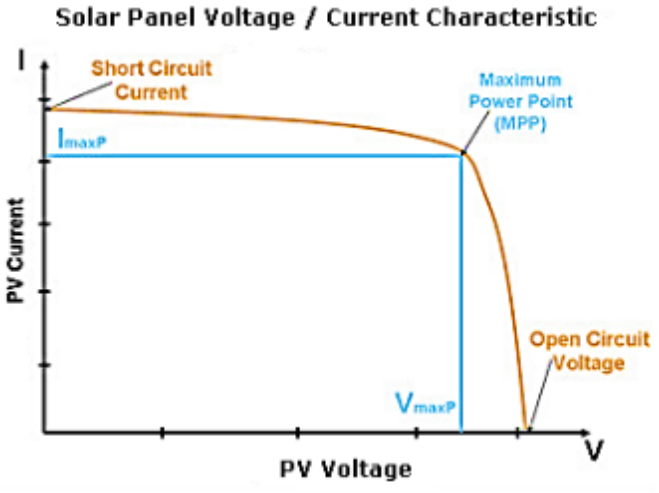

Figure 7. Typical PV Cell I-V Characteristic for MPPT [10]

There are three important factors that are considered when extracting the maximum amount of power from a PV panel [36]:

- Irradiance: changes PV panel current operating point
- Temperature: changes PV panel voltage operating point
- Load: used as a reference for the current and voltage

From understanding the PV panel power relation to power voltage and power current, we can define a Maximum power point tracker (MPPT) as a system that optimizes voltage input and voltage output matching between the PV panel and the battery to achieve maximum panel efficiency. Using current sensors and voltage sensors to detect the operating conditions of the PV panel, various sampling algorithms can be used to calculate the MPP. To perform many simple MPPT algorithms, the four following parameters are measured to operate controllers and are typically provided in PV datasheets:

- V_{OC} – open circuit voltage
- I_{SC} – short circuit current
- V_{MPP} – max power point voltage
- I_{MPP} – max power point current

The open circuit voltage is the maximum output voltage of the panel with no power drawn. The short circuit current is the absolute maximum current provided by the panel. These two values can be used to calculate their respective MPPT values without a microcontroller. Maximum power point voltage, V_{MPP}, is linearly dependent on the open circuit voltage under varying irradiance and temperature conditions. V_{MPP} determines the maximum power point by periodically disconnecting the system from the load to measure V_{OC} and can be calculated using Equation 7, where the constant k_v represents the configuration of the PV panel. [36]

$$V_{MPP} = k_v * V_{oc} \quad (7)$$

This method of calculating the maximum power point, or fractional open circuit voltage, typically causes temporary loss of power and is not typically advised to use as an MPPT method. Similarly, there is a fractional short circuit method in which the maximum power point current is linearly dependent on the short circuit current and can be calculated using Equation 8:

$$I_{MPP} = k_i * I_{sc} \quad (8)$$

To determine the short circuit current using this method is also disadvantageous. The short circuit current method results in increased power loss and heat dissipation. Also, the circuit would require an additional switch and current sensor to properly extract the value. [36]

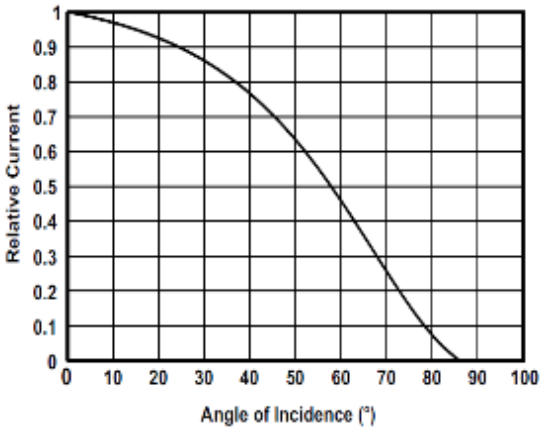

Figure 8. Angle of Incidence vs Relative Output Current [20]

It is important, however, to note that the two current values, I_{SC} and I_{MPP}, are proportional to the irradiance. More specifically, I_{sc} is proportional to irradiance, while I_{MPP} changes in proportion to irradiance as demonstrated in Figure 8. The power current's relationship with irradiance is important for mobile applications since the angle of incidence of irradiance varies especially when the PV panel will be moved to different locations and angles relative to available sunlight. As seen in Figure 8, if the angle of incidence is not zero, the amount of effective irradiance is reduced resulting in a decrease in current. This mobile situation would require a faster tracking system due to the potential angle changes. [20]

The parameters V_{OC}, I_{SC} , V_{MPP}, I_{MPP} and their relationship with irradiance determines the type of MPPT algorithm necessary to compute to maximum power output of the PV panel. Different combinations of these parameters characterizes algorithm efficiency and capability to determine the MPPT. [10]

2.3.2 MPPT Control Algorithms

There are many ways to maximize the power of a PV system such as using a simple method of voltage relationships to complicated sample based analysis. [20] Most commonly implemented MPPT algorithms include, but are not limited to, the constant voltage (CV), perturb & observe (P&O), incremental conductance (INC), open-circuit voltage (VOC), and short-circuit current (ISC) methods. The type of method chosen for a system is typically based on the level of expected irradiance. For instance, methods such as VOC and ISC are better for low levels of irradiance and are usually more immune to noise. Iterative methods are usually better when the PV cells are arranged in series. Searching methods are implemented when the angle of incidence changes or for a panel that will experience shade. In the case of portable devices, our system needs to perform efficiently under dynamic irradiance conditions and under the occurrence of the shadow effect. [20] A comparison on how each method operates and achieves MPP can be seen in Table 1.

Characteristics of methods	P&O	INC	VOC	CV	ISC
Choose a maximum power point using a predetermined value or ratio of values			x	x	x
Measurements of the PV open circuit voltage are taken, and an approximation for V_{MPP} is calculated as approximately 0.76-0.78 of V_{OC}			x	x	
Determines I_{MPP} as a ratio of I_{sc} to locate the maximum power point (MPP)					x
Provide dynamic MPPT under changing irradiance, temperature, and voltage conditions	x	x			

Table 1: Comparison of P&O, INC, CV, VOC, and ISC characteristics of each method

From Table 1, we can observe that three of the algorithms, CV, VOC, and ISC, choose a maximum power point using a predetermined value or ratio of values. For the CV and VOC methods, measurements of the PV open circuit voltage are taken and an approximation for V_{MPP} is calculated as 0.76-0.78 of V_{OC}. [39] The ISC method works similarly to the CV and VOC techniques but instead determines I_{MPP} as a ratio of I_{sc} to locate the maximum power point (MPP). The primary issue with the CV, VOC, and ISC methods is that they rely on assumed values for V_{MPP} and I_{MPP}, which do not accurately or efficiently account for changes in PV panel conditions. Only the P&O and INC methods provide dynamic MPPT under changing irradiance, temperature, and voltage conditions and are therefore addressed in detail within this paper.

Perturb and Observe (P&O)

To efficiently perform MPPT under varying input conditions, the Perturb & Observe algorithm is commonly used in MPPT controllers. P&O maintains maximum power by introducing a change in the panel's output voltage and observing if the output power increases or decreases in response. The algorithm then provides the appropriate modifications to the duty cycle of the DC-DC converter to account for modifying the panel voltage.

Figure 9 indicates that if the change in power is positive on the left side of the MPP, $dP/dV > 0$, then the output has moved closer to the MPP, and the controller will continue to perturb the PV panel in the same direction. If $dP/dV < 0$ on the right side of the MPP, the output has moved further from the MPP, and the controller switches to perturb the voltage in the opposite direction. The size of the step is proportional to the size of deviation, or oscillation, around the MPP. [39, 36]

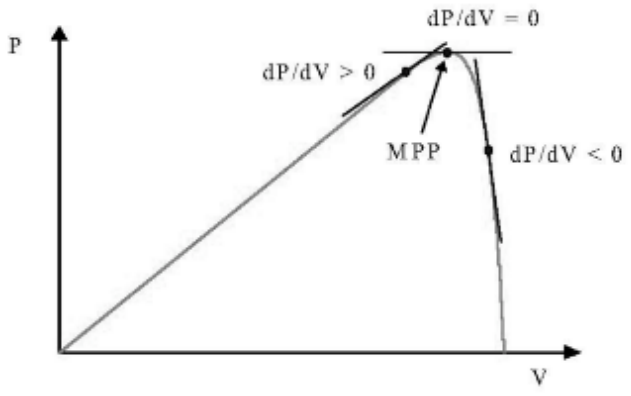

Figure 9. Signs of dP/dV with reference to MPP [38]

More clearly, the P&O method uses a fixed step to increase or decrease the voltage in attempt to match MPP:

- By decreasing voltage on right side of MPP, power increases towards MPP
- By increasing the voltage on left side of MPP, power increases towards MPP

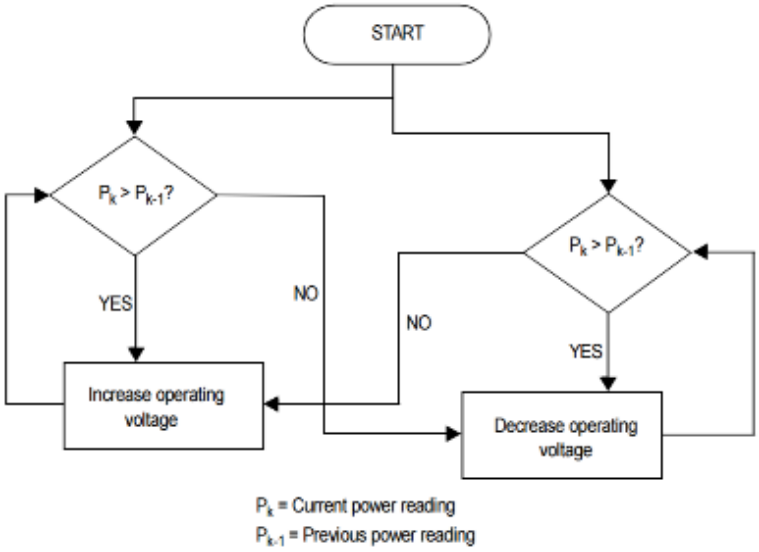

Figure 10 .Flowchart of P&O MPPT method [36]

The decision making process of the P&O method described previously can be visually described through the flowchart as shown in Figure 10. P&O is a simple algorithm to implement, however, sudden changes in irradiance can cause the algorithm to perturb in the wrong direction, and the algorithm can also be prone to steady-state error from oscillations around the MPP. [39]

Incremental Conductance (INC)

The incremental conductance (INC) algorithm is a method similar to P&O in that INC also can handle dynamic irradiance and temperature conditions. Instead of directly calculating $\frac{dP}{dV}$ like P&O method, INC uses compares the incremental conductance, $\frac{dI}{dV}$, to the instantaneous conductance, $\frac{I}{V}$. The INC algorithm will regulate the duty cycle signals until MPP (when $\frac{dI}{dV} + , \frac{I}{V} = 0$) is reached . In other words, when the incremental conductance equates the instantaneous conductance, the maximum power point has been reached. In general, the INC method calculates the relation of the power curve derivative and the voltage at zero which indicates the MPP. Any value on the left side of MPP is a positive slope and anything on the right side of MPP is a negative slope. Thus, the comparison is actually the positive incremental conductance versus the negative instantaneous conductance.

Equation 9 shows the derivation of the incremental conductance equality to instantaneous conductance from the principle: when the MPP is reached, $\frac{dP}{dV} = 0$. [39, 36]

$$\frac{dP}{dV} = \frac{d(VI)}{dV} = 0$$

$$I \times \frac{VdI}{dV} = 0$$

$$\mathrm{I} \times \frac{dV}{dV} + \mathrm{V} \times \frac{dI}{dV} = 0$$

$$\mathrm{I} + \mathrm{V} \times \frac{dI}{dV} = 0$$

$$-\frac{I}{V} = \frac{dI}{dV}$$

Equation 9. Derivation of Incremental Conductance Condition

Figure 11 shows the group of INC conditions in terms of power curve derivative as Equation 1 and Equation 2 the group of INC conditions in terms of incremental conductance and instantaneous conductance after the derivation shown in Equation 9. [36] As seen in Equation 9, the INC algorithm requires both the panel's output voltage values and output current values. Because of the more complicated method, this algorithm typically needs the higher processing ability of a PIC or DSP.

$$(1)\begin{cases} \frac{dP}{dV} = 0, at\ MPP \\ \frac{dP}{dV} > 0, left\ of\ MPP \\ \frac{dP}{dV} < 0, right\ of\ MPP \end{cases} \longrightarrow (2)\begin{cases} \frac{\Delta I}{\Delta V} = -\frac{I}{V}, at\ MPP \\ \frac{\Delta I}{\Delta V} > -\frac{I}{V}, left\ of\ MPP \\ \frac{\Delta I}{\Delta V} < -\frac{I}{V}, right\ of\ MPP \end{cases}$$

Figure 11, INC Conditions in Power Curve Derivative Form and Incremental Conductance Form [36]

The complex decision making process of the INC method described previously can be visually described through the flowchart shown in Figure 12. Most INC algorithms use a fixed step size for the panel output voltage updates.

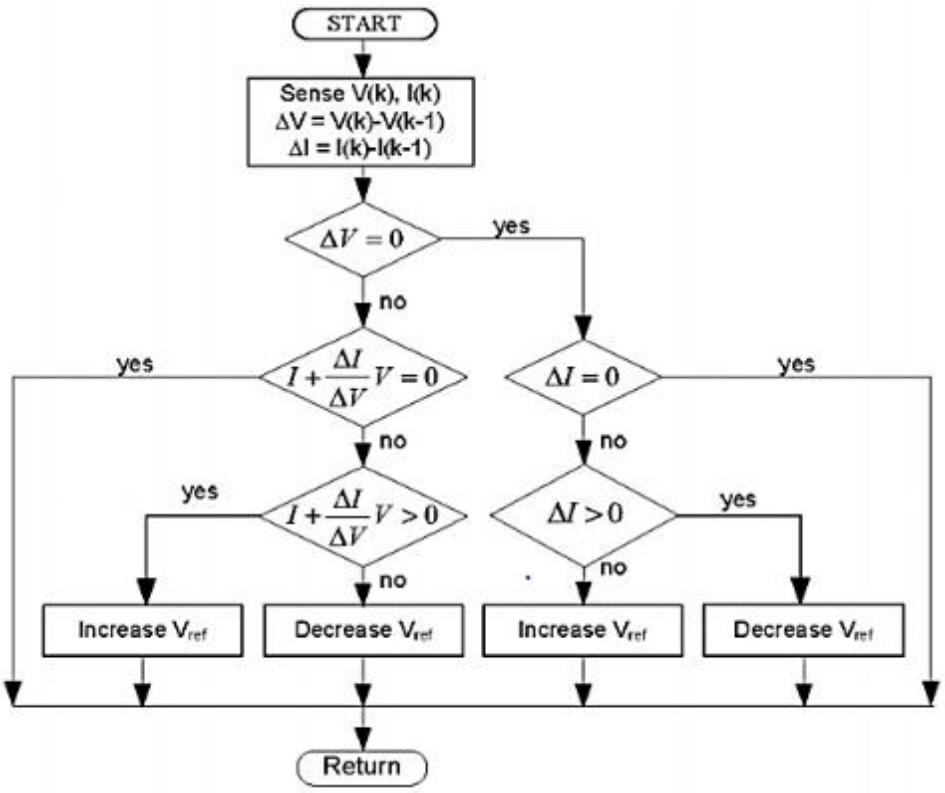

Figure 12. Flowchart of INC MPPT method [39]

From the comparing the flow chart in Figure 12 to the flowchart for P&O, the difference between INC and P&O can be observed. Because INC can compute the sign of $\frac{dP}{dt}$ without perturbation, steady-state error is reduced near the MPP meaning there is less oscillation around the MPP. The decrease in error of INC gives this method an advantage over P&O, but at the cost of complexity of implementation.

INC and P&O Comparison

From a study regarding the performance of P&O and INC methods under dynamic weather conditions, the INC and P&O methods were compared in a simulation and graphed as in Figure 13. In this case, MPPT efficiency was weighed against insolation slopes, and the averaged results are shown in Figure 13. By observing the results, the INC insolation slope has a higher efficiency curve than the P&O insolation slope. Although the P&O graph has a lower efficiency, due to a slower MPPT algorithm than INC, it provides overall better efficiency in medium to high insolation. INC proves to operate more efficiently at the extreme ends of isolation, and it is relatively steady through the range of insolation slopes. The INC, overall, performs more efficiently under dynamic conditions than P&O. The sensitivity range of INC is conducive for a portable device that will be exposed to dynamic irradiance and temperature conditions. Nevertheless, INC and P&O are relatively close in MPPT efficiency rating, where even at high slopes the INC efficiency is 98.6% and P&O is 98.45% with a difference of 0.15%. [25]

Thus, depending on the expected weather conditions for the panel, either choice is a reasonable method to implement in a solar charger.

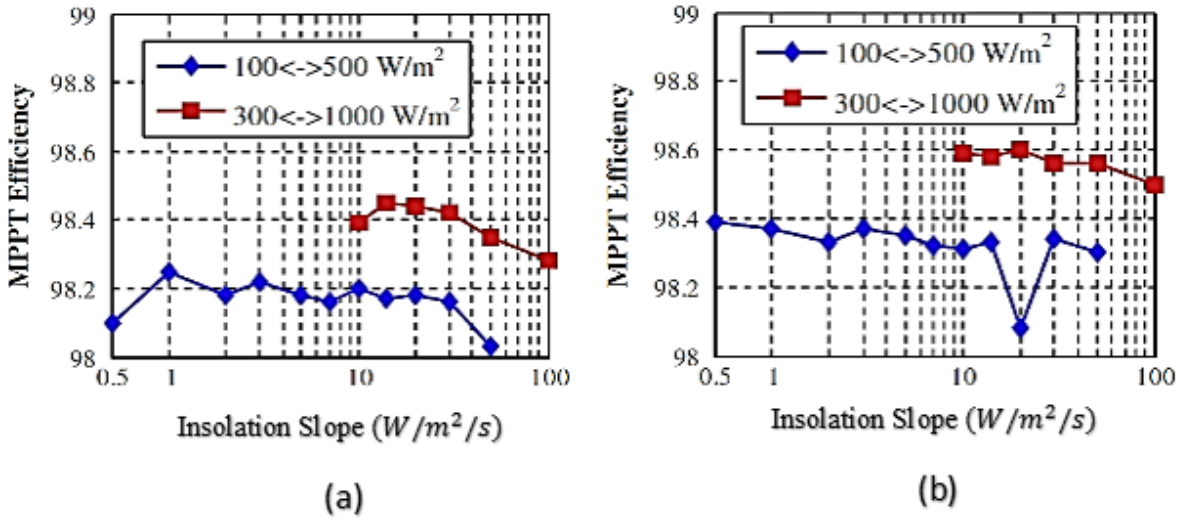

Figure 13. Average MPPT slope efficiency a. P&O and b. INC [25]

2.4 Energy Conversion Implementation

The implementation of MPPT involves the MPPT algorithm communicating the input voltage that the DC-DC converter will receive and instructions to the converter about to handle the input voltage appropriately. More specifically, the MPPT algorithm is executed through a controller, and the controller changes the duty cycle of the converter to regulate the input voltage to the required load voltage. The power conversion efficiency depends on voltage converter typology and how it is controlled. Therefore, it is necessary to explore the different typology configurations that would increase the output power efficiency. It is also necessary to understand how the DC-DC converter and controller communicate and produce an output voltage to match the load requirement. In this section, DC-DC converter typologies are discussed and their characteristics, parameters, and drawbacks are compared. In addition, once the components are described, the control and feedback of the system is explored to understand how the MPPT and the DC-DC converter operate as a unit.

To convert PV energy to the desired load, a DC-DC converter needs to be employed in the system. To account for varying conditions, the DC-DC converter should either increase or decrease the voltage level from the PV panel with minimal power loss to meet the requirements of the load. In our case the load is likely a battery.

2.4.1 Switched Mode Power Supplies: Typologies and Operation

DC-to-DC converters are a type of switched mode power supply (SMPS) that converts a DC power source, which either has a higher or lower power voltage than the load requirement, to a stable DC voltage that matches the load. SMPSs consist of using power switches, inductors, capacitors, and diodes to adjust and transfer the input power to the load. [35, 11]

Typologies

DC-to-DC converters are divided into two typologies: Non-isolated and Isolated. Isolation refers to the separation between the input and output of the converter. An isolated DC-DC converter users a transformer to break the electrical path between the input and output. A non-isolated DC-DC converter retains the electrical path between the input and output by using an integrated controller. [11] The focus of this paper will be on non-isolated DC-to-DC converters which are typically applied to lower voltage, portable devices, whereas an isolated typology is useful for higher voltage and power distribution applications. In addition, a converter's typology can determine if the voltage output will be the negative of the input, "inverted", or remain positive, "non-inverted". The output requirements of our project will be connected to a charge controller and needs to have a positive output voltage meaning that the converter requires a non-inverting typology. [18]

There are five general types of DC-to-DC isolated converters that were considered: Buck, Boost, Buck-Boost, SEPIC, and Cúk. With consideration of our project goal, Buck-Boost and SEPIC topologies are discussed in this paper due to their ability to both step-up and step-down voltage, and their capability to produce a non-inverting output. The reasoning to focus on Buck-Boost and SEPIC is based on elimination of the typology characteristics as seen in Figure 14, with the orange blocks representing the typologies that are suitable for portable device charging and the grey blocks representing the typologies that cannot achieve charging for portable devices.

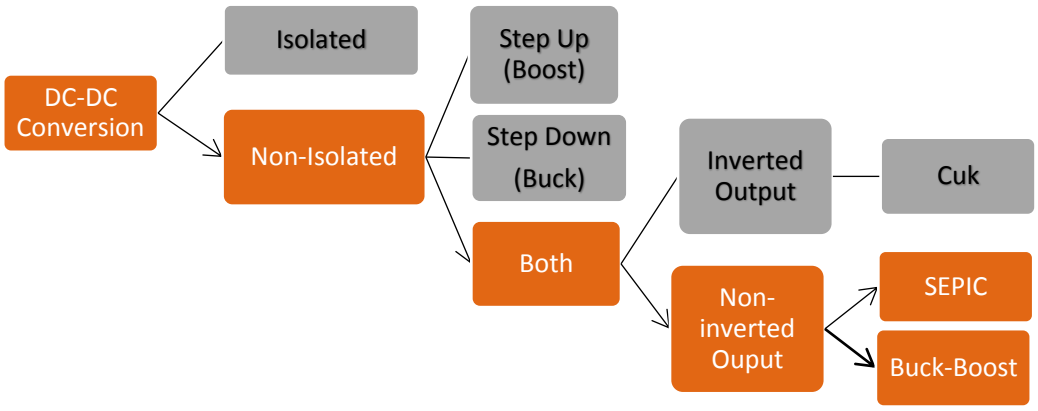

Figure 14. Hierarchy of Voltage Regulator Typology in Relation to Focused Design Selection

Operation

Since the typologies are characterized by their components and the way they are driven, it is important to discuss the basic principles of how a DC-DC converter operates. Considering a simple buck –boost circuit in Figure 15, the main components are a MOSFET (metal-oxide semiconductor field-effect transistor) switch, an inductor, a diode, and an output capacitor. By studying the voltage flow of the circuit, we can derive the basic operation of a buck-boost converter. The fundamental principle of operation for a DC-DC converter, to transform voltage, is based on the PWM controlled high frequency switching of the MOSFETs and the voltage it passes to the inductor. During this time the capacitor is either charging or discharging the regulated voltage to the load, while the diode dictates the direction of current when switching ON and OFF. [30] Table 2 explains how the voltage across the inductor drives the voltage conversion process through the inductor charging and discharging cycles.

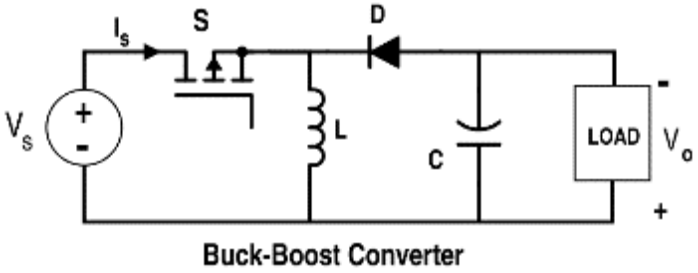

Figure 15. Typical Single Switch Buck-Boost Converter [1]

Inductor Charging Cycle	Inductor Discharging Cycle
• Inductor current increases linearly • Capacitor in discharging state supplies output current to load	• Energy stored to inductor flows to capacitor and to load • Capacitor in charging state • Inductor voltage decreases linearly
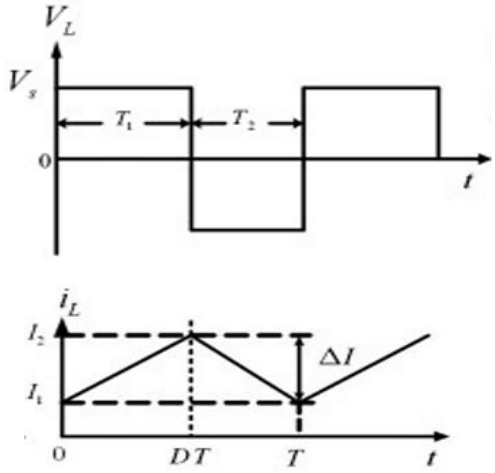 Figure 16a.Inductor voltage and current during charging (T1) and discharging (T2) modes	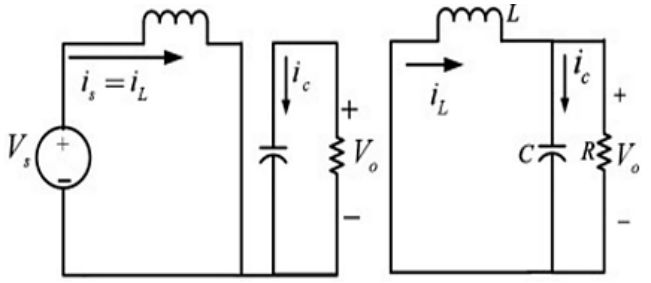 Figure 16b. Left. Inductor charge mode Q1, Q3 ON, Q2, Q4 OFF Figure 16c. Right. Inductor discharge mode Q1, Q3 OFF, Q2, Q4 ON
$V_S = L(I_2 - I_1)/T1$ $V_S = \left(L\frac{\Delta I}{T1}\right)$ (10a)	$V_{OUT} = \left(L\frac{\Delta I}{T2}\right)$ (10b)

Table 2. Description of Inductor Charging and Discharging Cycles for DC-DC Converter [26]

From observing Equation 10a and Equation 10b, and relating these to Equation 11 and Equation 12, where $T = T1 + T2$ and the duty cycle is $D = T1/T$,

$$T1 = D * T \quad (11)$$

$$T2 = (1 - D) * T \quad (12)$$

We can define the average output voltage as:

$$V_{OUT} = (D/1 - D) * V_S \quad (13)$$

With Equation 13, duty cycle's relationship to the output and input voltage is defined as the ratio of the time on (ON) or time off (OFF) over the total switching time period. Due to the function of the duty cycle, by controlling the period of the inductor charging cycle and discharging cycle, the circuit can operate in buck mode and boost mode under one duty cycle.

Since the duty cycle, or the fraction of the time period when the signal is active, of the switches determines the ON and OFF time of the switch, it also regulates how much power is transferred to the output. The configuration of the components and the duty cycle characterizes the different DC-DC converter typologies as step-up, step-down, or both. Because SMPSs require a higher operation frequency, voltage ripple, current ripple, and EMI become limiting parameters when considering designs for DC-to- DC converters. [35, 11]

2.4.2 Buck-Boost Converter

Unlike the inverting buck-boost converter that can only use buck-boost mode, a non-inverting buck-boost converter can operate using characteristics of a buck converter and boost converter separately, or in a combined buck-boost mode. These modes are available for either a two or four-switch buck-boost typology. The buck-boost design is a cascaded combination of a buck converter leg followed by a boost converter leg. To understand the functions of a buck-boost converter, we shall briefly define the difference between buck and boost:

- buck: adjusts input voltages higher than output voltage as current increases
- boost: adjusts input voltages lower than output voltage as current decreases

Due to strict input voltage range requirements to operate, both the buck circuit and the boost circuit cannot handle variability of input voltages outside of their restricted input range. Since the buck-boost circuit includes both the step-up and step-down conversion abilities, it can handle input variability above or below the output. [11, 18] In addition, the buck-boost circuit can handle a situation where the supply voltage is relatively close to the load voltage. This operational mode is considered the buck-boost mode, and it is possible because the converter has both buck and boost legs.

Two-switch Buck-Boost Converter

Figure 16 demonstrates the different operational modes of the two-switch buck-boost typology with their respective ideal voltage and current waveforms at each component. The two-switch buck-boost converter uses two MOSFETs as the active switches and two diodes as the passive switches. Conversely, the inverting buck-boost converter which only uses a single MOSFET and a single diode as the switching components. The two switch approach enables this typology to perform the three operational modes: buck mode, boost mode, and buck- boost mode as seen in Figure 16 a, b, c. These modes are defined by the duty cycles of the two MOSFETS, Q1 and Q2.

To operate the buck-boost circuit in Figure 16a, all the power components need to be ON. Q1 and Q2 switch ON and OFF simultaneously allowing either a buck or boost operation to occur when provided a specific duty cycle. During this operation, the diode, D1, ensures that the current is directed towards the load during the OFF cycle to prevent reverse current from entering Q1. Similarly, D2 directs the flow of the current from Q2 towards the load. The buck and boost circuits seen in Figure16b and Figure 16c use less power components during operation. For the buck circuit, Q2 is always OFF inhibiting the boost leg of the circuit. D2 restricts the flow of the current from accessing Q2 when the inductor discharges and only allows the buck leg to be active. For the boost circuit, D1 is always off inhibiting the buck leg of the circuit, but still allows current and voltage flow to the boost leg.

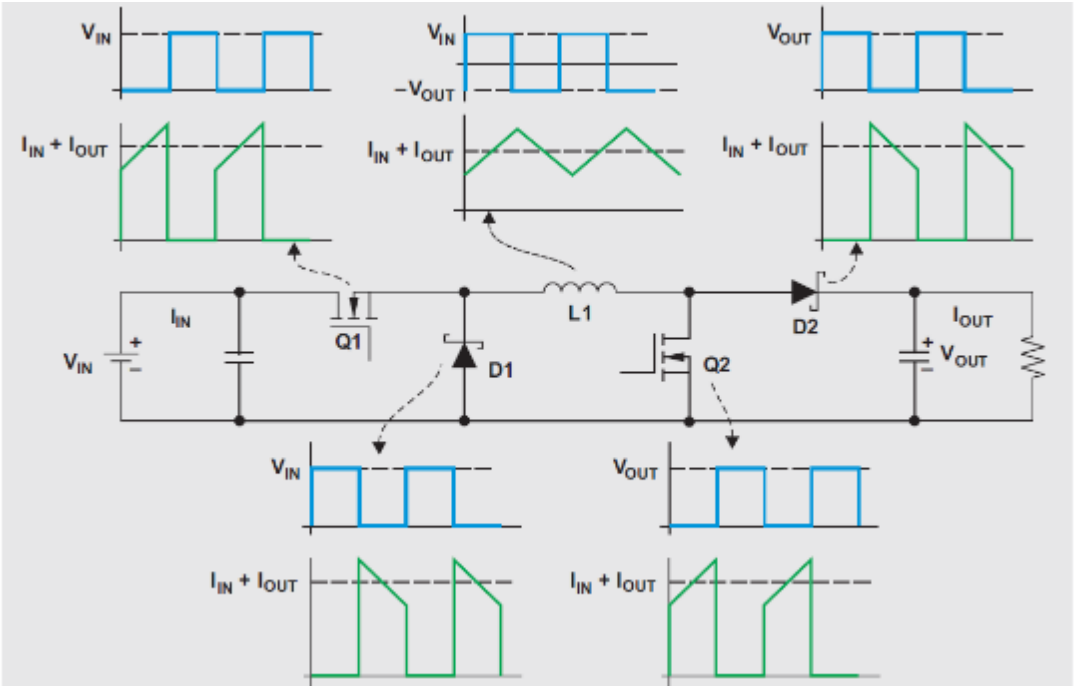

Figure 16a.Two-switch buck-boost in buck-boost mode

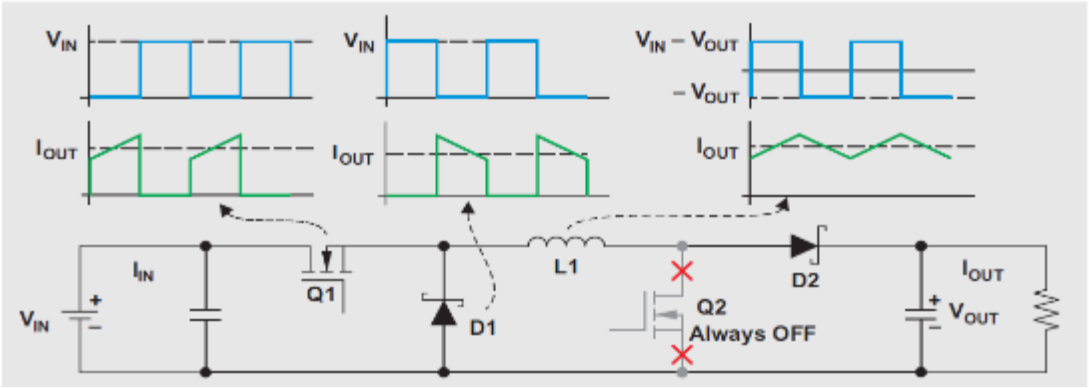

Figure 16b. Two-switch buck-boost in buck mode

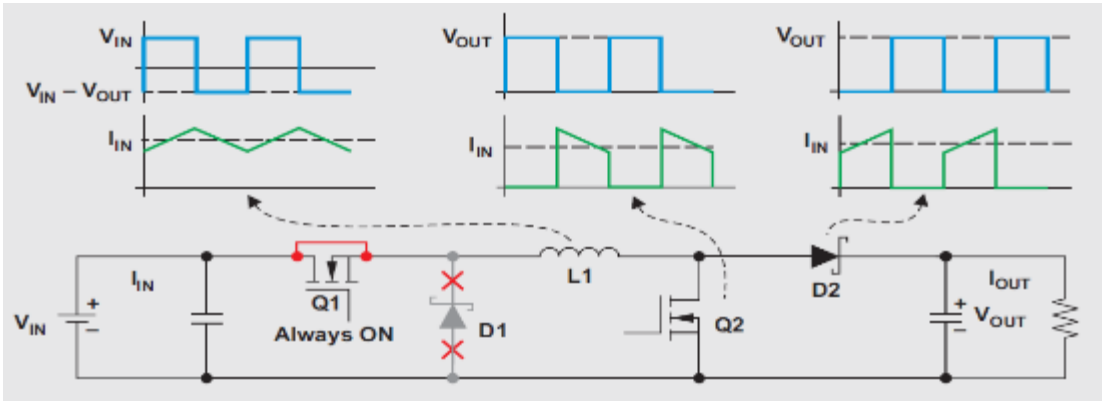

Figure 16c. Two-switch buck-boost in boost mode [18]

Table 3 explains the three different modes from Figure 16 in terms of the MOSFET operation and the voltage conversion ratios calculated using the duty cycles, *D*. [18]

Operational Mode	Q1 and Q2 states	Voltage Conversion Ratios
Buck-boost	Turn Q1 and Q2 ON and OFF simultaneously	$\frac{V_{out}}{V_{in}} = \frac{D}{D-1}$
Buck	Q2 is always OFF, output voltage is regulated by Q1	$\frac{V_{out}}{V_{in}} = D$
Boost	Q1 is always on, D1 is reverse biased and stays OFF, output regulated by Q2	$\frac{V_{out}}{V_{in}} = \frac{1}{1-D}$

Table 3. Buck-boost Operational Modes Defined by Q1 & Q2 States and Voltage Conversion Ratios [18]

The voltage conversion ratios in Table 3 characterize the inductor charging relationship between the duty cycle, the output voltage, and the supply voltage. For the buck converter, the current will increase linearly and decrease linearly because the supply voltage (V_{in}) is linearly proportional to the output voltage (V_{out}). However, for the boost and buck-boost modes, the inductor will not charge linearly, affecting the output voltage in terms of the duty cycle. The difficultly in non-linear voltage charging of the inductor impacts the efficiency of the power conversion from the supply to the load. [26] Thus, these operational modes are the foundation to the converter's efficiency. The number of power devices and the high current stress in the buck-boost mode limits the converter from being efficient. [18] However, if the operational modes are used in response to the provided input voltage, such as buck mode would be used if the input voltage is consistently higher than the load, the two-switch buck-boost converter will have higher efficiency than the inverted design. The full-buck and full-boost modes are inherently more efficient operational modes than simply the buck-boost mode because the single operational modes use fewer power devices which lowers the overall current stress on the components. Thus, it is important to consider which combinations of operational modes should be implemented for the converter to be efficient in the system. However, control circuitry, which would complement the desired operational mode capabilities, must be in place to execute these combinations. Table 4 describes the operational modes of the two-switch buck-boost in reference to control complexity and efficiency when performing a step-up and step-down.

Operation Modes	Control Complexity	Efficiency ($V_{in} > V_{out}$)	Efficiency ($V_{in} < V_{out}$)
Buck-boost	Simple	Low	Low
Buck and buck-boost	Moderate	High	Low
Buck-boost and boost	Moderate	Low	High
Buck, buck-boost, Boost	Complicated	High	High

Table 4 Comparison of Operating Modes in Terms of Control Complexity and Efficiency [18]

From examining Table 4, we can observe that although controlling buck-boost mode is the most simple to implement, this mode is the least efficient when bucking or boosting the input voltage. All three operation modes used separately is the most efficient in bucking and boosting. However, this operational capability requires the control to handle multiple modes of operation and performing the transitions accurately between each mode. We further discuss the control complexity of the buck-boost converter with respect to the operational modes in Section 4.5.

Non-Inverting Synchronous Buck-Boost Converter

Another typology of buck-boost is a four-switch buck-boost converter. In this typology instead of one MOSFET and one diode, two MOSFETs each are used to form the buck leg and boost leg of the circuit as denoted in Figure 17. This type of design implementation is referred to as synchronous rectification. Synchronous rectification is defined as using a rectifying transistor, typically a MOSFET, to perform current rectification, or driving the current in a specific direction. For the leg to work in a complimentary manner, one of the MOSFETS is ON and the other is OFF in the pair [44]. In this way, the buck-boost converter can operate in either buck, boost, or buck-boost mode to handle variations of voltage supply by controlling the MOSFETs. [26]

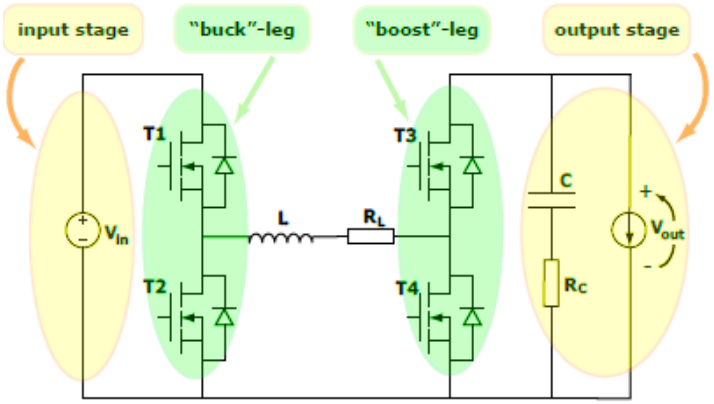

Figure 17. Non-inverting Synchronous Buck-Boost Converter Design [44]

Figure 18, Figure 19, and Figure 20 demonstrate the buck mode, boost mode, and buck-boost mode of the non-inverting synchronous buck-boost converter during inductor charging and discharging.

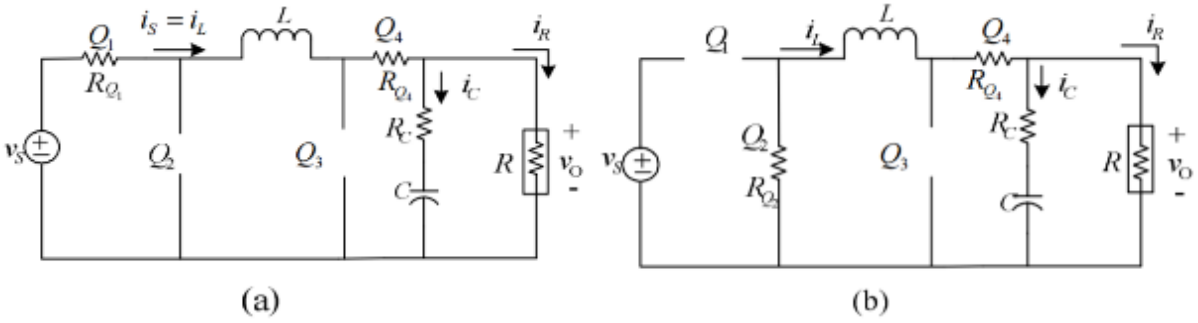

Figure 18. Buck mode (a) Inductor Charging (b) Inductor Discharging [26]

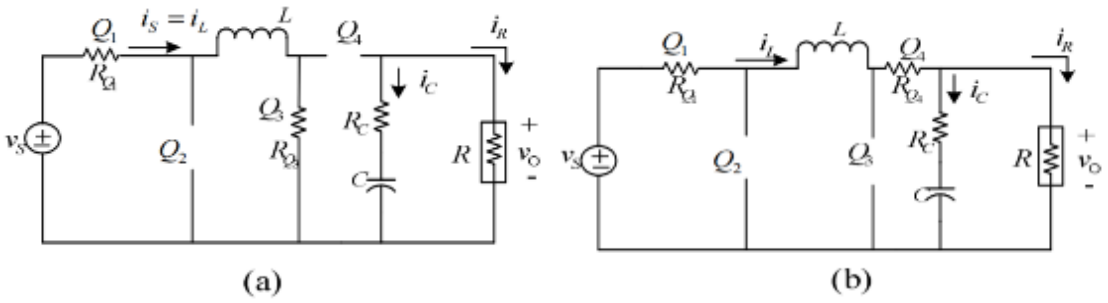

Figure 19. Boost mode (a) Inductor Charging (b) Inductor Discharging [26]

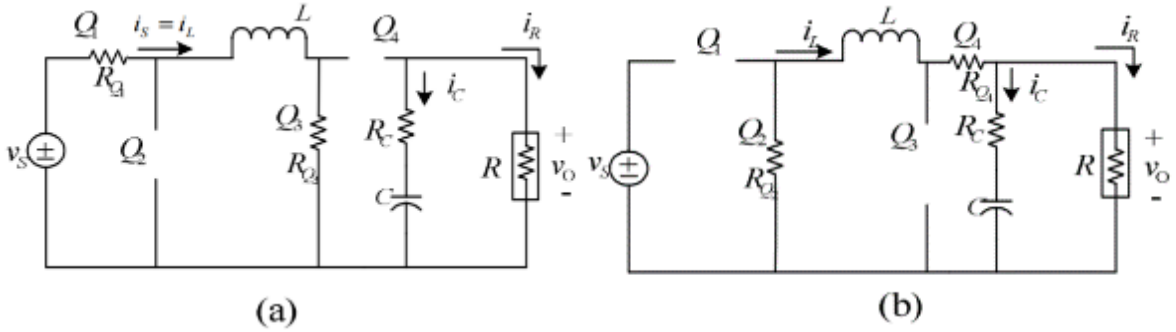

Figure 20. Buck-Boost mode (a) Inductor Charging (b) Inductor Discharging [26]

Table 5 explains how the MOSFETs are driven to set up the different operational modes of the buck-boost converter. During inductor charge, the supply voltage is charging the inductor, and the capacitor is discharging current to the load. During the inductor discharge, the inductor's voltage and current charges the capacitor and the load. During the inductor charging and discharging cycle, a pair of switches remains either always ON or always OFF to direct the supply voltage to the designated leg of the circuit to create the necessary operational mode.

Operational Mode	**Inductor Charge and Discharge**	**Inductor Charge**	**Inductor Discharge**
Buck	• Q3 is always OFF • Q4 is always ON	• Q1 is closed • Q2 is open	• Q1 is open • Q2 is closed
Boost	• Q1 is always ON • Q2 is always OFF	• Q3 is closed • Q4 is open	• Q3 is open • Q4 is closed
Buck-boost	• Q1 and Q3 work together • Q2 and Q4 work together	• Q1 and Q3 are closed • Q2 and Q4 are open	• Q1 and Q3 are open • Q2 and Q4 are closed

Table 5. Operational Modes of Synchronous Buck-Boost Converter during Inductor Charge and Discharge [26]

Similar to the two-switch buck-boost converter, the voltage conversion ratios are the same for the operational modes of the four-switch buck-boost converter. The voltage conversion ratios define the

operational modes for any typology. As long as the converter has the voltage conversion ratio of the buck mode, it will perform power conversion like a buck converter, and similarly for the other operational modes. However, the control mechanisms behind inducing the operational mode will be different for each typology. In this case, we can reproduce the buck, boost, and buck-boost modes using four MOSFETs instead of two MOSFETs and two diodes. It is then possible to compare efficiencies of typologies by comparing how efficient the typology performs power conversion in their operational modes. We further examined the control mechanisms of synchronous rectification in Section 2.4.5. In order for the four-switch buck-boost converter to be driven efficiently, conduction losses and switching losses need to be adjusted such that they are balanced between the components of both legs of the circuit. In addition the controller used to drive the circuit requires the ability to access all three operational modes similar to the two-switch circuit. The advantages of synchronous rectification is discussed further in Appendix B, "Increasing Efficiencies during Low Loads". From observing both the two-switch and the four-switch buck-boost converters, a controller must be chosen to meet the requirements of the operational modes desired for the buck-boost converter. The limitations of the buck-boost design is the number of power components and the current stress on the circuit.

Variations of Two-Switch Buck-Boost Typology

In addition to the two-switch and four-switch buck-boost configurations, there are different configurations of buck-boost converters that can produce a non-inverted output with varying efficiencies. Examples of modified buck-boost typologies can be seen in Table 6, where L denotes inductor, C denotes capacitor, S denotes switches, CR denotes diodes, and D1 and D2 are the duty ratios of S1 and S2.

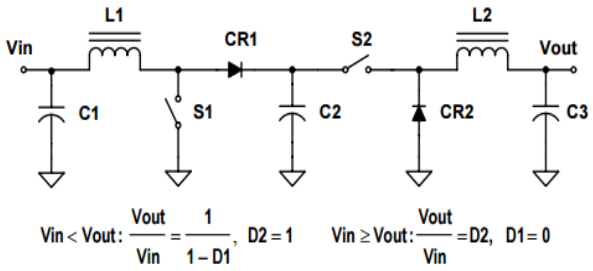 Figure 21a. Boost-Buck Example 1	**Example 1: Boost followed by Buck** Boost: drive S1 with PWM, hold S2 ON continuously Buck: drive S2 with PWM, hold S1 OFF Vin=Vout: no switched mode power processing required Limitations: C2 has discontinuous current from CR1 (boost) and from S2 (buck)
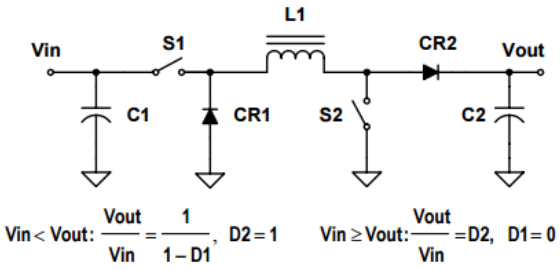 Figure 21b. Buck-Boost Example 2	**Example 2: Buck followed by Boost** Boost: drive S2 with PWM, hold S1 off Buck: drive S1 with PWM, hold S2 off Vin=Vout: no switched mode power processing required Limitations: input and output currents are discontinuous
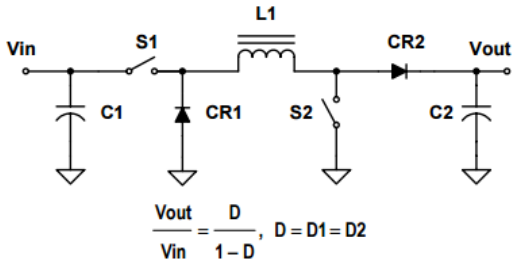 Figure 21c. Buck-Boost Example 3	**Example 3: Buck followed by Boost** Boost: drive S2 and S1 with PWM Buck: drive S2 and S1 with PWM Vin=Vout: inductor conducts twice input current Limitations: more complex and less efficient due to both switches being driven, causing all switching components (S1, S2, CR1 and CR2) conduct twice the current resulting in power losses

Table 6. Examples of Different Buck-Boost Configurations with Functional Descriptions [32]

These examples were simulated and analyzed through PSPICE as seen in reference 32. Mullet concluded that the Example 2 buck-boost converter is the most efficient circuit typology when the input voltage is close to the output voltage, and the Example 1 boost-buck converter displayed best performance with a larger range of input voltages. Further discussion to compare these results with a SEPIC converter will be seen in Section 2.4.4 Typology Comparison. We will first establish the functionality and characteristics of a SEPIC Converter before discussing comparisons.

2.4.3 Single-ended Primary Inductor Converter (SEPIC)

A SEPIC converter is a type of DC-DC voltage regulator, similar to a non-inverting buck-boost converter that can accept a wide range of input voltages. We can observe the similarity in the typology by considering the voltage conversion ratio in Equation 14.

$$M = \frac{V_{out}}{V_{in}} = \frac{D}{1-D} \qquad (14)$$

Contrary to a buck-boost converter, SEPIC has a different configuration to perform step-up and step-down regulation. [27] More specifically, a SEPIC converter uses two magnetic windings which can be wound on a common inductive core or on two separate cores, and an extra capacitor. Similar to an inverting buck-boost, a SEPIC only requires a single MOSFET, and a single diode. Since the configuration of a SEPIC is similar to the inverting buck-boost design, the SEPIC converter will have similar voltage and current requirements and will experience similar power losses to the inverting typology. [18]However, with an additional capacitor and inductor, the design becomes a non-inverting SEPIC. The extra capacitor inhibits DC components between the input and output, but requires a second inductor to cause the diode to direct current toward the load [27].

Because the same voltage is applied to the two inductors, some designs suggest to couple the inductors on the same core to reduce the number of components in the design. However, this approach is more expensive because winding both inductors on same core requires a customized component that is not typically sold.

As illustrated and explained in Figure 22 and Table 7, the SEPIC operates by being driven by a simple controller applying PWM to the switch transistor (Q1). In Figure 22, L1 and L2 denotes the two inductors, C1 and C2 are the capacitors, and D1 is a Schottky diode.

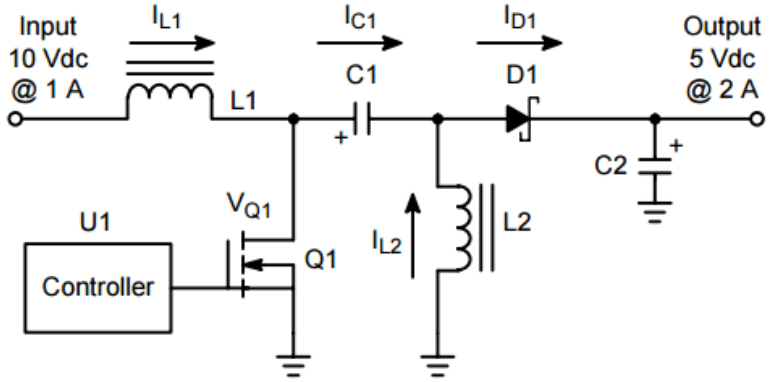

Figure 22. An Example of a SEPIC Converter [32]

Transistor state: Q1 ON	Transistor state: Q1 OFF
• Current flows from the input across L1 to Q1 to ground • Current increases and energy is stored in L1 • If a previous cycle has already occurred, C1 would have been charged, during this state, C1 would discharge to charge L2 • D1 is reversed biased allowing C2 to discharge if previously charged	• Current stored in L1 flows through C1 to D1 and to the output • Inductor L2 provides stored current to D1

Table 7 States of Switching Transistor and Corresponding Components [32, 34]

The average inductor currents of L1 and L2, I_{L1} and I_{L2}, are equal to the input current and output current. The capacitors C1 and C2 can be coupled as an ac-coupling capacitor or they can be left separately. The choice in either capacitor implementation will cause extra power loss and reduce the converter's overall efficiency. In order to minimize power loss from these components, ceramic capacitors with low Equivalent Series Resistance (ESR) should be used but are more expensive. Both the additional inductor and capacitor increase the PCB board size and increases the overall cost of the converter. Advantageously, SEPIC converters experience reduced noise, because SEPIC uses a clamped switching waveform.

2.4.4 Topology Comparison

Having described the non-inverting buck-boost typology and SEPIC typology, we compare the advantages and disadvantages of these typologies. From these comparisons, an appropriate converter can be evaluated based on the most advantageous for a portable solar charger.

The following compares the non-inverting buck-boost typologies mentioned in Table 6 against the SEPIC converter mentioned in the previous section. From Figure 23 we observe that the boost-buck model performs most efficiently over a range of input voltages compared to SEPIC and buck-boost.

The two inductors of the boost-buck model smooth the input and output current, which reduces the component stress caused by

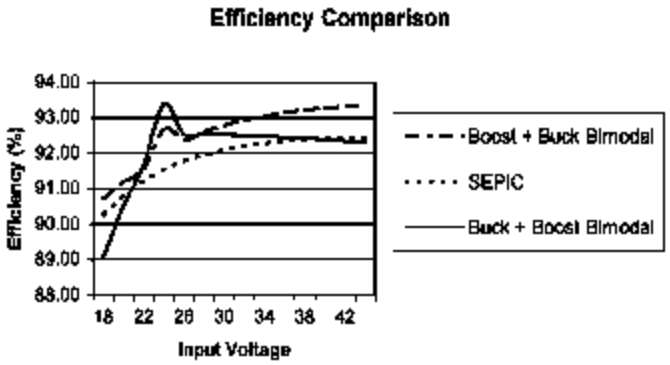

Figure 23. An Efficiency comparison of Example 1 Boost-Buck, Example 2 Buck-Boost, and a SEPIC [32]

current ripple. The boost-buck model and the buck-boost model perform with efficiencies around 92% to 93% when an input voltage is close to the output voltage (24V), whereas the SEPIC, although efficient, only handles the input voltage at an efficiency around 90% to 91%. [32, 27]Typically, the SEPIC is less efficient than the buck-boost model because of the parasitic capacitances and impedances. Table 8 compares the advantages and disadvantages previously discussed in the buck-boost section and SEPIC section of this paper.

Typology	Non-Inverting Buck Boost	SEPIC
Advantages	• Typically less components than SEPIC • High efficiency over a large range of input voltages • Different configuration styles and different order of buck or boost mode allow variety in operation	• Non-inverting output design • Less active components and only uses one controller • Clamped switching waveform reduces noise caused by high-frequency switching
Disadvantages	• More complex design, requires an accurate controller for better efficiency • Higher power loss and more noise due to more power components	• Complex design due to inductors • Reduced efficiency due to parasitic capacitances and inductances

Table 8. An Efficiency comparison of Example 2 Buck-Boost, and a SEPIC Converter [32]

By comparing these two converters, it is evident that the non-inverting buck-boost converter has multiple possible typologies available to implement and higher efficiency with a larger input voltage range, whereas the SEPIC only has a couple of typologies to implement with lower efficiency and narrower supply voltage range. In the case of a portable solar charger, implementation of the buck-boost would be easier but the cost and controlling complexity are limiting factors. Although the SEPIC converter has lower efficiency, it requires less components. Nevertheless, the limitations of the non-inverting buck- boost are trade-offs for its higher efficiency and wider supply voltage range. We can further observe the differences in component selection for the calculations for determining the component values as seen in Appendix A. These equations define how these structural parameters characterize the behaviors of each typology.

2.4.5 Control and Feedback

After establishing the basic typologies of buck-boost and SEPIC converters, the control and feedback mechanisms of the DC-DC controller are explored to understand how the DC-DC converter is controlled by an MPPT algorithm and together acts as a system. In general, we consider the controller, power stage, and feedback loop as the major components of the system. Figure 24 illustrates the flow of this process. The controller manages the switching operation to regulate the output voltage. The power stage involves the switching elements converting the input voltage to the desired output voltage. The feedback loop connects the power stage and controller by comparing the actual output voltage to the desired output voltage and communicates the difference (error) to the controller. In this way, a feedback loop is necessary to provide information about the output for the controller to calculate appropriate adjustments that will drive the power stage. [28] By understanding this system flow, we can conceptualize how the input voltage is converted to a regulated output voltage in relation to the system elements.

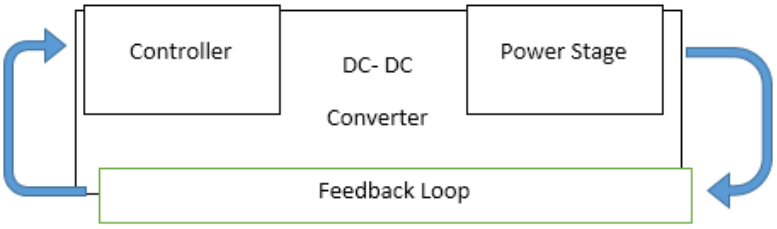

Figure 24. Control Operation of DC-DC converter in Three Steps: Controller, Power stage, Feedback loop

Controller: Microcontroller and Driver

The controller maintains the stability and precision of the input voltage supplied by the PV panel. In typical applications, controllers use Pulse Width Modulation (PWM) to regulate the power voltage. There are two components that define the controller: microcontroller and driver. These components and methods define how the controller operates and its efficiency of operation.

Operating a non-inverting DC-DC converter requires a PWM driver and a microcontroller to determine the value of the PWM. Either a half-bridge driver or full bridge driver can be employed depending if the converter circuit uses two MOSFETs or four MOSFETs for either non-synchronous or synchronous applications. These drivers provide the duty cycle by driving the PWM signal from the microcontroller to the N-Channel MOSFETs. The driver can employ a few methods to generate the PWM. The PWM

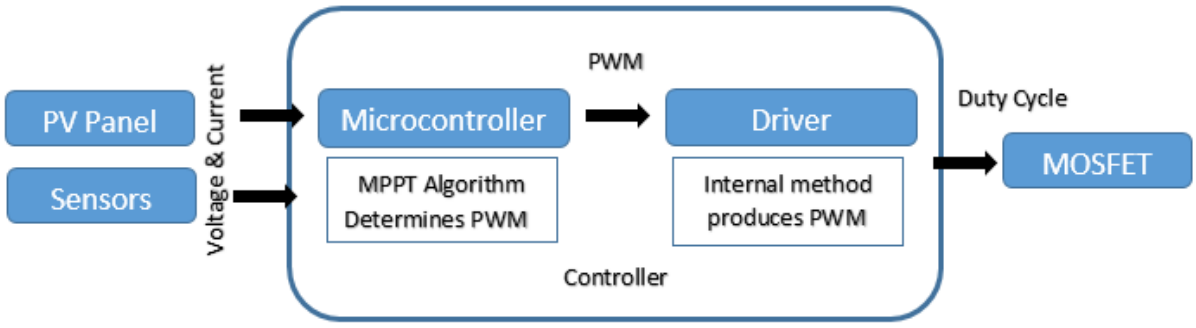

Figure 25. Operation of Controller: Microcontroller and Driver

successively turns the MOSFETs ON, OFF, and switches them at specific frequencies and duty cycles. It is important to distinguish that the microcontroller determines the duty cycles of the PWM outputs to indicate which operational buck-boost mode should handle the input voltage. The driver simply provides the microcontroller-specified PWM to the MOSFETs. In this way, the microcontroller is the bridge between the sensors and the circuit, since the microcontroller uses the MPPT algorithm with information from the input sensors to calculate the appropriate operational mode to meet the MPP demands of the PV panel. [26, 40] The controller defined for a non-inverting DC-DC converter is illustrated in Figure 25.

Driver Control Scheme

The driver circuit's purpose is to provide enough current to control the transistor and limit each MOSFET's drain-source voltage. The pulse of the PWM sent to the MOSFET gate controls how the MOSFET operates. [26, 40] There are two different conduction modes in which the driver can provide the appropriate duty cycle control:

- Continuous conduction mode (CCM): current in energy transfer never goes to zero between switching cycles
- Discontinuous conduction mode (DCM): current goes to zero between switching cycles

We have previously provided the buck-boost typology operation in CCM in Section 2.4.2 when we first presented the inductor charging and discharging cycle. Appendix E has detailed conditions which buck mode and boost mode enter DCM, as well as operational consequences of DCM. As seen in Table 2 in Section 2.4.2 and Appendix E, entering CCM or DCM is dependent on the current through the inductor. Due to this dependency, it is important to choose the converter's inductor based on the load variation and how much time the converter will spend in low-power mode. Although a larger inductor can be employed to reduce the peak-to-peak current, a larger inductor also requires more circuit surface area, is more expensive, and can reduce the converter's efficiency. [30]
There are two typically applied methods to generate PWM in either CCM or DCM: voltage-mode control and current-mode control. Both usually use a fixed frequency PWM, or constant switching, to limit

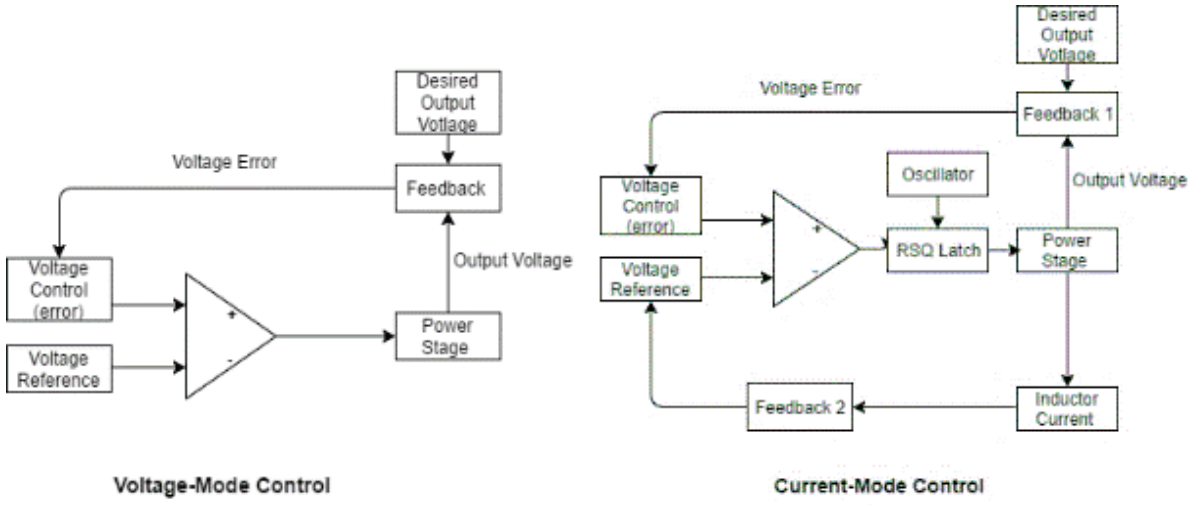

Figure 26. System Diagrams of Voltage-Mode (top) and Current-Mode Control (bottom)

electromagnetic interference from the power supply. Figure 26 illustrates the basic system diagram used for voltage-mode control and current-mode control.

Voltage-mode control was developed first, and it had operational limitations such as slow response to load variation and varying loop gain with input voltage. The current mode control was developed afterwards to address the voltage-mode limitations. However, current-mode control had its own limitations such as requiring two feedback loops and limiting duty cycles to 50% or less which restricts the input voltage range of the source. Table 9, briefly describes the how each method functions, their advantages and disadvantages. It is important to choose the appropriate method of control based on its application so that the control method operates most effectively for the application. Appendix C provides a detailed checklist to assess which control method to implement in a system based on the advantages and limitations previously described. From this checklist, current-mode control method is the most suitable for a portable solar charger application because it has a fast response time, handles dynamic regulation, and is compatible with high frequency switching.

Method	**Voltage-Mode Control**	**Current-Mode Control**
Functionality	• PWM generated by connecting a control voltage (V_c) to positive end of a comparator and a sawtooth voltage waveform (V_{ramp}) of fixed frequency • Duty cycle of PWM is proportional to V_c • V_c (or error voltage) is the difference between actual output and reference voltage	• PWM generated by adding a second feedback loop indicating inductor current • Feedback signal includes both AC ripple current and DC inductor current • Feedback signal is amplified and is connected to a comparator and compared to the error voltage
Advantages	• Single feedback loop design allows easier circuit analysis • Large amplitude waveform allows reasonable noise margin for stable modulation	• Decreases response time due to immediate response of line-or-load voltage changes • Eliminates loop-gain variation with input • Higher gain bandwidth than voltage-mode
Disadvantages	• Slower response time • Requires an output filter that is unable to handle loop gain variation	• Two feedback loops complicate circuit design and analysis • Limited duty cycle to <50% and limited input voltage range • Resonances from inductor can increase loop noise

Table 9. Descriptions, Advantages, and Disadvantages of Voltage-Mode and Current-Mode Control [30]

Feedback: Current and Voltage Sensors

For MPPT algorithms to acquire the current and voltage panel operational values, sensors are used to bridge information about current and voltage values between the PV panel, the load, and the microcontroller coded with the MPPT algorithm. Because the sensors provide input and output information, the sensors create the feedback loop for the system. The type of sensors chosen for the system directly affects the accuracy of the MPPT method's step size. For an accurate and efficient MPPT, it is ideal to have a fast update rate and a small increment step size.

A sensor's ability to provide information to the algorithm is driven by the PI loop which is essentially the microcontroller's error calculation between the set point and the measured value. The speed of the calculation depends on how long it takes for the sensor to measure the load voltage and the PV panel output voltage, and directly affects the MPPT update rate. The MPPT update rate determines the efficiency of reading a new panel operational value. The PI loop update rate has the most impact on the MPPT update rate because between MPPT updates, the PI loop needs to have enough steps to direct the panel output voltage towards the maximum power point voltage and to determine its difference between the set load voltage. Thus, sensors update rate must be faster than the MPPT update rate, typically around 25 times faster. For example if the MPPT update is running at 40Hz, then the PI loop needs to operate at 1 kHz. These frequencies also help determine which microcontroller has a fast enough processing power necessary to meet the needs of the PI loop, MPPT update, and the algorithm calculations. The other significant limiting factor to the MPPT update rate is the input capacitor. The input capacitor affects the accuracy of the algorithm in low irradiance conditions, for it will slow down the variations in the panel output voltage. [36]Along with these design limitations of the MPPT, the choice in typology of the DC-DC converter affects the system's power efficiency.

Power Stage: Dynamic Characteristic

In order to ensure efficient voltage regulation of the DC-DC converter, typically a stability analysis of the converter's duty cycle is conducted for each operational mode. For the scope of this project, we do not need to know exactly how the stability analysis is performed, but it is important to understand how the stability of a buck-boost converter's dynamic characteristics affects the control and operation of the converter, which affects the efficiency of voltage regulation. By using state-space averaging techniques, Reference 26 derived the dynamic characteristic equations of a non-inverting synchronous buck boost converter, and Reference 40 derived the transfer function form as seen in Equation 15, where D is the duty cycle, D' = 1-D, v_o is the desired output voltage, v_s is the supply voltage, R_C, is the capacitor's resistance, I_L is the current over the inductor, L is the inductor inductance, and C is the capacitor capacitance.

$$v_o(s) = \frac{\frac{(DD'R_C)}{L} * \left(s + \left(\frac{1}{R_C C}\right)\right)}{\left(s^2 + \frac{1}{RC}s + \frac{D^2}{LC}\right)} * v_s(s) - \frac{I_L R_C \left(s + \left(\frac{1}{R_C C}\right)\right)\left(s - \left(\frac{D'V_o}{DL\,I_L}\right)\right)}{\left(s^2 + \frac{1}{RC}s + \frac{D^2}{LC}\right)} * d(s) \qquad (15)$$

From Equation 15, we can observe that the system is characterized by the inductor and the capacitor. Since the system is dependent of the inductor and the capacitor, the stability margins of the system also depend on them and the load condition. Due to this dependence, by increasing the capacitance or

decreasing the inductance within the design limits, the stability margins can be improved. [26]The dependence on inductance and capacitance was previously discussed using circuit analysis in Section 4.2 and Section 4.3. When determining these values there are important factors that need to be considered for each component as outlined in Table 10.

Factors to Determine Inductor (L)	**Factors to Determine Capacitor (C)**
• Input Voltage range • Output Voltage • Maximum inductor current • Switching frequency	• Inductor current ripple • Switching frequency • Desired output voltage ripple

Table 10.Factors that Determine Inductor Inductance and Capacitor Capacitance [26]

The transfer function also reveals that the system has a zero in the Left Half Plane (LHP) and a Right Half Plane (RHP) zero due to the duty cycle, d(s). A detailed explanation of the significance of the RHP zero is found in Reference 6, but we will summarize the RHP zero's effects for a buck-boost converter. In buck-boost systems there is a right-half-plane (RHP) zero in CCM which is not present in DCM. The RHP zero causes the system to have two effects:

1. *Over compensates duty cycle*: The system temporarily uses a larger duty cycle than necessary which increases the inductor peak current with every switching cycle. The result is a higher average inductor current delivered to the load.
2. *Current delivered is below load requirement*: Due to the increase in duty cycle, the amount of conduction time for the passive switch (diode or MOSFET's diode) decreases. The passive switch current, which drives the output current, decreases with an increase of the duty cycle. The result is the output current being 180 degrees out of phase with d(s). In terms of the transfer function, the result is the RHP zero. [6]

These effect makes it more difficult to stabilize a converter with dynamic response to switch between buck mode, boost mode, and buck-boost mode as previously mentioned in Section 4.3. To fix phase margin, a compensator loop is usually employed. The compensator's function is to cross at frequency lower than the RHP zero frequency. The crossover frequency may be limited by at least a decade of the actual operational frequency restricting full dynamic response of the converter. A simple implementation is choosing one operational mode since the power stage frequency will maintain about the same. A more complex implementation is using all three operational modes because the power stage frequency will change significantly when switching between these modes [40].

Since the location of the transfer function's poles and zeros vary with the duty cycle, the converter requires compensation for the lowest frequency poles and zeros, or when the duty cycle is at its peak. Duty Cycle limiting using slow-start and dynamic reference control bypass circuit, and dead time control in the synchronous typology are two methods of frequency compensation. [37] Descriptions of the

compensation technique's implementation to prevent inherent frequency-caused problems is found in Table 11.

Compensation Technique	Problem	Implementation
Duty Cycle Limiting	• During startup and transients, the duty cycles varies between it extremes • can be seen if the reference voltage is higher than the feedback voltage • PWM comparator output would reach the negative rail during the entire switching period causing switching M1 and M3 to be ON and the output voltage will stay the same • Since inductor current can still increase, it can damage the power components	• Provides a supply voltage to the feedback control that is less than the peak value of the reference voltage, which limits the duty cycle to less than unity or less than its peak • slow-start circuit: when the supply is turned on, the reference voltage for the converter is the output voltage from a slow charging capacitor • Once the converter's reference voltage reaches the predetermined threshold, the controller initiates dc-dc converter operation.
Dead Time Control	• Shoot-through current occurs when both the rectifier switch and complementary passive switch are both conducting current simultaneously	• Synchronous rectification • Advanced designs of dead time can be employed to reduce body-diode conduction, gate-drive, and switching losses

Table 11. Descriptions of Compensation Techniques: Duty Cycle Limiting and Dead Time Control [37]

Power Stage: Synchronous Rectification Control

Efficiency of the power stage can be improved for low voltage applications by using MOSFETs instead of rectifying diodes. Using four MOSFETs instead of two MOSFETs and two rectifying diodes in a design is known as synchronous converter typology.

There is a time delay known as dead time between T_{ON} and T_{OFF} to prevent shoot-through current. During dead time, the inductor current passes through the diodes of the MOSFETS, M2 and M4. Figure 27 explains delay time operation through the duty cycles of each MOSFET (T1, T2, T3, T4) as the following:

- *Dead time*: short periods of time between switching that the MOSFETS are off
- d_1: time when T1 is ON, T2 is OFF
- $1- d_1$: time when T1 is OFF, T2 is ON

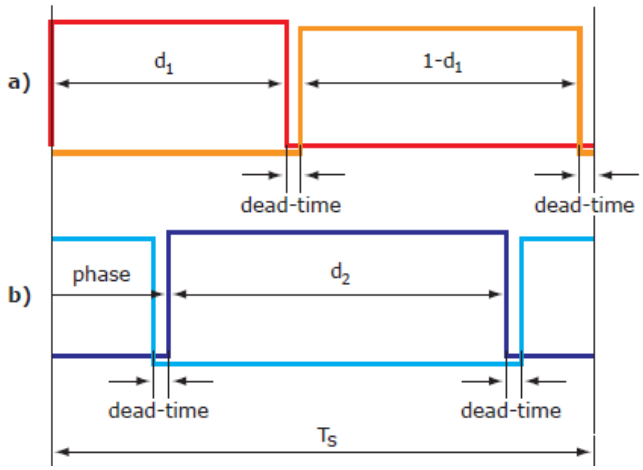

Figure 27. Gate signals sent to (a) buck leg ,T1 and T2 (b) boost leg, T3 and T4 [44]

The association of d_1 and $1- d_1$ with *T1* and *T2* is similar to that for d_2 and $1- d_2$ with *T3* and *T4*. The duty cycles d_1 and d_2 can also be shifted relative to each other by inserting a phase between them which determines the amount of energy transferred, and affects the behavior of the converter to adjust to the desired output voltage. [44] Having control of all four duty cycles increases the overall performance of the converter because it provides more accurate control of the different operational states that the converter can achieve.

We derived that the relationship of the duty cycle with T_{ON} and T_{OFF} in Equation 16 where *T* is the switching period of the cycle.

$$Duty\ cycle = \frac{T_{ON}}{(T_{ON}+T_{OFF})} = \frac{T_{ON}}{T} = \frac{D}{1-D} \qquad (16)$$

Because the duty cycle affects the switching of the MOSFETs, the duty cycle's value determines the operational mode, buck, boost, or buck boost, for a non-inverting synchronous buck-boost converter [37]:

- Duty Cycle = 0.5, $V_{OUT} = V_{IN}$
- Duty Cycle < 0.5, $V_{OUT} < V_{IN}$ (buck)
- Duty cycle > 0,5, $V_{OUT} < V_{IN}$ (boost).

From these relationships we observe that to adjust the output voltage in the power stage, the duty cycle must change. With more control over the duty cycle, the converter can utilize full dynamic response, and appropriately convert the power to the desired load.

2.5 Energy Storage

The final step for the solar charger to perform is “energy storage”. For the application of a portable solar charger, the solar charge controller must connect to a battery of a device so that the power collected from the PV panel can be stored and be used by the device. There are several steps that occur for the storage (charging) process. To store energy in a portable Li-ion battery pack, the charge flow is determined by a USB bus and the state of charge must be appropriately determined by through Li-ion charge controller. Output voltage regulation is important in battery charging since the batteries require a specific charging method with various voltage and current level for each specific stage. The charging methods determine the battery life and the battery performance. The charge controller performs the voltage and current adaptations to allow long battery life.

2.5.1 Lithium-ion Battery Charging

A Li-ion battery is charged from a current-limited fixed voltage source, also referred to as constant voltage charging. A constant voltage (C-V) charging is described in the following two steps:

- C-V charger provides current to the battery as to force the battery’s voltage to a predetermined value (set-point voltage)

- After the set-point voltage is reached, charger provides only enough current to maintain the value of the set-point voltage constant [41]

Currently, Li-ion specifications recommends about 4.2 V set point voltage, and 1 A-hr (1c) maximum charging current rate. Coulomb counting estimates the state of charge (SoC) by measuring the in-and-out flowing current by one coulomb per second (1C/s = 1 Amp) or in one hour discharging at 1A will be 3,600 C. This works well with Li-Ion batteries that offer high coulombic efficiency and low self-discharge. [3] The accuracy of the set-point voltage directly affects the battery life, i.e., if the voltage is too high, the battery life shortens, and if the voltage is too low, the cell will never fully charge. The typical charge profile for a Li-ion under recommended operating specifications is shown in Figure 28.

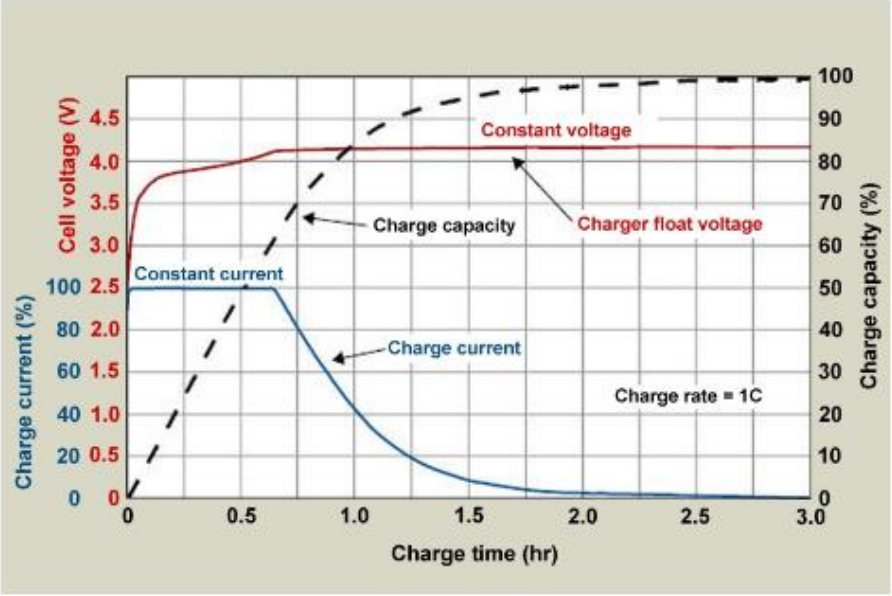

Figure 28.Typical C-V Charge Profile using 1c Constant Voltage Charging [2]

From Figure 28, we can observe how the constant charging cycle is divided into two phases: current limit phase and the constant voltage phase. Table 12 describes both phases in relation to the charging state of the battery.

Current Limit Phase	Constant Voltage Phase
• Maximum charging current flows into the battery • Battery voltage below set point • Charger tries to force battery voltage up • About 65% of total charge delivered • Assuming 1c charging current, maximum charge time is 40 minutes	• Begins once charger senses that set-point is reached (4.2V) • Charger reduces charging current to maintain constant voltage, resulting in exponential decay waveform • Decrease in current causes charge time during constant voltage phase is about two hours • About 35% of total charge delivered

Table 12.Descriptions of Current Limit Phase and Constant Voltage Phase of Charging Cycle [41]

By comparing the two phases from Table 12, the constant voltage phase, although only 35% the charging cycle, takes twice as long to charge the battery then when in the current limit phase which is 65% of the charging cycle. The limited constant voltage phase occurs because every Li-ion cell has an internal ESR (Equivalent Series Resistance), and voltage sensed by the charger is the sum of voltage drop across the ESR and the cell voltage. During the voltage limit phase, the internal ESR is negligible since there is barely any current flowing through it, and the cell-voltage is 4.2V. During current limit phase, the ESR is not negligible, so the battery reaches 4.2V over 65% of the charge capacity delivered. [41]

2.5.2 Lithium-ion Battery Charger

One of the most common ways to connect to electronic portable devices is through a Universal Serial Bus (USB). Each USB connection contains a power bus with a maximum power rating of 5.25V/500mA, which is optimal for charging a single-cell Li-Ion battery. Figure 30 illustrates the steps of charging a Li-Ion battery using USB power bus for an electronic portable device receiving the power. [13]
From the block diagram, the voltage bus provides the necessary power voltage to the power switch. The

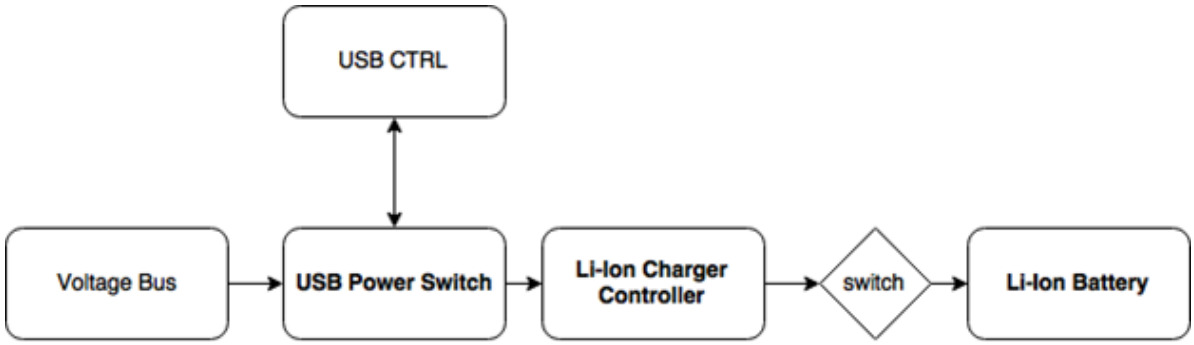

Figure 30. Block Diagram of USB-powered Li-ion Battery Charger

power switch isolates the battery charging circuit from the bus during start-up as to prevent overloading the bus with charge current. The USB control indicates when the USB power switch can connect the power from the voltage bus to the charge circuit. The power is then sent to the Li-ion Charger Controller which controls a switch based on the state-of charge of the battery, and the switch that allows the current to flow into the Li-ion battery.

There are some restrictions of using the USB power bus as a charging device as stated in its specifications. Some of these limitations include:

- Only 500mA at a maximum can be drawn from the bus during normal operation for a high-power function. Typically, only 400mA is drawn from the bus by implementing a current-limit resistor, and the remaining 100 mA allows other functions, such as USB control to operate.

- During device start-up or when the device initially connects to the USB bus, the device cannot draw more than 100mA until USB system is configured.[13]

In addition, the charging time is restricted by the USB specification of input voltage to the battery charger controller. The input voltage specification takes into account that the USB cable and connectors resistive drops equate to about 350 mV. The system with a USB supply voltage closer to the minimum requirement will charge the battery slowly, or can prevent a full battery charge. Thus, to charge the battery within an optimal charge time, the maximum charge current should be sent to the battery until it achieves full-charge voltage. For example, the optimal charge time for a 4.2V battery occurs if the input voltage to the charge circuit is at or above 4.7V. If the input voltage to the USB is at 4.6V, the available charge current will be reduced by 50% which results in slower charging time. At 4.5V input

voltage, the battery will not reach a full 4.2V charge. [13] To prevent the slow charging event and the under-charging event, the voltage at the input to the charging circuit must be high enough. Thus, in order to have optimal charge time for a portable device, the solar charge controller circuit must provide the USB with a constant supply voltage high enough to charge the battery consistently.

2.6 Summary

In the background section, we have explored the fundamental processes of a solar charger: energy collection, energy conversion optimization, energy implementation, energy storage. By considering each major process, we have described the essential components or procedures that occur within each solar charger process and how these components must operate together to achieve charging a Li-ion battery. The characteristics of each process affects the whole energy conversion process. By understanding how the processes relate to each other, we can understand how to design an efficient solar charger. Table 13 displays the key concepts of each process discussed and the importance of each with respect to our project.

Energy Processes	**Key Concepts**	**Why it's important**
Collection	• PV cells are similar to PN junction of photodiode. • PV output current depends on solar cell irradiance and temperature.	• Because PV cells absorb photons (energy and convert energy to current like a photodiode, we can model a PV panel to observe output current or voltage. • Power conversion efficiency of panel depends on temperature and irradiance. The dynamic conditions determine the supply voltage range of panel.
Conversion Optimization	• MPPT detects and determines the maximum voltage and current that can be provided by PV panel under dynamic conditions. • V-I characteristic of PV panel shows where MPP is located. • MPPT calculates the MPP depending on both load input and PV panel output. • P&O and INC are two examples of MPPT algorithms that are typically implemented.	• MPPT allows solar charger to extract as much available power from PV panel from a wide supply voltage range and utilize it to charge the load. • We need to understand how the PV panel operates in terms of voltage and current in order to create an MPPT method. • To determine the MPP, sensors are required to monitor both PV supply and the power delivered to load. • We found that INC is more efficient over a larger range of input voltage under dynamic conditions.

Implementation	• The fundamental principle of operation for a voltage regulation is based on the PWM-controlled high frequency switching of the MOSFETs and the voltage it passes to the inductor. • By comparing SEPIC and non-inverting buck-boost typologies, it is evident that the non-inverting buck-boost has higher efficiency with a larger input voltage range, whereas the SEPIC has lower efficiency and narrower supply voltage range. • With more control over the duty cycle, the converter can utilize full dynamic response, and appropriately convert the power to the desired load.	• By controlling the duty cycle of the inductor charging cycle and discharging cycle, the circuit can operate in different modes: buck mode, boost mode, and buck-boost mode. • The limitations of the non-inverting buck- boost is a trade-off for its higher efficiency and wider supply voltage range. • A non-inverting synchronous buck-boost converter is able to provide an efficiently regulated voltage under dynamic conditions due to its control complexity.
Storage	• Charge time for a portable device is dependent on the constant supply voltage high enough to charge the battery consistently. • To charge the battery within an optimal charge time, the maximum charge current should be sent to the battery until it achieves full-charge voltage.	• . Output voltage regulation is important in battery charging since the batteries require a specific voltage and current level for each charging stage. • The charging methods determine the battery life and the battery performance.

Table 13. Main Energy Processes within a Solar Charger

3. Problem Statement

3.1 Introduction

After studying and exploring the fundamental system dynamics and processes of a solar charge controller, we found many design improvements that can be made to current on the market portable solar charge controllers. In this section, we present our problem statement in detail based on our findings from our previous section. We also provide our objectives and requirements of our project.

3.2 Project Statement, Goals, and Objectives

The typical portable solar charger is inefficient and underutilizes the power output of the solar panel under varying temperature and irradiance because the voltage regulator used can only handle voltages above the battery load requirement, and the regulator is connected to a simple controller that drives the regulator only within the converter's designated range. The result of using a simple buck solar charge controller are potentially premature battery failure and wasted potential solar power due to inconsistent charging and limitations of the converter's design.

Project Goal

Our project was to research, simulate, design, and prototype a solar charge controller that regulates power small PV panels (5-15W) using Maximum Power Point Tracking (MPPT) with a wide range input voltage DC-DC converter under dynamic panel conditions to charge Li-Ion battery connected portable devices.

Objectives

To accomplish our goals, we developed the following objectives:

- Test the power capabilities of a portable PV panel
- Evaluate different non-isolated switched mode power supply typologies and several MPPT algorithms based on handling dynamic and wide range supply voltages
- Simulate and study the power conversion efficiencies of different converter typologies using Multisim
- Design, build, and test an MPPT solar charge controller application circuit similar to our design and compare the power efficiency measured to the simulated power efficiency

3 Requirements

The following requirements of the solar charge controller are based on the foundation of our research conducted for energy collection, energy conversion optimization, energy conversion implementation, and energy storage. Each of these major stages are associated with the main components that create the solar charge controller.

With regard to these fundamental processes, the charge controller should provide power conversion under dynamic irradiance and temperature while achieving the following requirements:

- Power conversion efficiency >95%
- Wide Input voltage range of 2V to 23V
- Output voltage of 5V± 0.25V (USB)
- Minimum output current of 500mA

Specific requirements associated with each energy stage of the solar charge controller are displayed in Table 14.

Energy Process	Design Requirements	Justification
Collection	• PV Panel should be rated as 5W – 15W • PV panel should produce about 1W under indoor testing conditions.	• PV panel size needs to be small enough to be transportable. • PV panel power needs to be testable under artificial lighting.
Conversion Optimization	• MPPT algorithm needs to calculate MPP with at least 90% efficiency under dynamic conditions.	• The supply voltage and current will vary due to changing irradiance and temperature conditions on the panel.
Conversion Implementation	• DC-DC converter should handle an input voltage range of about 2V to 23V. • Power conversion efficiency of converter should be at least 90%. • DC-DC converter should provide a consistent output voltage of 4.75V to 5.25V, and minimum output current of 500mA	• Due to dynamic panel conditions, the input voltage will vary. To efficiently use the available power voltage, the converter should respond to a wide input voltage range. • Typical solar charge controllers using MPPT have at least 90% power conversion efficiency. • The load of the converter should provide a charge for typical portable device battery requirements.
Storage	• 5V USB connected to Li-ion battery.	• Portable devices use Li-ion batteries as a power source that are charged over a 5V USB cable connection.

Table 14. Requirements and Justification for Each Energy Stage of the Solar Charge Controller Operation

Additional requirements of the solar charge controller are listed as:

- Size of solar charge controller system should be compact and portable.
- Total cost of the solar charge controller should be affordable: between $10 to $15

By following these system requirements, a portable solar charge controller that handles dynamic conditions can be designed.

4 Summary

From our project statement, we established the guidelines to design a solar charge controller as summarized in Figure 31.

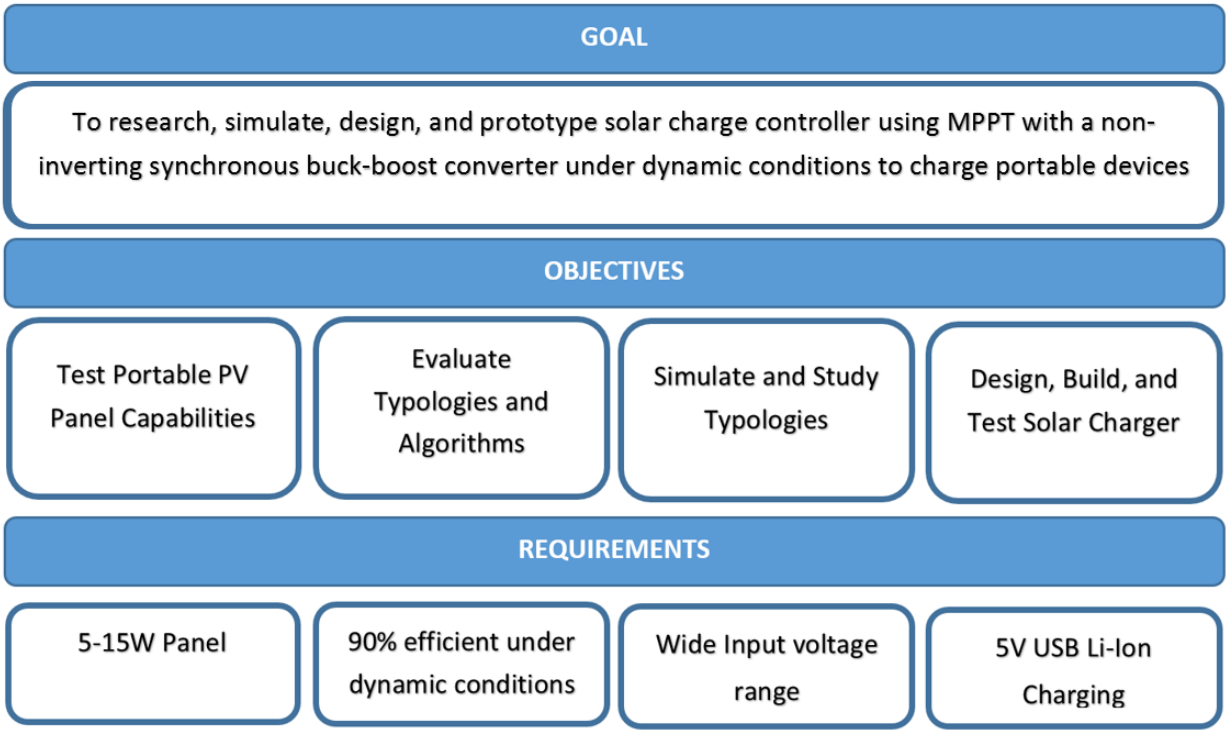

Figure 31. Project Statement Summary: Goals, Objectives, Requirements

From Figure 31, achieving our project goals depends on our system requirements. These system requirements are examined in the following section.

4. System Design

4.1 Introduction

Based on our design goals and requirements, and our background research, we developed a generalized system diagram of the solar charge controller as illustrated in Figure 32.

By understanding a general system operation of the solar charge controller, we applied our design parameters to our research and concluded that using Incremental Conductance as an MPPT algorithm with a non-inverting synchronous buck-boost converter was the most power efficient under dynamic conditions for portable application. However, for the scope of our project, we took the significant parameters of the proposed design, created a checklist, and researched an IC (integrated circuit) that was most similar to our proposed design criteria. In this section, we discuss why and how we determined our design choices for our actualized system implementation as illustrated in Figure 33.

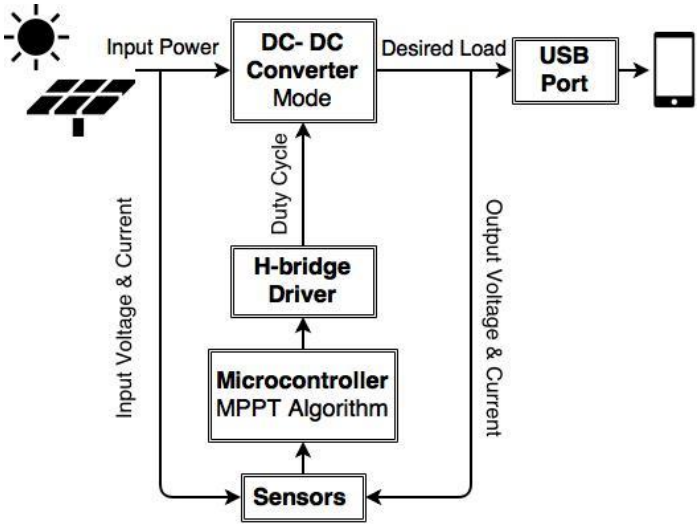

Figure 32. Proposed MPPT Charge Controller System Design

4.2 MPPT Integrated Circuit

To test the effects of an MPPT algorithm and dynamically driven DC-DC converter on power efficiency, we decided to employ an IC that had features such as MPPT algorithm, synchronous four-switch buck-boost converter compatibility, and Li-ion battery charging capability. Also, we chose an IC that met the most of our system requirements. Our decision making process to choose our implementation is seen in Appendix F.

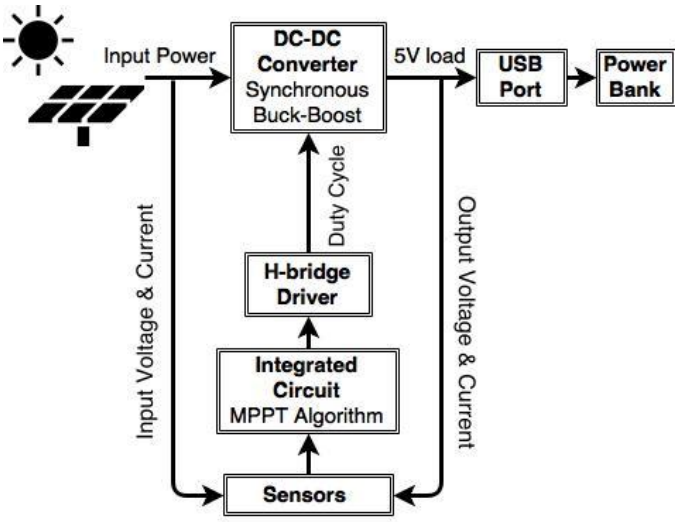

Figure 33. Actualized MPPT Charge Controller System Design

The IC that we chose was the SM72445 from Texas Instruments. In this section we only discuss the IC implementation in terms of system design. Technical details of the system design can be found in Section 6. Implementation. In order to understand how our implementation functions, it is important to discuss the differences between our ideal system design and our IC implementation in terms of our system requirements. Before we explore the differences, we first establish the key components and specifications of the ideal system design.

Ideal System Design

The key aspects of the ideal system design can be seen as two major parts: the infrastructure and the operational efficiency. By considering the design in two parts, we assessed the infrastructure as separate components and how they operate together as described in Table 15, and we evaluated which components had significant impact on system power loss and efficiency as described in Table 16.

Component	PV Panel	Sensors	Microcontroller	H-Bridge Driver	DC-DC Converter	USB Port
Operation Requirement	Power Source	Monitor system current and voltage	Perform MPPT calculations and general correct duty cycle to driver	Controls buck-boost charge and discharge current to DC-DC converter	Regulates and transforms supply to constant load	Delivers power to external battery

Table 15. System Design Described in Terms of Components and Requirement for System Operation

From our research, we found that the MPPT algorithm, the PWM driver, and the DC-DC converter impacted the system's efficiency and power loss the most. More explicitly as described in Table 16, the impact of these components by how they operate or by their internal parameters directly affects the overall system power conversion efficiency and power losses.

Component	**Effect on Efficiency or Power Loss**
MPPT Algorithm	• Increase power converted by calculating the voltage at which the PV panel can produce the MPP • By determining the duty cycle, adjusts voltage to current ratios of converter to deliver higher rated charge to load
PWM Driver	• Efficient control depends on driver method and complexity of operation • Power loss occurs when not driving converter in appropriate operation mode
DC-DC Converter	• Typology determines operational modes • Operation determines power conversion efficiency • Values of inductor and capacitor determine power loss • Power components contribute to power loss

Table 16. Components and How Their Operation Affects Efficiency and Power Loss

From Table 16, we observe the dependency of each of the three components and how each component affects the next in terms of efficiency and operation. The MPPT algorithm can increase power conversion efficiency by calculating the adjustment values of the voltage to current ratios for the converter. The driver then uses the duty cycle value to produce the associated PWM. When the driver delivers the PWM to the converter, the driver controls the operational mode of the DC-DC converter. The driver and the DC-DC converter should be chosen based on the types of operational modes are required of the DC-DC converter and the type of control required for those modes.

The components' effects on efficiency and power loss define the requirements of the ideal components. In addition, the system requirements for these components should also be compatible for portable application. Portability implies that the system can handle dynamic conditions such as temperature and irradiance, and should charge a battery load. Based on our research and the system requirements, we found that the Incremental conductance algorithm, the current- mode controlled full-bridge driver, and

the synchronous non-inverting four-switch buck-boost converter are the ideal key components of the system. Each of these components increase the system efficiency and decrease power loss as required. Table 17 contains brief description of each component and how their characteristics fulfill the component requirement for increased efficiency, reduced power loss, and portability.

Component	Operation Effect on System
Incremental Conductance Algorithm	• Efficiently calculates and accurately determines MPP under dynamic conditions and with wide range of supply voltage
Current-Mode Controlled Full-Bridge Driver	• Stable feedback loop with current sensing • Fast transient response to dynamic change in power supply • Compatible for synchronous application and could reduce switching losses
Synchronous Non-inverting Buck-Boost Converter	• Using all MOSFETs for switches eliminates diode conduction losses and diode inefficiencies, and maintains low power dissipation • All three operational modes available: buck, boost, buck-boost

Table 17. Ideal Components and Their Impact on the System

Having defined the key components of our ideal solar charge controller in Table 17, we describe the similarities and differences in our realized application compared to the ideal system design.

Final System Design

Using the ideal key components and the system requirements as a checklist, we evaluated that we should employ the SM72445 IC; however, the IC design only meets some of the system requirements. We compare the ideal system design and the final system design in terms of infrastructure and key components as done previously. Figure 34 highlights the changes in the system design infrastructure when including our IC implementation.

From Figure 34, we observe that the major differences include the following:

- Microcontroller interfaces with IC for I2C applications only such as battery charging and reading sensor values
- IC implements the MPPT algorithm, not the microcontroller
- Sensors feed into the IC instead of I2C
- IC provides PWM, not the microcontroller

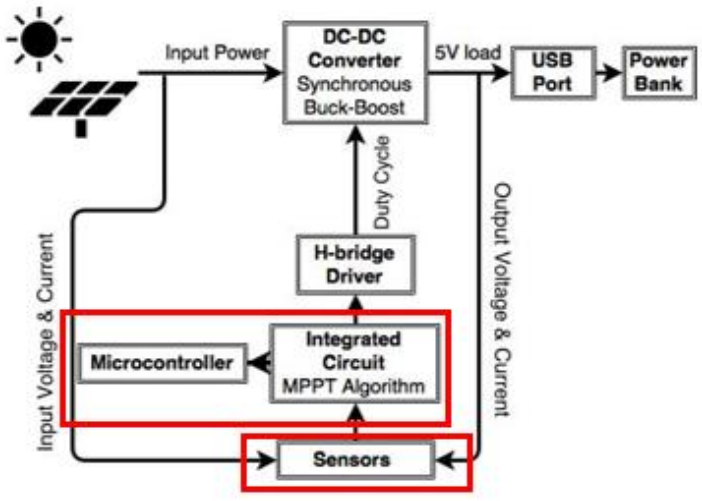

Figure 34.Final MPPT Charge Controller System Design: Differences Highlighted

These differences display how the IC is the major operator as a solar charge controller by reading in sensor values to control the MPPT algorithm, generating the correct duty cycle value to the driver, and communicating with an external microcontroller to monitor battery charge states.

Comparing the ideal key components to the implementation, the IC agrees with two of the three requirements. The IC is compatible to operate a synchronous non-inverting four-switch buck-boost converter by using a full bridge driver with current-mode control. However, the MPPT algorithm used by the IC is Perturb and Observe, which is less efficient than INC but still more efficient than most algorithms as asserted in Section 2.3.2 MPPT Control Algorithms. We determined that a different algorithm was our trade-off to have the synchronous non-inverting four-switching buck boost converter, because P&O is still over 90% efficient for the mid-range of input voltages. Additionally, the IC is compatible with the following system design requirements: Li-ion battery charging, switching frequency at least 100 kHz, power conversion efficiency of at least 90%, and wide input voltage range (about 5V to 60V).

4.3 Summary

The ideal system design and the implemented system design were outlined and compared in terms of infrastructure and key components. We found an IC compatible with most of the system requirements and the ideal system design. One of our trade-offs was the MPPT algorithm being Perturb and Observe rather than Incremental Conductance. The ideal system and IC implemented system comparison is summarized in Table 18.

System Component/ Requirement	Ideal	Actual
Controller	Microcontroller (Arduino)	Integrated Circuit
MPPT Algorithm	Incremental Conductance	Perturb and Observe
Driver and Control Mechanism	Current-Mode Controller Full Bridge Driver	Current-Mode Controller Full Bridge Driver
DC-DC Converter	Synchronous Non-inverting Buck-boost	Synchronous Non-inverting Buck-boost
Sensing	Current and Voltage	Current and Voltage
Load	Li-ion Battery	Li-ion Battery or Lead Acid
Switching Frequency	100 kHz	100 kHz
Handle Dynamic Conditions	Yes	Yes
Wide Input range	About 2V-23V	About 5V- 60V
Expected Power Conversion Efficiency	90%	90%

Table 18. Summary of Ideal System Design and Implemented System Design Comparison

With the specified requirements of both the ideal system design and actual system design, it was possible to explore and observe how we might expect our system to work using simulation. Through simulating our system designs, we could study the potential efficiencies and power losses expected of our design, and verify if our system design will meet the system requirements.

5. Simulation

5.1 Introduction

To simulate the DC-DC converter circuit topologies, models of Buck, Boost, cascaded Boost-Buck, and Full-Bridge Synchronous Buck-Boost converters were created in NI Multisim 13.0. Simulations of each topology were performed for the following purposes:

- Confirm theoretical behavior of the selected topologies
- Assist in component value selection for a DC-DC converter application circuit
- Identify sources of converter inefficiency

The construction, testing, and results of the four simulations are discussed in this section.

5.2 Buck Converter Simulation

The simulated buck DC-DC converter model was constructed in Multisim as shown in Figure 35. The converter used an inductor of 120µH, an input capacitor of 0.1µF, and an output capacitor of 15uF. Each component was connected in series with a 0.1Ω resistor to simulate an equivalent series resistance. The component values for the buck converter were based off of the calculations provided in Reference 21. The diode model chosen was the 1N5821G Schottky Diode with a forward bias voltage of 0.34V at 1A.

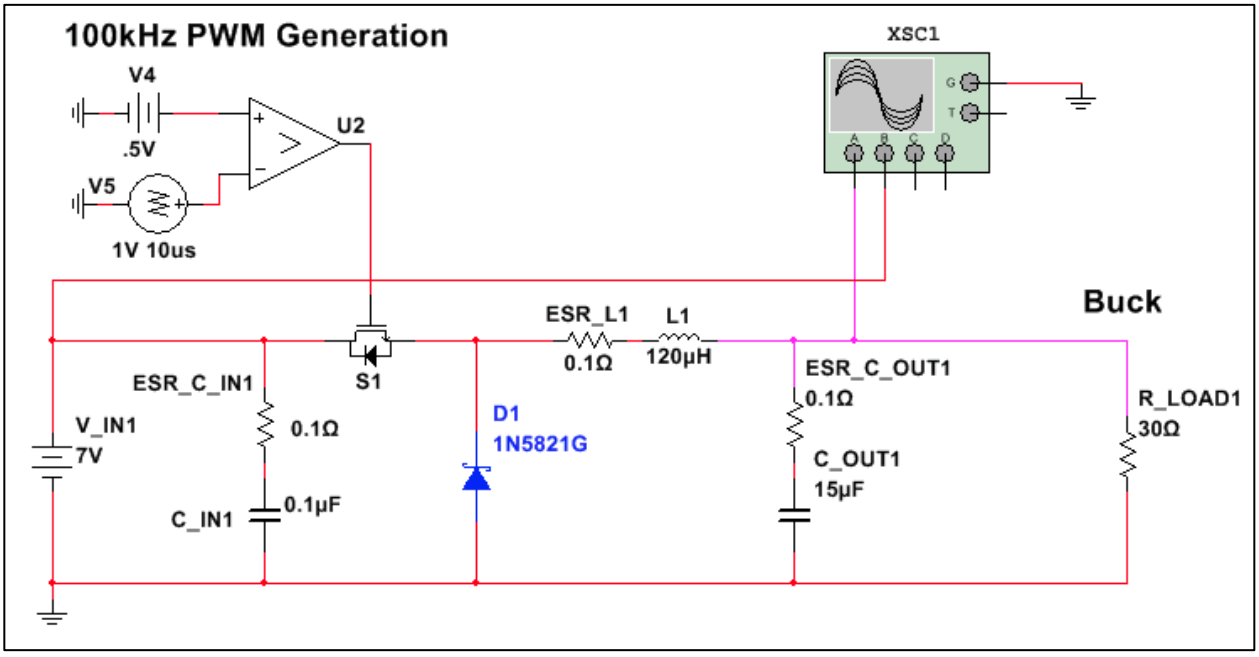

Figure 35. Multisim Buck Converter Model

To drive the converter, a 100kHz PWM signal, D1, was generated using a comparator and a sawtooth wave generator with a peak amplitude of 1V and a period of 10µs. By setting the comparator reference voltage (V4 in Figure 35) between 0V and 1V, the duty cycle of the PWM waveform was directly controllable between 0 and 1. The PWM waveform output connected to the gate of an n-channel enhancement mode MOSFET, with body diode, S1. The Multisim four-channel oscilloscope tool was used to observe the input and output voltages of the converter.

Testing & Results

The converter was tested at duty cycle values of D1 that were between 0 and 1. For each test the duty cycle was incremented by 0.1, and the input and output voltage levels were measured after a runtime of 5ms. The 5ms simulation runtime, before measurement, allowed for any transients in the converter to settle before the measurement was taken. A constant DC input voltage of 7V served as the input of the converter to test the gain of the circuit using a constant source. Figure 36 shows the converter input and output voltages at D1 = 0.5.

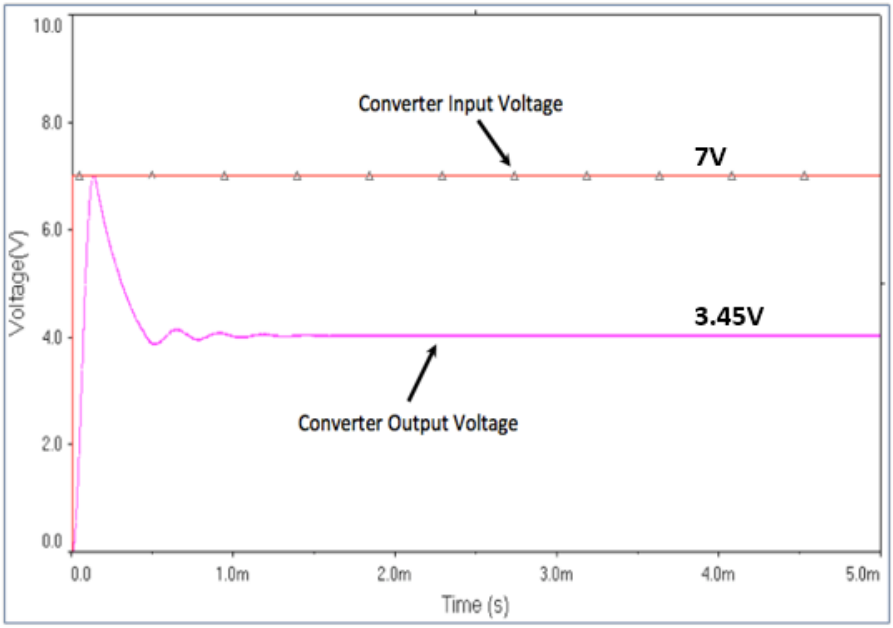

Figure 36. Buck Converter Voltage, D1 = 0.5

At D1 = 0.5, the converter produced an output voltage of 3.45V from a DC 7V input; a gain ratio of approximately 0.493. For a buck converter, the output was expected to be equal to the input voltage multiplied by the duty cycle (see Table 3, Section 2.4.2). In this case, the measured output voltage of 3.45V was close to the expected value of 3.5V, and the gain ratio of 0.493 had an error of 1.4% from the expected ratio of 0.5. For D1 = 0.5, the output also had an initial transient that rose to 7V but settled within 1.5ms to a steady-state value of 3.45V. Figure 37 shows the complete range of output voltages produced from values of D1 between 0 and 1.

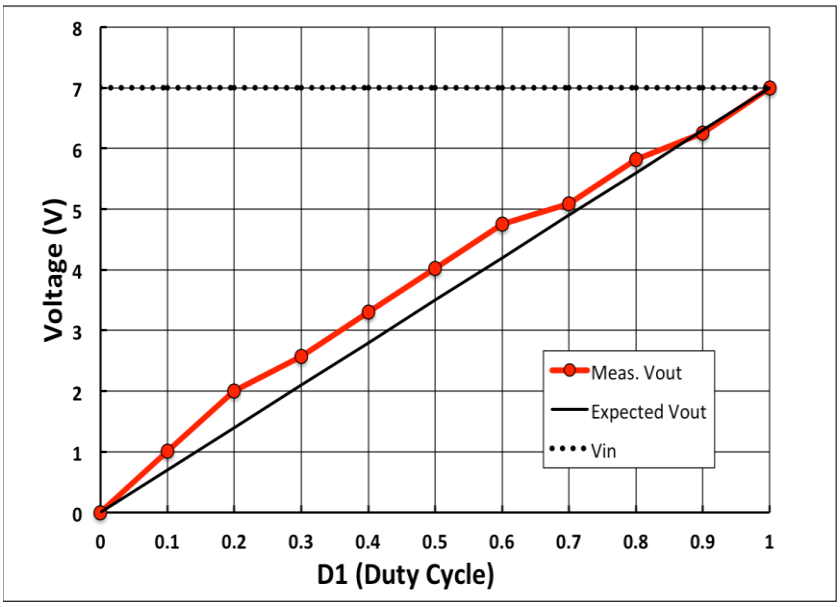

Figure 37. Buck Converter Output Testing

The buck converter behaved closely to the theoretical operation of a buck converter, however, the simulated converter produced a slightly higher than expected voltage for all duty cycles except for D1 = 0.9.

5.3 Boost Converter Simulation

The Multisim boost converter simulation consisted of the same component values as the buck converter simulation (L = 120 µH, C_IN = 0.1µF, C_OUT = 15µF) but with a different layout of components. The inductor in the boost converter was placed in series between the input and the Schottky diode. Instead of being connected to the input directly, such as in the buck converter, the switching MOSFET, S2, connected from the inductor output to GND. The MOSFET S2 was driven by a 100kHz PWM signal similarly to the buck converter. The boost simulation circuit is shown in Figure 38.

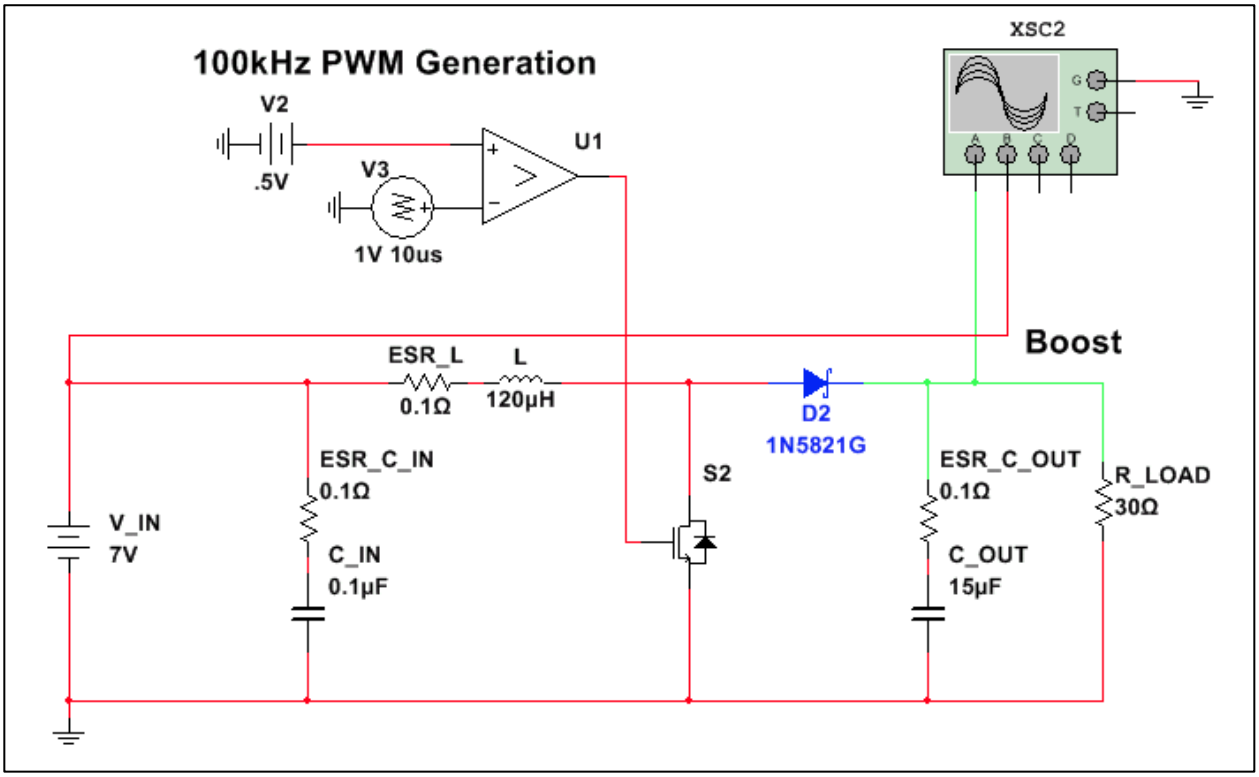

Figure 38. Multisim Boost Converter Model

Testing & Results

The boost converter was tested at duty cycles between 0 and 1 in increments of 0.1. Like the buck converter, the boost converter was measured after 5ms of runtime to allow for transients in the output voltage to settle to a steady-state value. Figure 39 captures the output and input voltages of the simulated boost converter at a duty cycle D1 = 0.5. For D1 = 0.5, the converter produced an output voltage of 13.525V from a 7V input; a ratio of 1.93. For the boost converter, the theoretical value of the output voltage is equal to the input voltage multiplied by 1/1-D1 (see Table 3, Section 2.4.2). The measured gain ratio of 1.93 had an error of 3.39% from the expected gain of 2.

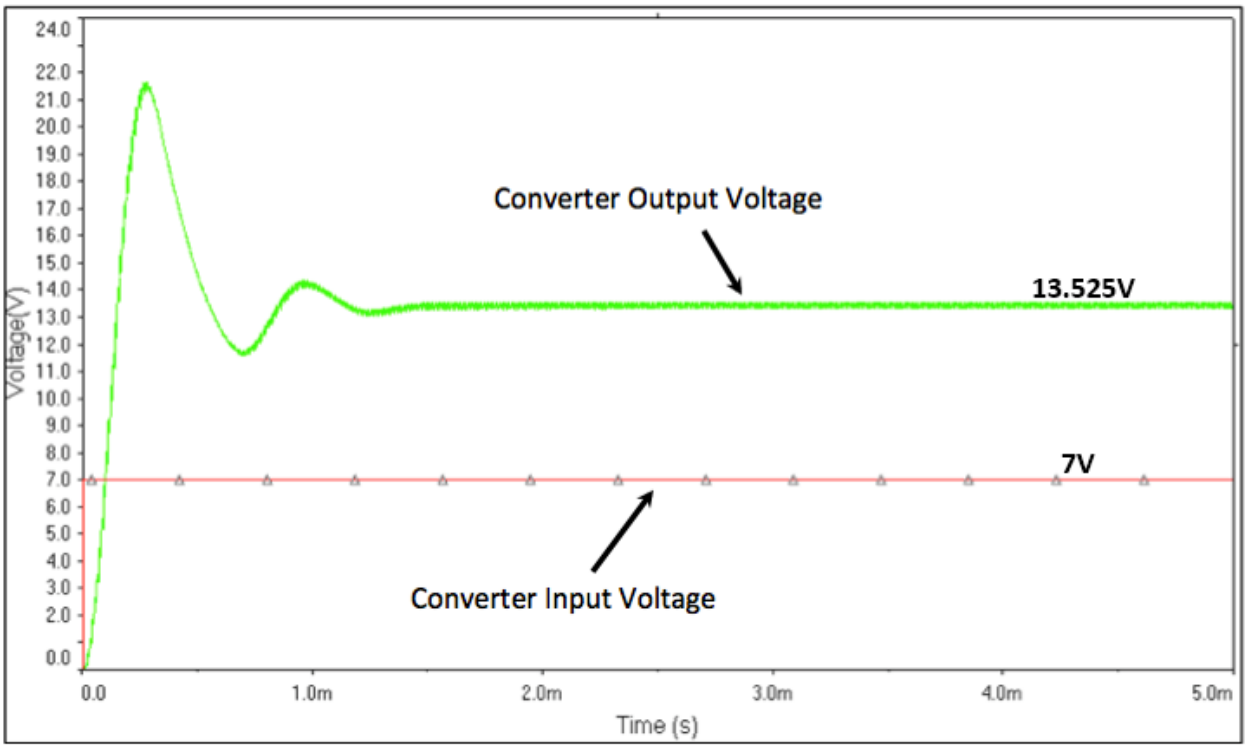

Figure 39. Multisim Boost Converter Voltage, D1 = 0.5

In Figure 40, the results of the converter output for a range of D1 values from 0 to 1 are shown, and the input voltage starts at 7V.

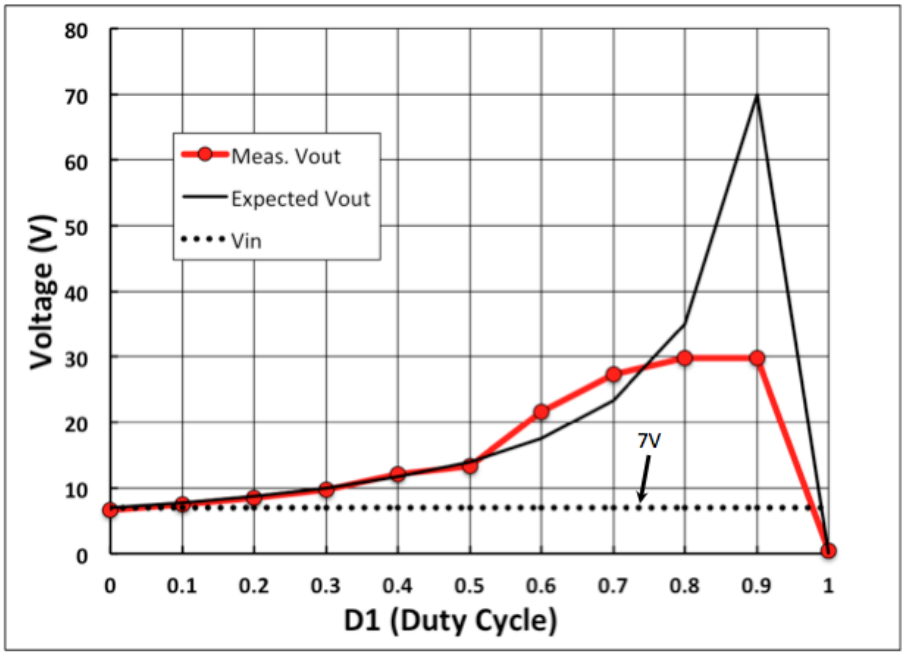

Figure 40. Multisim Boost Converter Output Testing

The boost converter performed close to the expected behavior with the exception of duty cycle D1 = 0.9. At D1 = 0.9, the converter hit a maximum output voltage of 30.945V. The resulting gain of 4.42 had an error of approximately 55.8% compared to the expected gain of 10.

5.4 Boost-then-Buck Converter Simulation

From the boost and buck circuit topologies, a cascaded boost-buck converter simulation was constructed as seen in Figure 41. The boost-buck converter consisted of a two switch (two MOSFET) topology with S2 controlling the boost leg of the circuit and S1 controlling the buck leg of the circuit. Like in the buck and boost simulations, equivalent series resistances of 0.1Ω were added in series with each inductor and capacitor. The first input capacitor, C_IN1, was set to 0.1µF to filter transients in the input voltage. The second input capacitor, C_IN2, was set to 10µF and acted as the output capacitor for the boost leg of the circuit. The output capacitor, C_OUT, was again set to 15µF. Both the boost and buck leg inductors were selected to have values of 120µH.

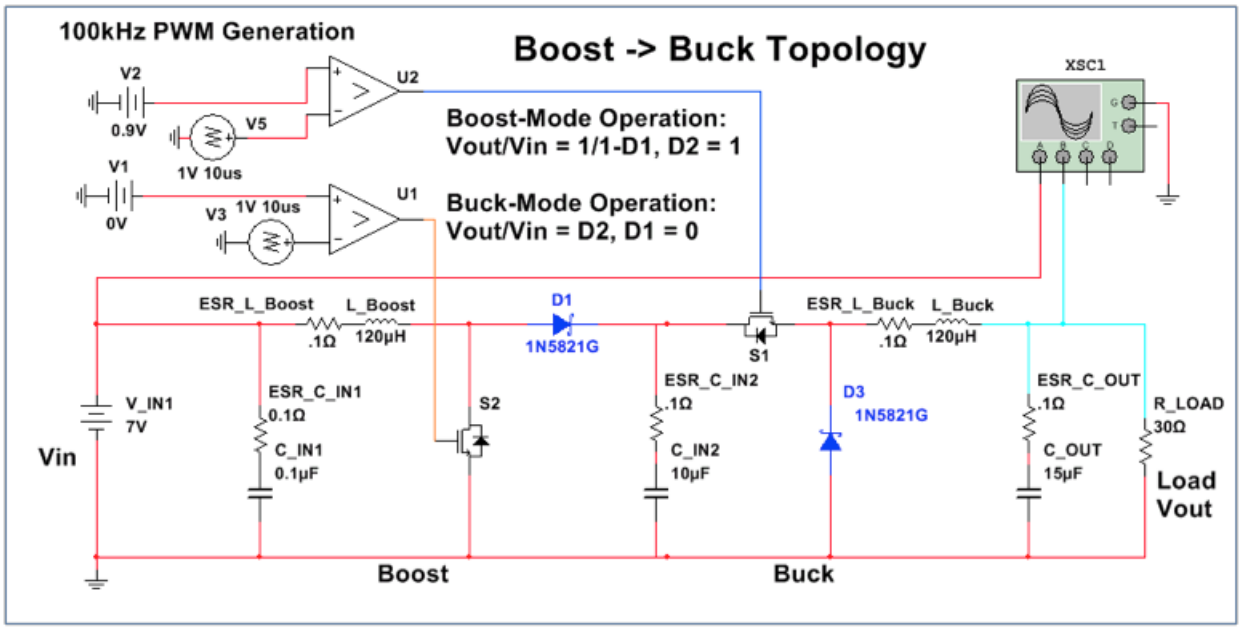

Figure 41. Multisim Boost-Buck Converter Model

To control the operation of the boost-buck converter, two independent PWM generation circuits were constructed using comparators and sawtooth wave generators. Reference voltages V1 and V2 controlled the duty cycles D1 and D2 respectively. A constant 7V DC source acted as the input to the converter.

Testing & Results

To test the functionality of the converter, the simulated circuit was tested in both the buck and boost modes. In buck mode, D1 was set to 0 to keep the switching MOSFET, S2, from conducting to GND. In this way, the input voltage was unaffected by the boost leg and only the buck leg of the circuit was activated. Figure 42 shows the converter input and output voltages while the converter is in buck mode with a D2 = 0.5.

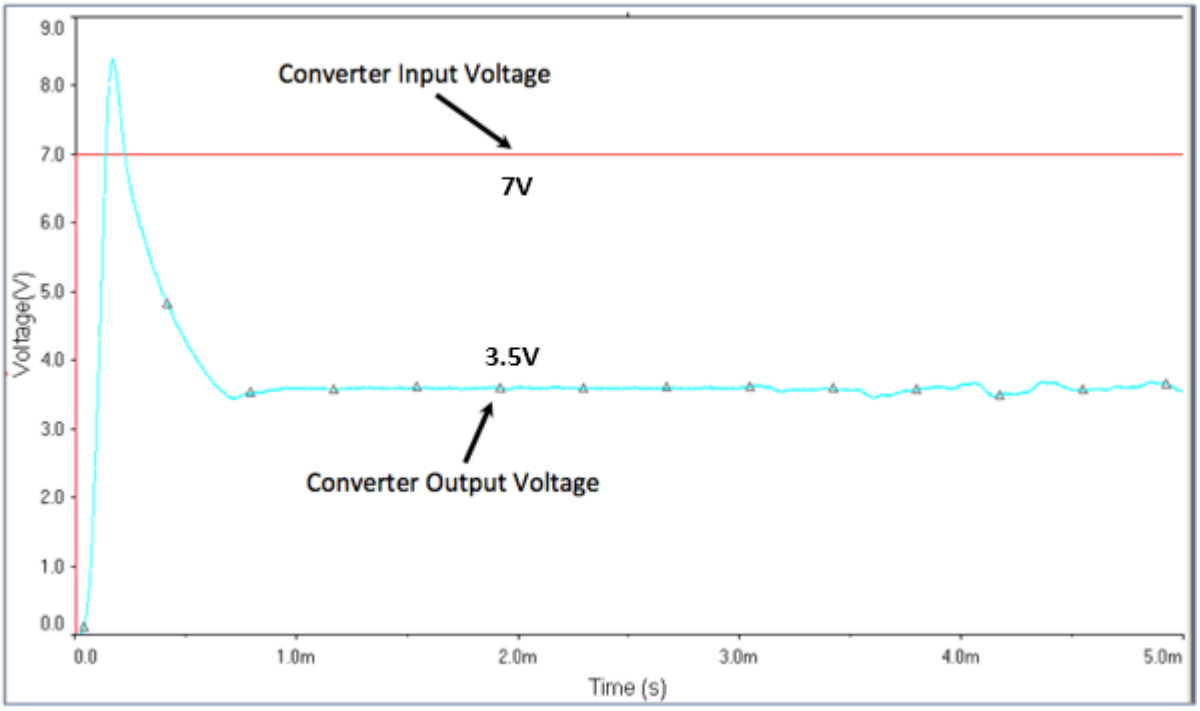

Figure 42. Multisim Boost-Buck Converter, Buck Operation, D1 = 0, D2 = 0.5

As shown in Figure 42, the converter produced a steady-state output voltage of 3.558V from an input voltage of 7V. For buck mode the circuit was expected to produce an output voltage equal to the input voltage multiplied by D2 (see Table 3, Section 2.4.2). The measured gain ratio of 0.508 had an error of approximately 1.69% of the expected gain ratio of 0.5. To test the buck operation of the circuit across a range of values, duty cycle D2 was incremented in increments of 0.1 from 0 to 1. Figure 43 shows the converter output voltages across the range of duty cycles that operate in buck mode.

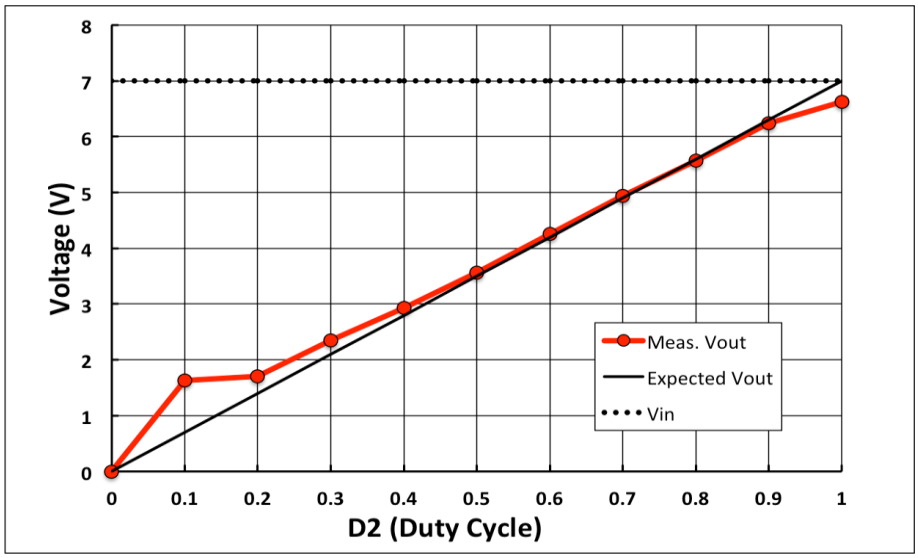

Figure 43. Multisim Boost-Buck Converter, Buck Operation Testing, D1 = 0

As shown in Figure 43, the converter produced close to the expected output in most situations, however at D2 = 0.1, the output voltage (1.625V) was 132% higher than the expected voltage of 0.7V. Duty cycles for D2 below 0.7 produced slightly higher than expected output voltages while duty cycles above D2 = 0.8 produced slightly lower voltages than expected.

To test the boost functionality of the circuit, D2 was set to 1 to deactivate the buck leg of the circuit. With S1 constantly open, D1 was varied between 0 and 1 to provide different levels of voltage boost without buck operation. Figure 44 shows an example case where D1 = 0.5. The circuit produced an output voltage of 13.374V from an input of 7V. The measured valued had an error of 4.47% from the expected voltage of 14V.

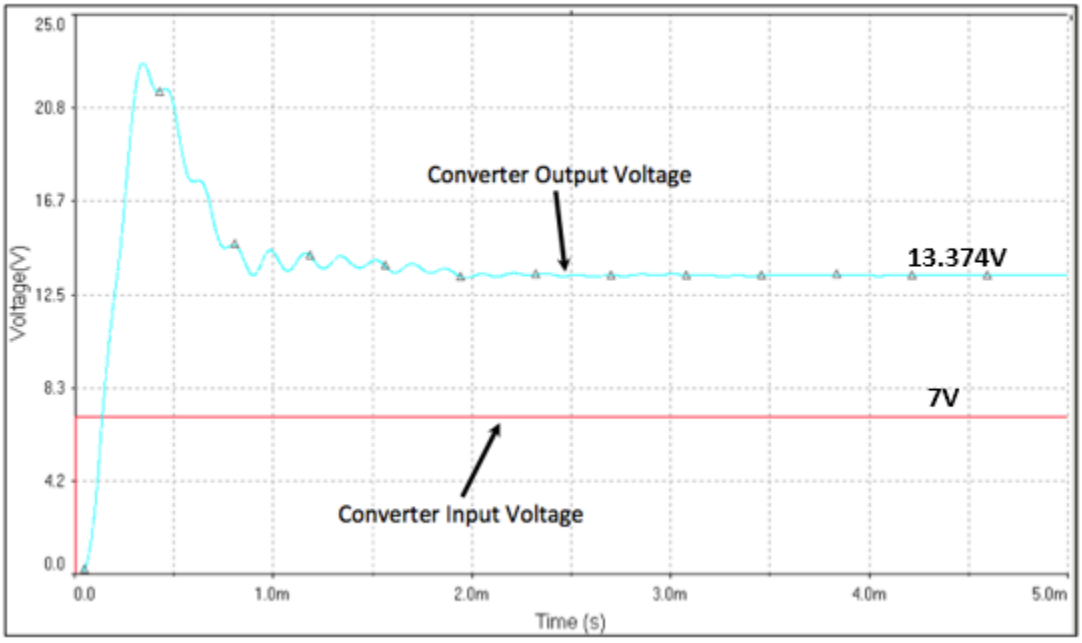

Figure 44. Multisim Boost-Buck Converter, Boost Mode Operation, D1 = 0.5, D2 = 1

Figure 45 shows the operation of the converter in boost mode across a range of values for duty cycle D1 from 0 to 1. For duty cycles below D1 = 0.5, the converter output voltages were within 6% or less of the theoretical output value. Above D1 = 0.5, the error increased and the output voltage was limited to a maximum of 29.842V. At D1 = 0.9, the converter produced an output voltage with an approximate error of 57.4% from the theoretical output voltage.

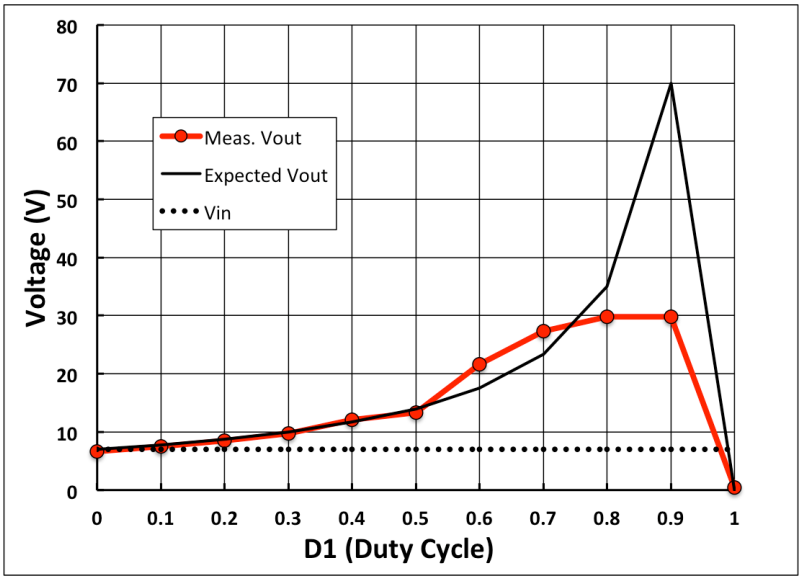

Figure 45. Multisim Boost-Buck Converter, Boost Mode Operation Testing, D2 = 1

5.5 Full-Bridge Synchronous DC-DC Converter Simulation

Multisim Advanced PV Panel Model Parameters

To demonstrate the Full-Bridge Synchronous converter model in relation to solar MPPT, a photovoltaic panel model was used to simulate the characteristics of a PV panel input. [7] The Multisim Advanced PV Model was acquired from National Instruments' online forums and was edited to have characteristics close to the Goal Zero Nomad 7W Solar Panel. The parameters used in the PV panel model are listed in Table 19.

Model Parameter	Value	Unit
I_{SC}	0.96	A
V_{OC}	8.85	V
R_{series}	0.5	Ω
R_{shunt}	2000	Ω
ns	28	# of PV cells
nd	1.397	-
k_v	-0.16	-
k_i	-0.025155	-

Table 19. Multisim Advanced PV Model Parameters

The model short-circuit current, I_{SC}, was set to be identical to the tested current of 0.960 A. The open-circuit voltage, V_{OC}, was set at 8.85V, slightly higher than the tested V_{OC} of 8.51V, as the model was shown to operate at a slightly lower voltage than given. The series resistance, R_{series}, and shunt resistance, R_{shunt}, were selected through trial and error to closely approximate the I-V characteristic of the Nomad 7W Panel. Ns, the number of PV cells was set to 28, the number counted on the Nomad 7W Panel. Nd, k_v, and k_i were ideality constants left to their default values.

To operate the PV model in Multisim, the pins of the PV model were connected to three elements: an irradiance voltage, V_Irrad (pin 1), V_Bias (pin 3), and GND (pin 2) as shown in Figure 46.

The irradiance voltage simulates the level of sunlight incident in the solar cell with 1000V equal to 1000W/m^2. [37] V_Bias is used to hold the panel output to a voltage for testing. To use the circuit with a converter, pin 3 is connected as the input voltage source to the converter instead of V_Bias.

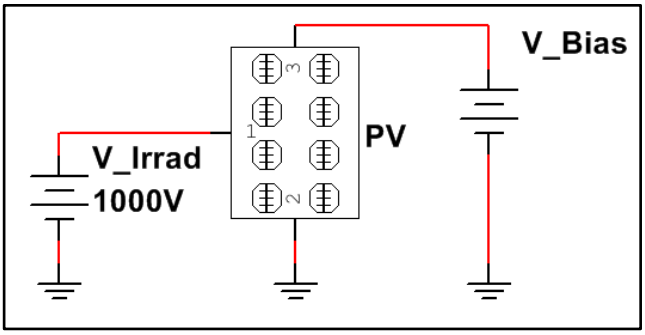

Figure 46. Multisim Advanced PV Panel Model

Model Comparison to Nomad 7W PV Panel

To check the accuracy of the Multisim Advanced PV Model, a DC sweep analysis of V_Bias was conducted to determine the I-V characteristic of the model. The model I-V curve and the GoalZero Nomad 7W I-V curve are compared in Figure 47.

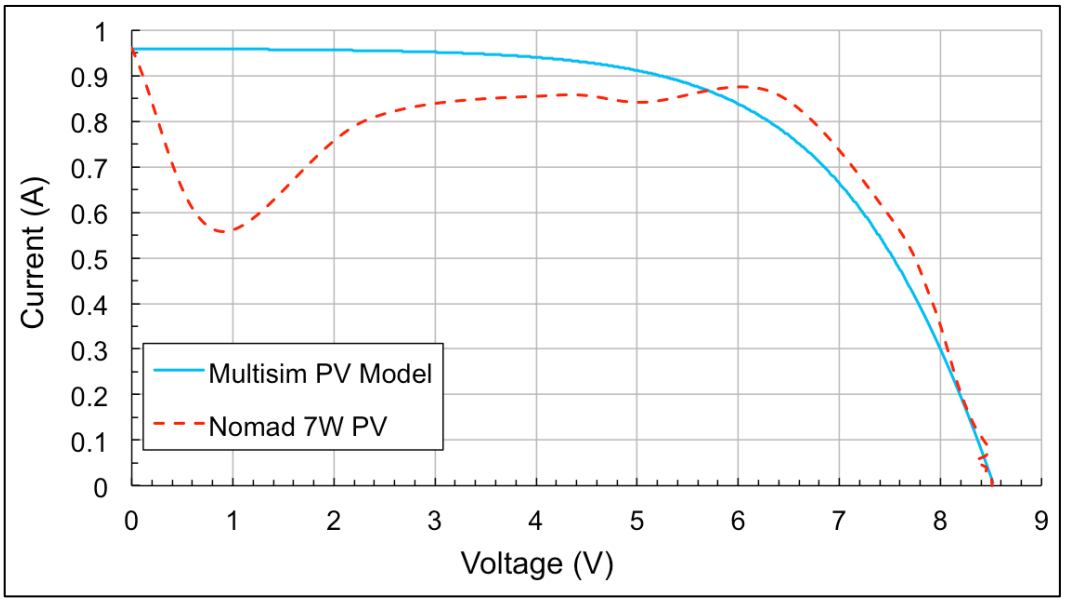

Figure 47. PV Model Comparison to GoalZero Nomad 7W PV Panel

The simulated I-V characteristic was shown to approximately follow the tested Nomad 7W Panel I-V characteristic with the exception of part of the low-voltage, high-current section of the curve (< 5V). The irregularity of the Nomad 7W Panel around 1V was caused by a mixture of temperature variation and accidental shading of PV cells during testing.

Full-Bridge Converter Construction

To simulate a full-bridge synchronous DC-DC converter used for MPPT, the NI Multisim Advanced PV Model with a V_{irrad} value of 1000V was connected as the input voltage to the converter. A 15uF input capacitor, C_{In}, with an equivalent series resistance of 0.1Ω, was connected in parallel to the input voltage. The input voltage was then wired to the buck leg of the circuit, which consisted of two MOSFETs (S2, S1). From the S2 source and the S1 drain node, a 120µH inductor and an equivalent series resistance of 0.1Ω connected the buck leg of the circuit to the boost leg. For the boost leg, the source of S3 and the drain of S4 were wired to the inductor, with the drain of S3 wired to the load, and the source of S4 wired to GND. The load was connected in parallel with a 10µF output capacitor, C_{out}, and a Schottky diode, D1, to handle reverse current with minimal switching losses. Watt-meters XWM7 and XWM1 were attached to the input and output, respectively, to measure converter efficiency. The simulated full-bridge converter circuit is shown in Figure 48.

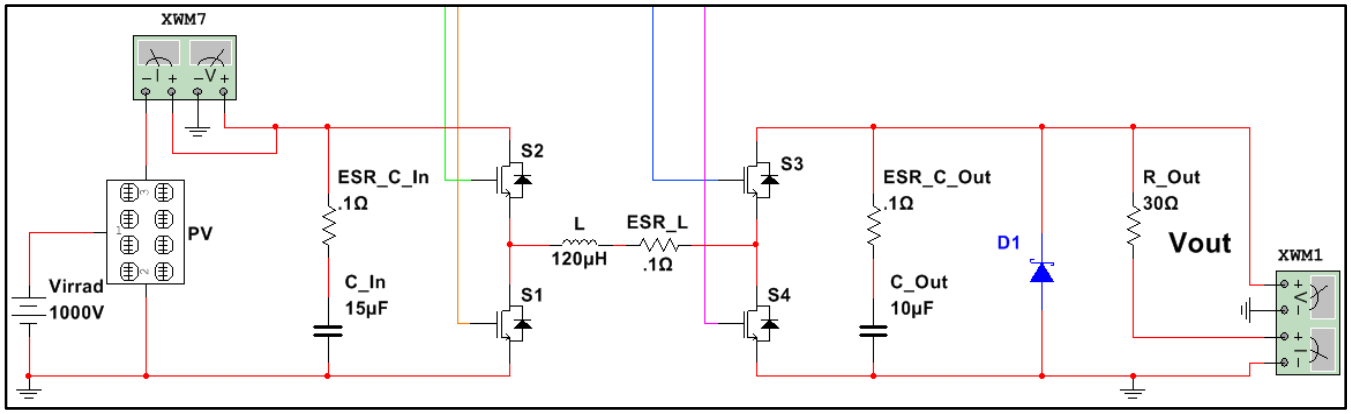

Figure 48. Multisim Full-Bridge Synchronous DC-DC Converter Model

To control the output voltage of the full-bridge circuit, four 100kHz PWM signals were generated as the gate inputs to S1, S2, S3, and S4 as shown in Figure 49.

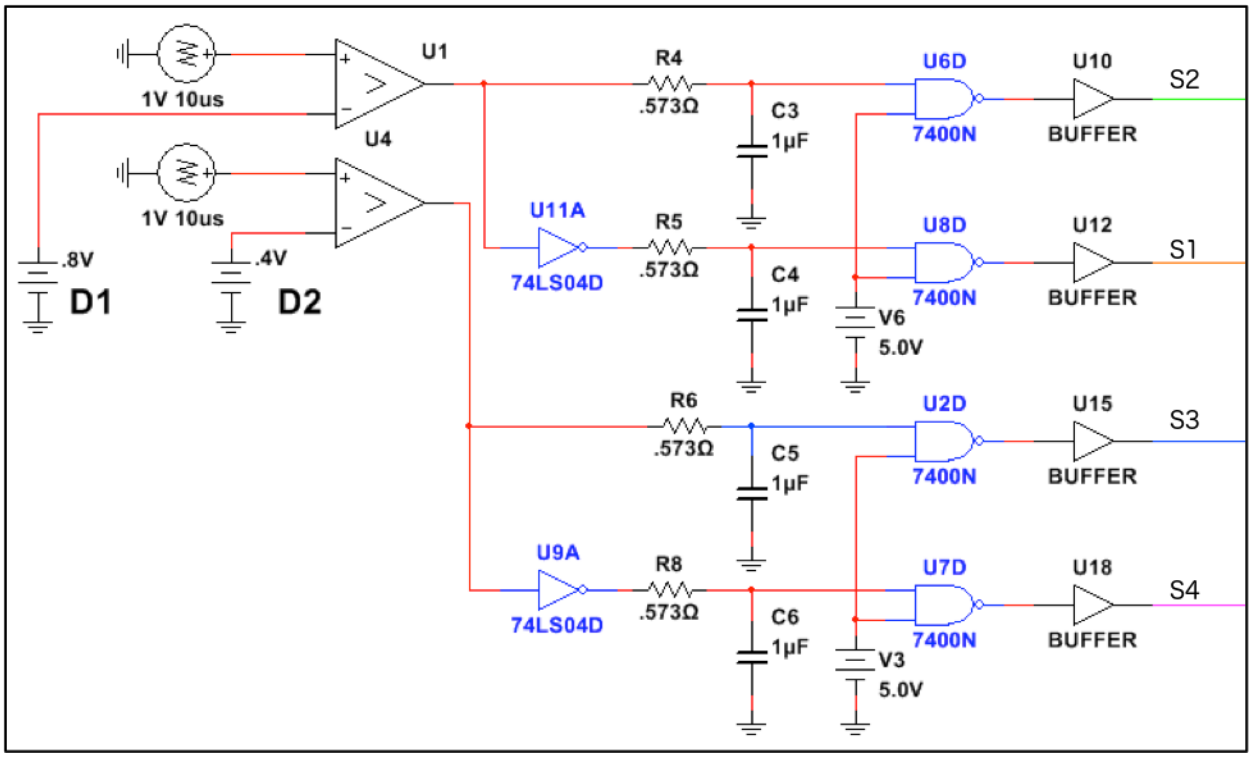

Figure 49. PWM Generation & Dead-Times Circuit

The PWM signals were generated using a comparator with a 100kHz, 1V-peak triangle wave input on the positive input compared to a constant reference voltage on the negative input. By modulating the reference voltages between 0V and 1V, the PWM duty cycles D1 and D2 were directly controlled between 0 and 1. To prevent cross-conduction, the signals for complementary MOSFETs were inverted and dead-times were added to all four signals. The dead-times were generated through the charging and discharging of an RC circuit as the input to a NAND gate. The NAND gate provided hysteresis such that dead-times were added to both the rising and falling edges of the PWM waveforms. The NAND gates

and inverters were implemented by using Multisim models of 7400 Series TTL (transistor-transistor logic) components.

Typical outputs from the PWM generation circuit are given in Figure 50.

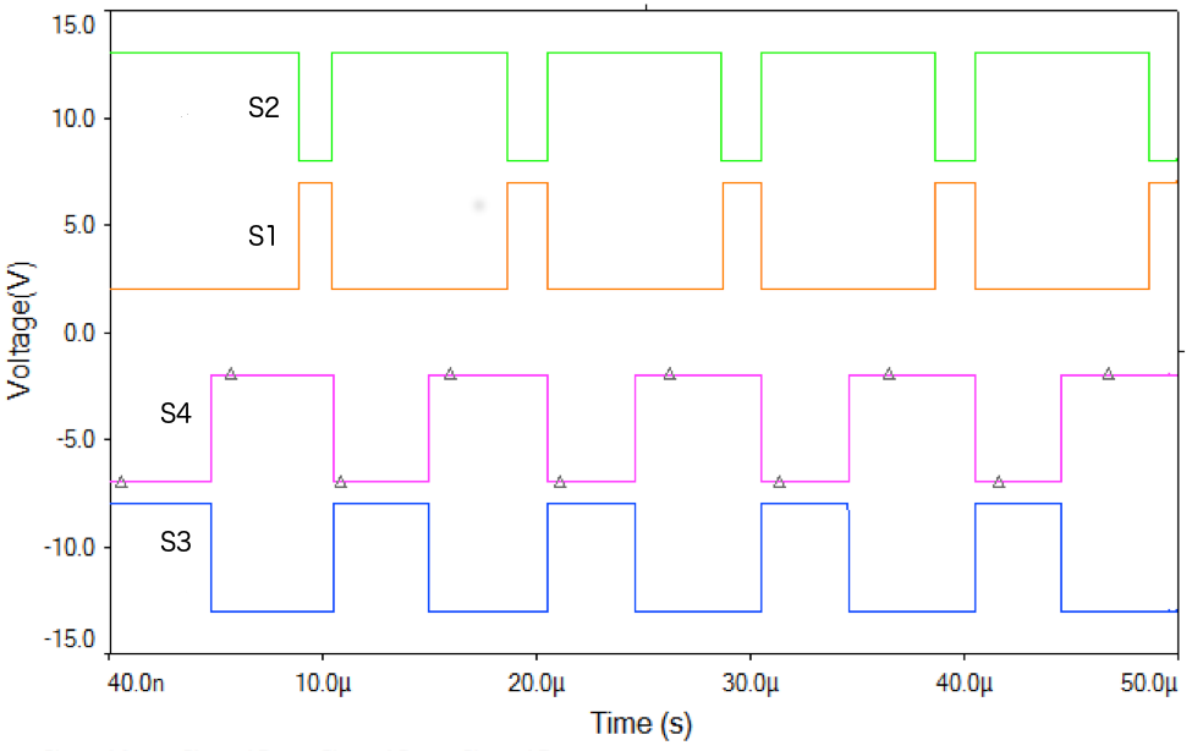

Figure 50. 100kHz PWM Signal Generation, D1 = 0.8, D2 = 0.4

For the buck leg, the two MOSFETs were controlled by the PWM waveform with duty cycle D1 (S2) and its respective complement (S1). For the boost leg, the MOSFETs were controlled by a PWM signal with duty cycle D2 (S4) and its complement (S3).

Testing & Results

To test if the simulated full-bridge circuit was funcitoning properly, the configured ciruit was tested at different combinations of duty cycles D1 and D2. At each combination, the voltage and power was measured in Multisim for both the input and output of the converter. To allow for transients in the converter to settle, the simulation end time was set to 3ms and measurements were taken at the end of the simulation run time. To change the duty cycles, the reference voltages of the PWM generation circuit were independently incremented by 0.1V for a corresponding 0.1 change in duty cycle. To be operating properly, the full-bridge converter is designed to produce an output voltage equal to the input voltage multiplied by the ratio of the duty cycles, D1/D2. The ratio of the two duty cycles, in this way, is equal to the theoretical voltage gain of the converter.

Buck Operation

To test the buck operation of the circuit, an example is shown in Figure 51 of a duty cycle combination of D1 = 0.3 and D2 = 0.6. The combination, with a ratio of D1/D2 = 0.5, was calculated to produce an output voltage that should be exactly half of the input voltage.

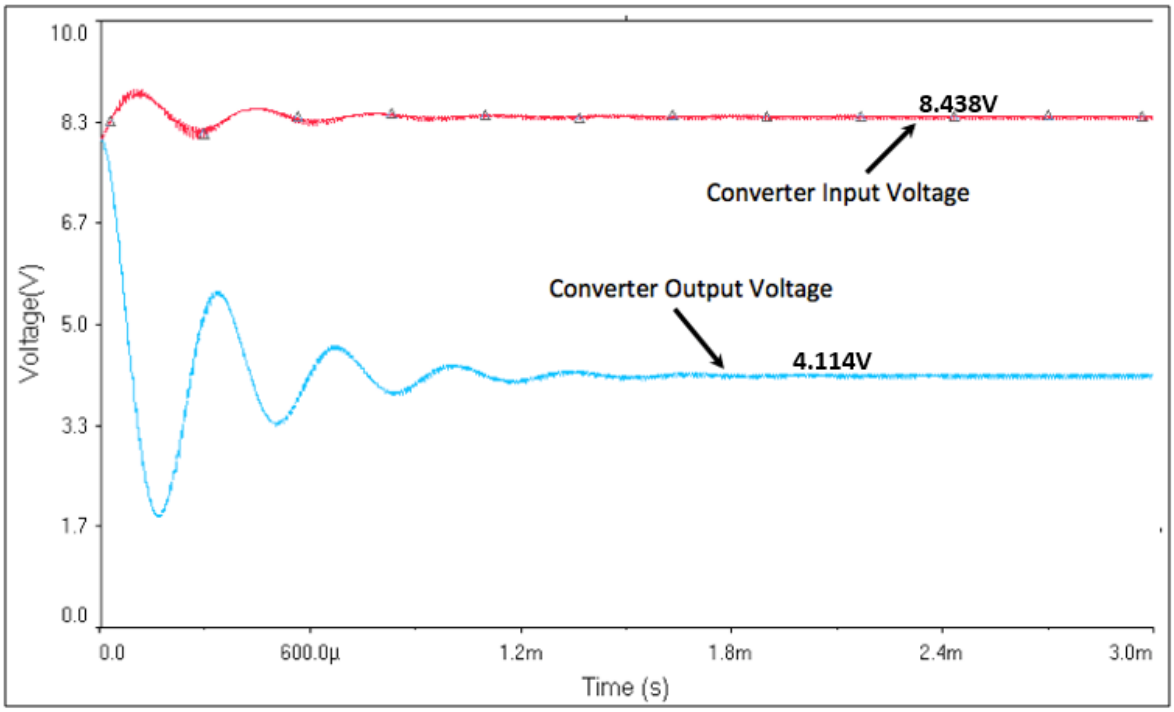

Figure 51. Simulated Full-Bridge DC-DC Buck Operation

The results of the combination of D1 = 0.3 and D2 = 0.6, produced an output voltage of 4.114V from a PV panel input of 8.438V. The resulting voltage was almost exactly as expected with a ratio of approximately 0.488 of the input voltage. The buck operation example combination had an efficiency of 98.8% and an output ripple voltage of 60mV peak-to-peak.

Boost Operation

To test the boost operation of the circuit, an example is shown in Figure 52 which depicts the output of the duty cycle combination of D1 = 0.8 and D2 = 0.5. The resulting ratio of duty cycles is 1.6 with the output voltage expected to be 1.6 times the input voltage. The simulation produced an output voltage of 11.288V from an input voltage of 7.251V; a ratio of about 1.56. The duty cycle combination of D1 = 0.8 and D2 = 0.5 also had an efficiency of 98% and an output ripple voltage of approximately 240mV peak-to-peak.

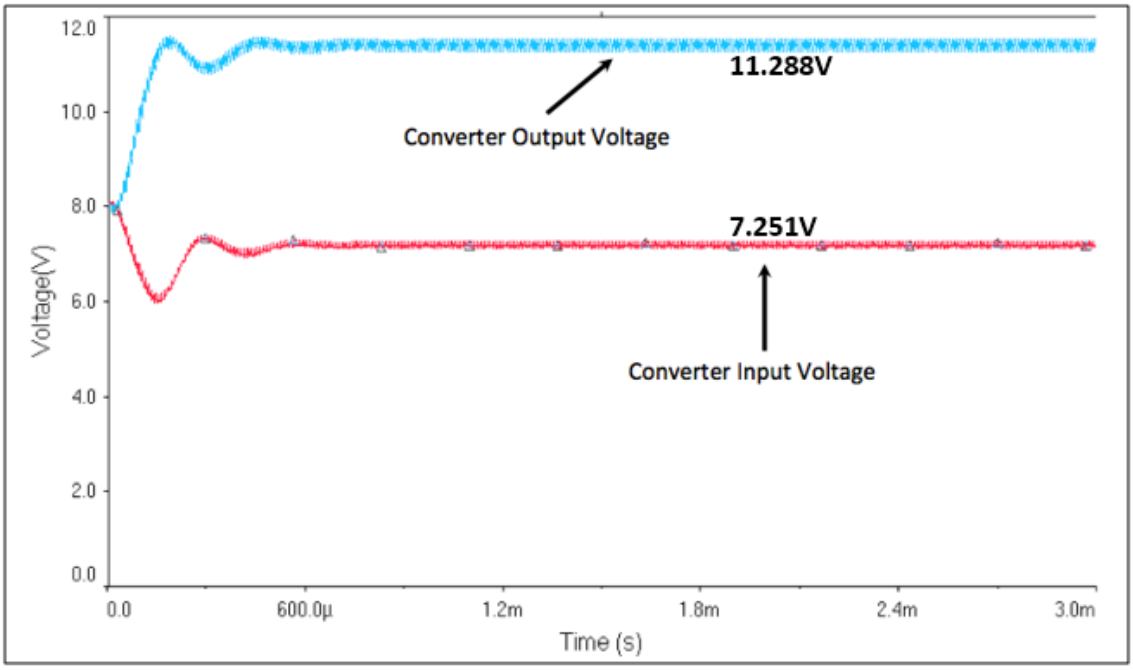

Figure 52. Simulated Full-Bridge DC-DC Boost Operation

Buck-Boost Operation

A third example combination of duty cycles D1 = 0.5 and D2 = 0.5 was chosen to demonstrate the cicuit in buck-boost operation. The resulting ratio of duty cycles was 1:1 and the circuit was expected to produce the same voltage out as the input voltage. Figure 53 shows the output of the converter during buck-boost operation.

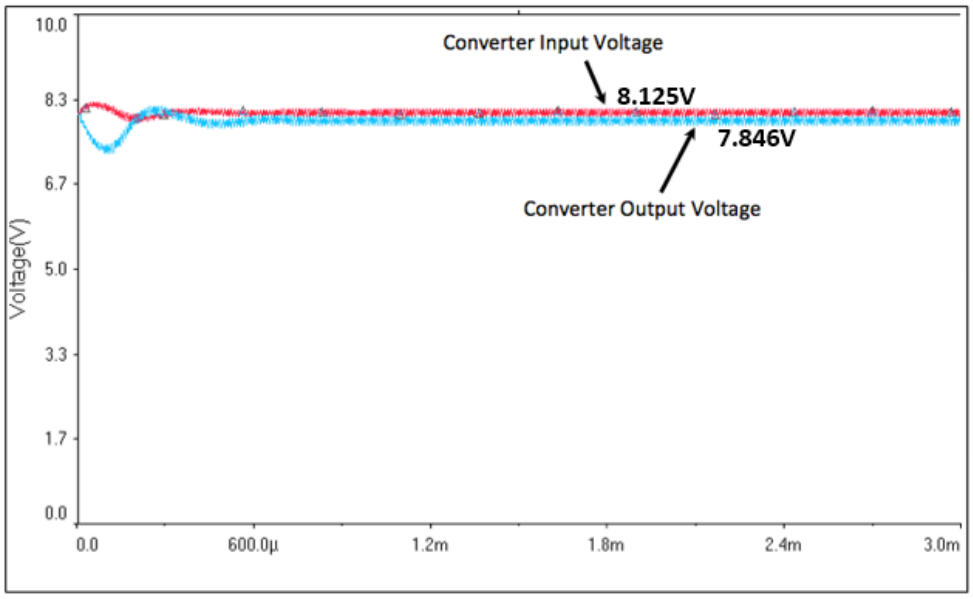

Figure 53. Simulated Full-Bridge DC-DC Boost Operation

When simulated the buck-boost unity gain configuration produced an output voltage of 7.846V from an input of 8.125V; a ratio of 0.97. The output voltage also had a voltage ripple of 106mV.

Converter Accuracy & Efficiency

To get a comprehensive idea of the operation of the simulated converter, all combinations of duty cycles in 0.1 increments between 0 and 1 were simulated and the results recorded. For simpler visualization of results, only the D2 values of 0.1, 0.3, 0.5, 0.7, and 0.9 are plotted. A full table of results can be found in Appendix F. Figure 54 shows the expected gain of each duty cycle combination compared to the measured voltage gain of the simulated converter.

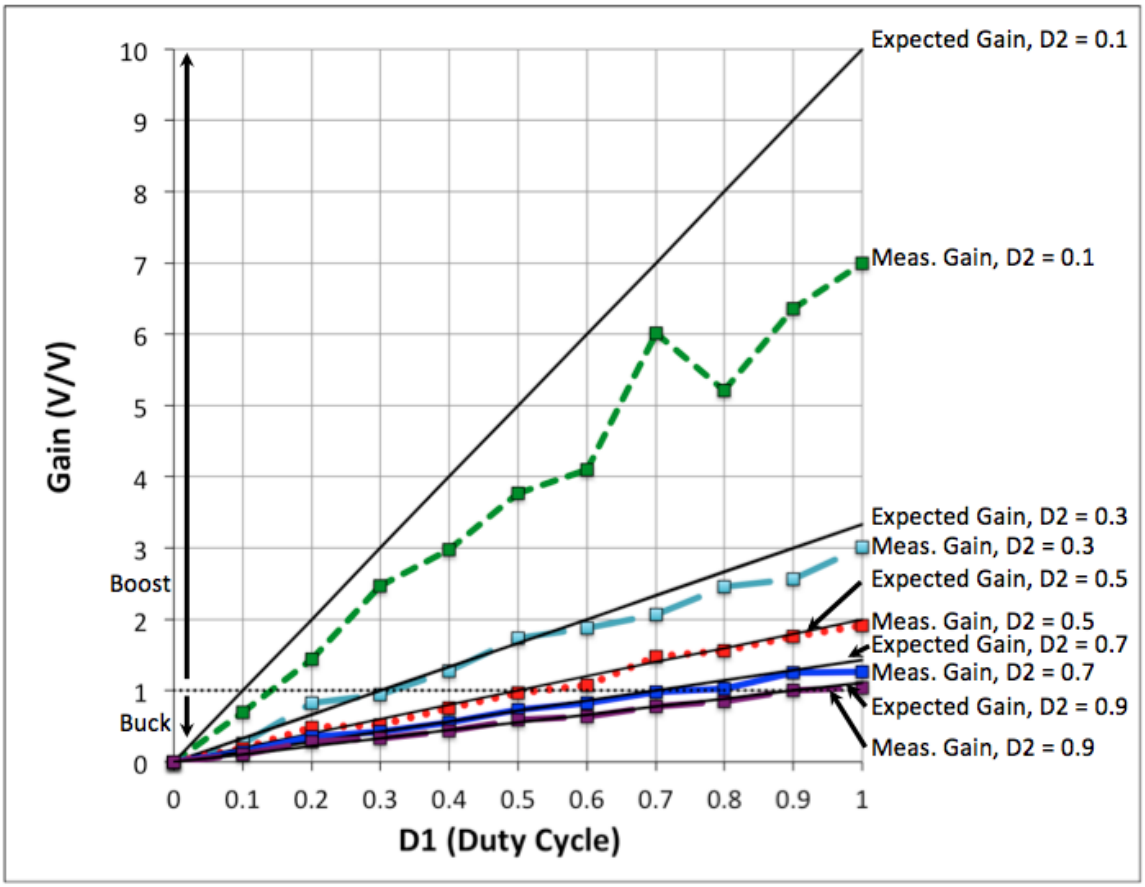

Figure 54. Simulated Full-Bridge DC-DC Converter Voltage Gain Results

For combinations of duty cycles where D2 = 0.1, there was an average error from the expected gain of 26.6%. For D2 = 0.3, the average was 11%, and for D2 = 0.5, D2 = 0.7, and D2 = 0.9, the combinations resulted in average error values of 7.2%, 6.1%, and 5.6%, respectively. The results showed that low values of duty cycle D2 (<0.3) resulted in larger deviation from the expected gain. Figure 55 provides the efficiency of the converter at different combinations of D1 and D2.

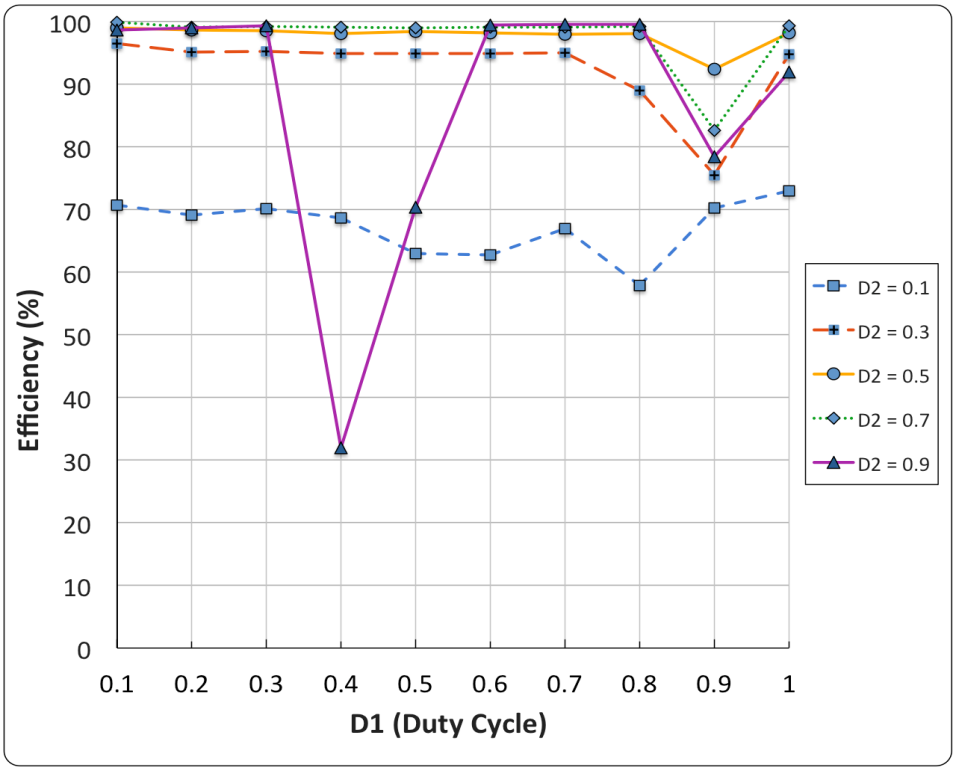

Figure 55. Simulated Full-Bridge DC-DC Converter Efficiency Results

As shown in Figure 55, duty cycle combinations with D2 = 0.1 resulted in efficiencies below 75%. There was also a significant pattern of decreased efficiency where D1 was equal to 0.9. For D2 = 0.9, there were also dramatic drops in efficiency for the values of D1 = 0.4 (31.9%) and D1 = 0.5 (70.3%).

To determine the cause for drops in efficiency, the transient behavior of some of the most inefficient combinations of duty cycler were observed using the Multisim oscilloscope tool. Figure 56 shows the resulting input and output voltages for the duty cycles, D1= 0.4 and D2 = 0.9.

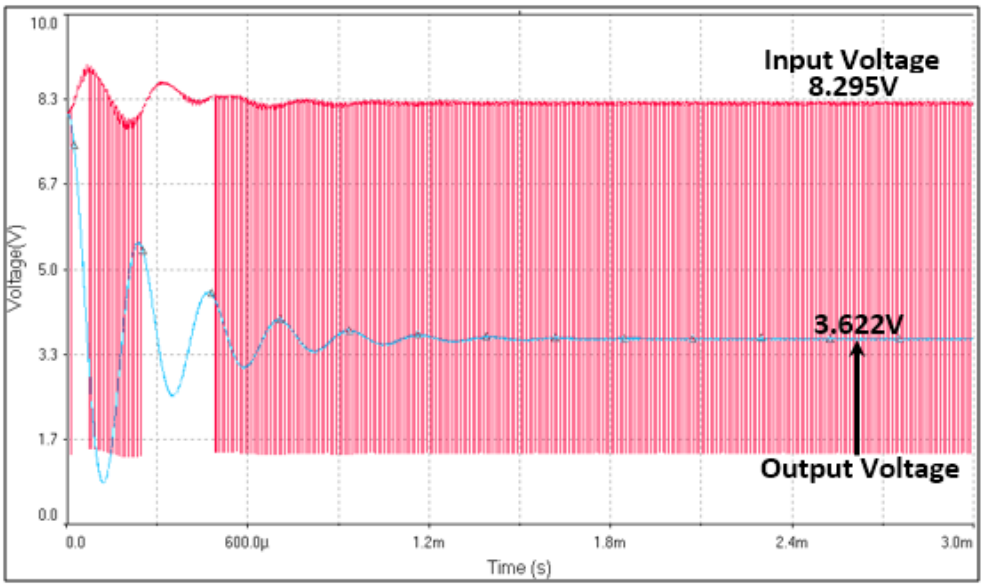

Figure 56. Simulation of Full-Bridge Converter Input and Output Voltages, D1 = 0.4, D2 = 0.9

.

At the combination D1 = 0.4 and D2 = 0.9, periodic drops in the input voltage of the converter occurred from a steady state value of 8.295V down to approximately 1.6V. After some investigation, the cause of the voltage drops was determined to be a regularly occurring short circuit across S2 and S1. The short circuit was caused by overlap of the ON time of the PWM signals used to drive the gates of MOSFETs S2 and S1. Due to the PWM generation at D1 = 0.4 and D2 = 0.9, both MOSFETs were being turned on simultaneously for approximately 15 ns per period. Figure 57 provides a snapshot of the S2 and S1 drive voltages during a short circuit condition.

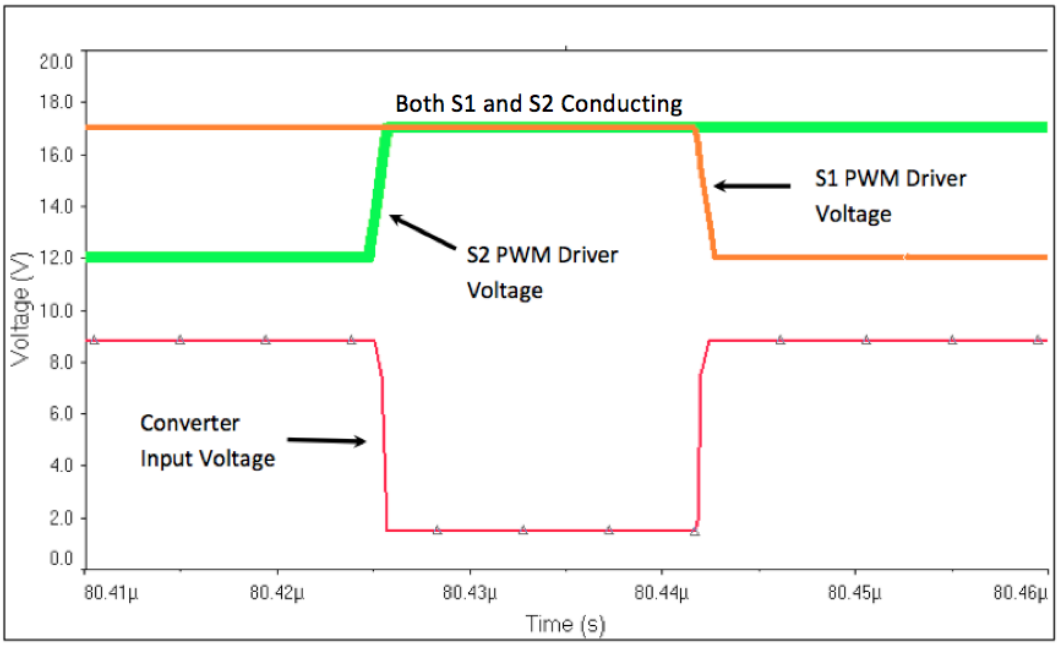

Figure 57. Full-Bridge Simulation Short-Circuit Condition, D1 = 0.4, D2 = 0.9

The short circuit issue was a result of missed dead times during some combinations of duty cycles. The missed dead times were most likely to occur when one of the duty cycles was in the range of 0.8 to 0.9. As shown in Figure 49 (PWM Generation & Dead-Times Circuit), the dead times were generated using an RC circuit and a NAND gate to prevent short circuit conditions during switching transitions. At high duty cycles, the capacitor of the RC circuit did not have adequate time to fully discharge before the next period of the PWM waveform. The partial discharging of the capacitor thus interfered with the generation of the dead times, leading to short circuit conditions and losses in efficiency. The short circuit problem was shared by the other outliers of low efficiency as well, however, the missed dead times often occurred inconsistently.

Efficiency Comparison

To determine the difference in efficiency between the cascaded boost-buck topology and the full-bridge topology, efficiency of the converters was tested at duty cycle combinations that would produce the same voltage gains in both converters. For comparison, the 7V DC source used in the boost-buck converter simulation was replaced with a Multisim Advanced PV Panel Model identical to the model

used in the full-bridge simulation. Duty cycle combinations from both converter simulations were selected for identical boost-mode voltage gains are shown in Figure 58.

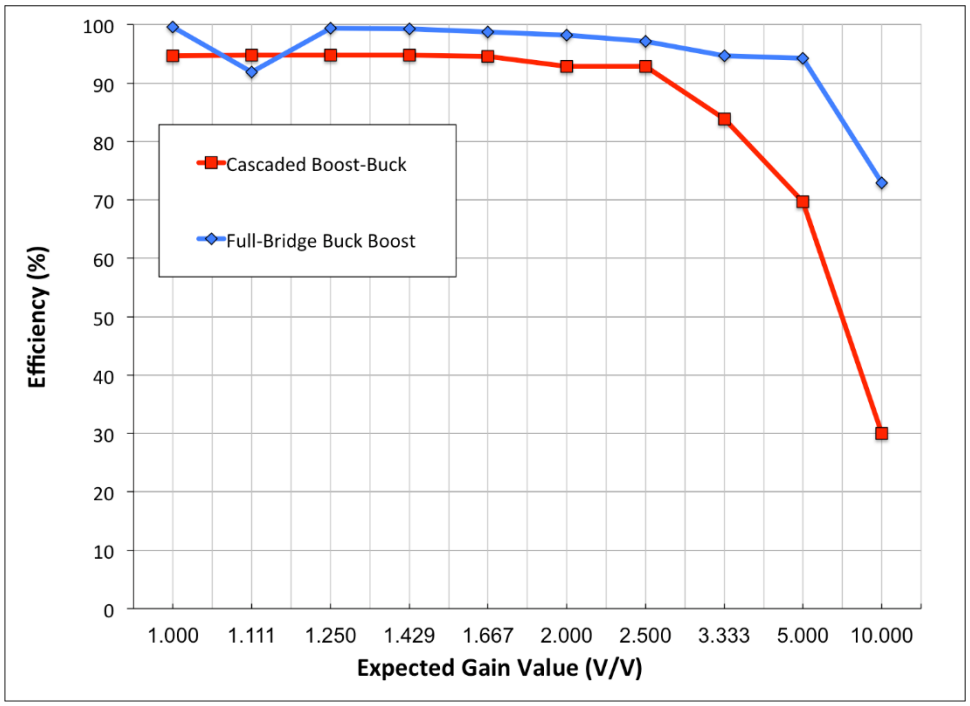

Figure 58. Converter Boost-Mode Efficiency Comparison

From the comparison, the cascaded boost-buck converter was consistently less efficient than the full-bridge model. The boost-buck converter had an average efficiency of 84.3% in boost mode, while the full-bridge had an average efficiency of 94.6%.

For buck-mode, another comparison was performed as shown in Figure 59.

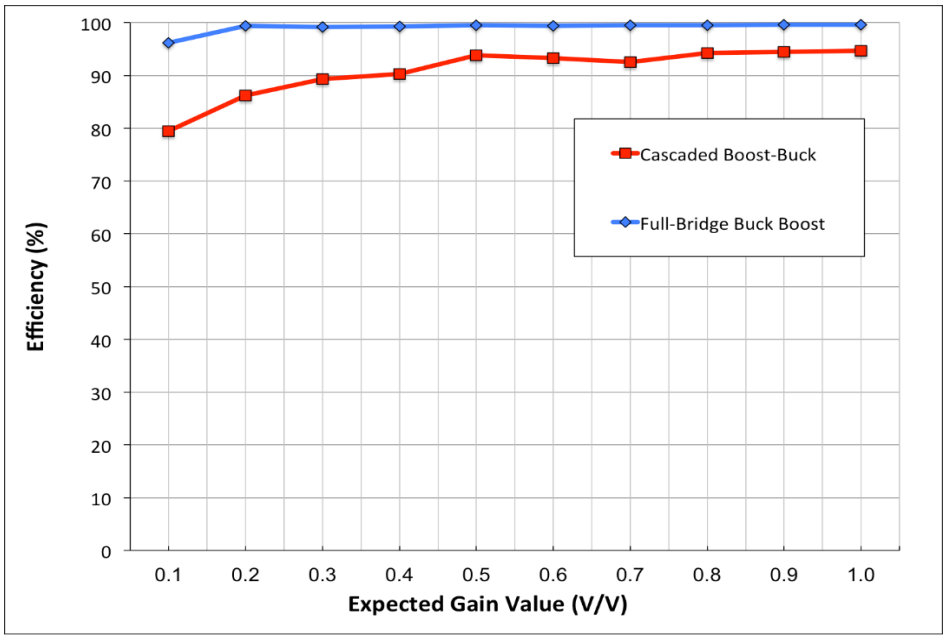

Figure 59. Converter Buck-Mode Efficiency Comparison

To compare the cascaded and full-bridge topologies in buck operation mode, the efficiency of each converter was tested at buck-mode duty cycle combinations that produced the same gain ratios in each converter. The average efficiency for the buck-mode, cascaded boost-buck converter was 90.8% compared to 99.1% for the full-bridge converter. Because of the increases in efficiency using the full-bridge design, the full-bridge topology was favored over the cascaded boost-buck design.

5.6 Summary

In testing the operation of the Multisim simulated buck, boost, cascaded boost-buck, and full-bridge buck boost converters, all of the converters were shown to behave closely to their theoretical values of voltage and efficiency. Only under certain combinations of duty cycle was efficiency and accuracy shown to be reduced. After the simulations of the four converter topologies were completed, the full-bridge converter was shown to be more efficient than the cascaded boost-buck topology while still being capable of both boosting and bucking voltage. Despite the full-bridge converter often operating at efficiencies above 90%, the simulated converter implementation still had difficulty generating PWM driver signals. To prevent cross conduction across adjacent MOSFET switches in the converter, dead times were added to the PWM waveforms, yet under certain combinations of duty cycles, the circuit still suffered from periods of cross-conduction and drops in efficiency of up to 30-60%. The simulation, in this way, was limited by the generation of MOSFET driver signals in the methods presented in this section. For physical implementation, using a pre-made MPPT integrated circuit or a microcontroller operated driver could prevent the cross conduction problem, and prevent losses of efficiency in real applications.

The simulation also had some limitations because we only simulated the DC-DC converter circuit without the MPPT algorithm. We did not implement MPPT into the simulation due to time constraints and the overall complexity of building a feedback loop that could respond to changes in the DC-DC converter's output voltage and current levels and perform MPPT. By implementing MPPT, the simulation could provide more useful information into how to optimize MPPT for low-capacity PV panels. Although the simulation did not simulate MPPT, the simulation was still useful for confirming the component values that would work for a physical application circuit. The inductor value (120µH) and capacitor values (input: 15µF, output: 10µF) were chosen from the results of the simulations. During trials of different component values, changes in the output voltage ripple, transient settling time, and accuracy of the converter all influenced component selection. By performing the simulations, the converter application circuit component values were chosen in confidence that the converter would operate in the voltage range required for MPPT of low-capacity solar panels.

6. Implementation

6.1 Introduction

We chose the Texas Instrument SM72445 “Programmable Maximum Power Point Tracking Controller for Photovoltaic Solar Panels” IC for our implementation. In this section, we describe how we examined the SM72445 datasheet and application notes to calculate the necessary external components of the circuit.

6.2 Texas Instrument SM72445 Integrated Circuit

From Section 4: System Design, we discussed important component parameters and system requirements that characterize our ideal design. From our research, we found that the Texas Instrument SM72445 was the most compatible IC for our intended application for an MPPT-driven, portable solar charge controller. Considering our outlined system design from Section 4, Figure 33, we will now describe the SM72445 IC more specifically in terms of the IC’s features and how we designed the supporting circuit required for implementation.

As seen previously in Figure 33, the MPPT IC replaces the microcontroller’s function to execute the MPPT algorithm and communicate with the full bridge driver. Specifically, the functionality of the SM72445 is to implement a Perturb and Observe MPPT algorithm, use sensors to collect data for the MPPT calculation, communicate with the full bridge driver, and communicate with a microcontroller. A block diagram of the SM72445 with the IC’s required external components is seen in Figure 60.

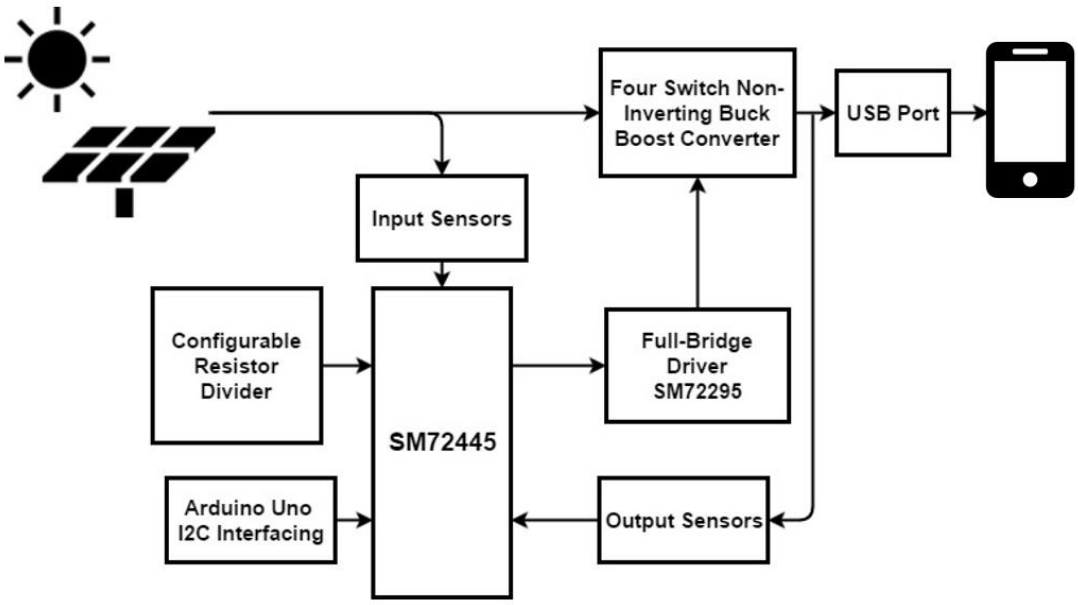

Figure 60. Block Diagram of SM72445 and External Components

Figure 60 is a representation of the detailed circuit diagram proposed in the SM72445 datasheet. The blocks illustrated in Figure 60 relate to key components that create a solar charge controller: solar panel, controller to implement MPPT algorithm, full-bridge (H-bridge) driver, DC-DC converter, sensors, and load. The configurable resistor divider and the Arduino Uno are additional necessary components to drive the SM72442. The configurable resistor divider allows the user to designate specific settings for

the SM72445. Similarly, the Arduino Uno (a microcontroller) can be programmed to configure the SM72445 digitally through an I2C bus. Also, the Arduino Uno can read from or write to the SM72445 using an I2C bus. In our implementation, we configured the SM72445 using the resistor divider design, and used the Arduino Uno to read values from the SM72445. Some of the configuration options are slew rate limit, MPPT exit threshold, maximum output voltage, and current limit. I2C interfacing with the Arduino include reading the configured values, and reading or writing values such as input voltage and output voltage, voltage and current offsets, and current thresholds. More details on the configuration options, I2C read or write options, and additional features can be found in SM72445 IC's datasheet from TI. The configurability and I2C communication bus are a couple of the SM72445 features.

6.3 Component Selection

For our implementation, we needed to design the recommended external components to drive the SM72445. From Figure 60, we have calculated component values for each block interfacing with the SM2445. We will briefly outline the components required for each external component block in Table 20. Specific component values calculated is found in Appendix G: Component Selection Calculation Sheet.

External Component Block	Circuit Representation	Component Description
Configurable Resistor Divider	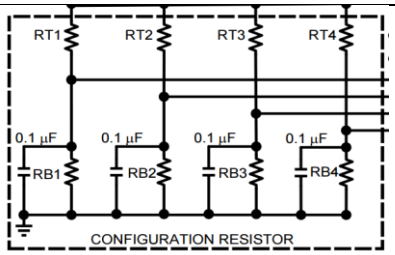	• Set of resistor dividers to configure SM72442 pins • Resistor values based on specific voltage settings for configuration as described in SM7224 datasheet
Four Switch Inverting Buck-Boost Converter	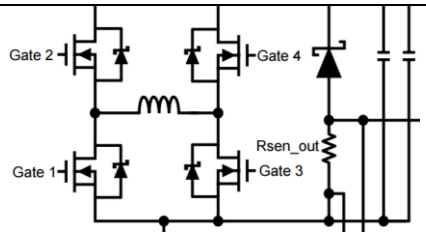	• Buck-boost converter typology using four MOSFETs and single inductor • To address voltage ripple, input and output capacitors recommended • Inductor and capacitor values based on simulation results
Current Sensors	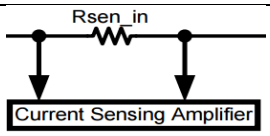	• SM72442 has internal current sensing amplifier • requires a resistor between the positive and negative terminals
Voltage Sensors	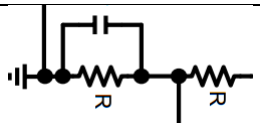	• Voltage divider circuit recommended for input and output voltage sensing • Circuit directly connects to SM7224

Table 20. External Component Selection Description and Circuit Representation [8]

The configurable resistor divider, four-switch inverting buck-boost converter, current sensors, and voltage sensors were designed using the circuit diagrams in Table 20 as reference and additional information provided by the SM72445 datasheet and the Solar Magic Application Note. The Arduino Uno block and the Full-bridge driver block were not included in Table 20 because they do not have a circuit representation, but rather the Arduino Uno is a microcontroller and the full-bridge driver is an

integrated circuit. The Arduino and driver were selected but not designed. The Arduino Uno was selected because it is easily programmable using computer software and can interface with I2C bus. The SM72295 full-bridge driver IC was recommended by the SM72445 datasheet to implement synchronous control, and the driver is designed to be compatible with the SM72445 IC.

6.4 Summary

Our implementation of our system design was employing Texas Instrument's SM72445 Integrated Circuit and designing its external components. We chose the SM72445 IC because the SM72445 IC's features and capabilities were compatible with our system design requirements. Because we used the SM72445 IC, we had to design the accompanying external components such as the four-switching buck-boost converter, the configurable resistor divider, and the voltage and current sensors. The components selected were based on recommendations from the SM72445 datasheet and the Solar Magic Evaluation Board Application Note. Using the datasheet, application note, and simulation results, we bought and built our solar charge controller as seen in Figure 61.

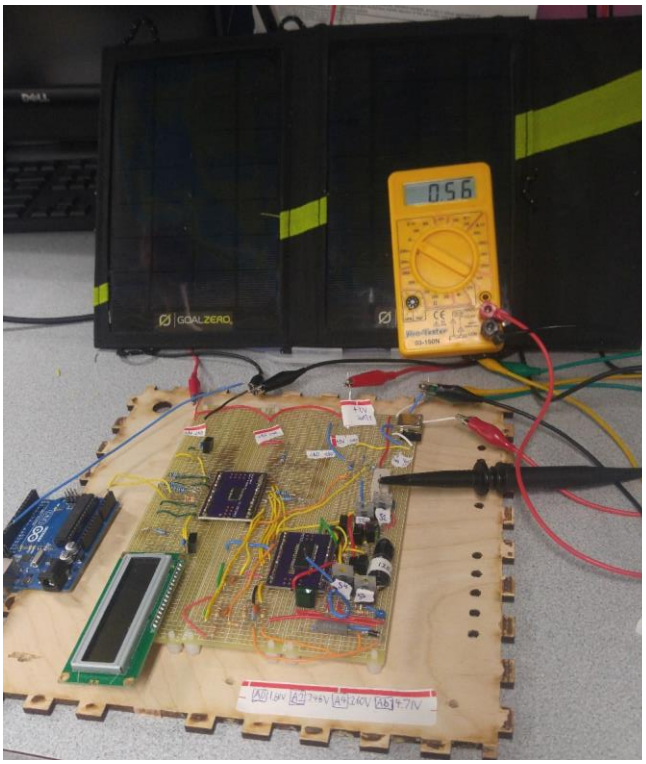

Figure 61. Our Solar Charge Controller Implementation

7. Discussion and Conclusions

7.1 Introduction

In this section, we present our findings from our tested results with our simulation results and expected functionality of the circuit. We discuss our conclusions based on our research, simulations, and testing. Also, we suggest potential improvements to apply to the MPPT solar charge controller.

7.2 Results

In order to determine the functionality of our implementation, we used the simulation and the SM72445 IC's datasheet and application notes to outline the criteria under which our circuit should be considered functional. We first establish the main differences between the simulation circuit and our implementation circuit. We employed a similar inductor value and capacitor values as the simulation for our DC-DC converter implementation. However, the simulation is not driven by a control loop, but rather the control of the DC-DC converter is determined by set parameters as briefly discussed in Section 5. Thus, the efficiencies provided in Section 5 are expected to be higher than our tested circuit.

By establishing the main differences between the simulation and implementation, we developed a general basis for which we can determine our actualized circuit as functional: if the control or PWM is communicating to the converter whether to buck or boost while the SM72445 IC is in MPPT mode, it is considered functional no matter the efficiency output of the circuit.

In addition to our generalized functionality statement, we expected the following:

- PWM to be 110kHz in MPPT operating mode
- Predetermined calibration resistor divider values to match read values and associated calibrated mode of operation (as calculated in Appendix G)
- The implementation to be less efficient than the simulation
- The output voltage to be a regulated around 5V

With the expectations and criteria for functionality, we built and tested our circuit as seen in Figure 62 and Appendix M. Our implementation seen in Figure 62. The points of interest are highlighted in Figure 55 including the MPPT IC, the driver IC, the buck-boost converter, the USB output, and the configuration resistor divider which were all checked during testing.

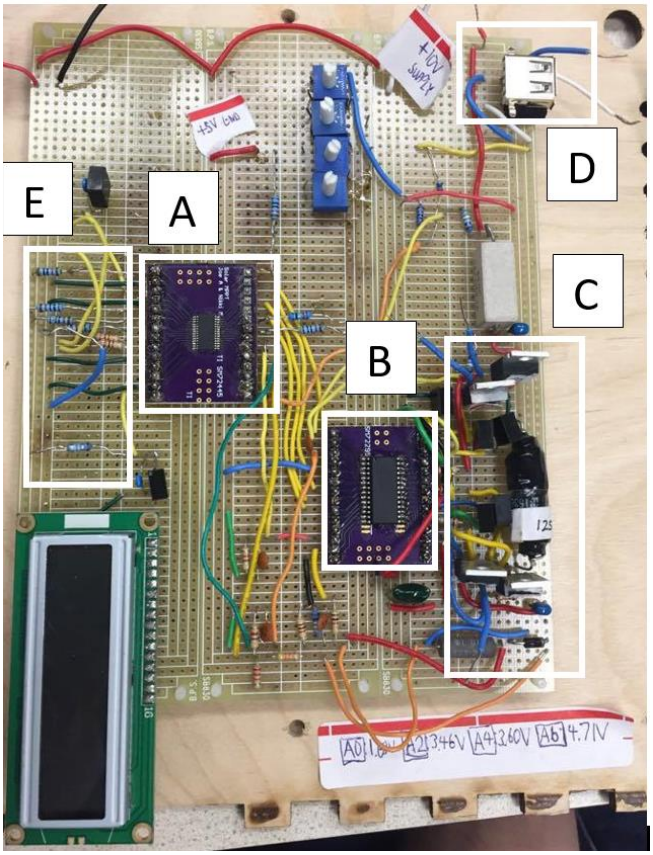

Figure 62. Actualized Circuit with (A) SM72445 IC, (B) Driver IC, (C) Buck-boost Converter, (D) USB Output, (E) Configured Resistor Divider

During our testing, we found many errors in our soldering and component setup as compared to the datasheets of the MPPT IC and the driver IC. We also discovered that the set values for pins A0 through A6 could be configured through the resistor divider or the Arduino (microcontroller). Thus, we determined not to focus on implementing the Arduino through I2C, but to just focus on the analog components When we consulted the datasheets of the SM72445 and SM72295 to check our circuit, the datasheets and application notes were vague as to how to implement the ICs into our circuit design and the circuit diagrams provided by the datasheets did not present how or why certain components should be connected together. Due to the setback of consistently adjusting our circuit design and the time constraint, we were only able to perform a few tests. We recorded our tests, circuit adjustments, and findings which is found in Appendix L: Testing Results and Log. We focused most of our testing on checking if the MPPT IC was functional because the MPPT IC determined the PWM waveforms that would determine the DC-DC converter mode. In order to test the MPPT IC, connected the 5V and 10V power supply to the circuit, provided the circuit an input voltage ranging between 0V and 10V, and probed the circuit using a Tektronix oscilloscope and two digital multi-meters (DMM) to read the input and output voltages.

From reviewing our log and test data, we achieved observing the SM72442 IC in panel mode, boost mode, and buck mode. When we were testing, we were only able to observe the panel mode, buck mode, boost mode until the last couple of changes were made to the circuit as documented in Appendix L. We saw that the criteria for the SM72445 to enter Panel mode (all switches in 50 kHz PWM, and enter panel mode when RST pin was high) in our testing agreed with the datasheet, but we were unsure how we were able to observe the boost mode. More specifically, we were able to recreate the Panel Mode (when voltage is close to the desired load, that the MPPT IC does not enter any operational mode) during all of our testing, but we were not able to recreate the test set-up for the boost mode to occur because its occurrence seemed to have been an accident. We assumed that the boost mode was caused by a misconnection on the board to the 10V power supply, but we cannot fully conclude the cause of the boost mode. The boost mode observations showed that it was capable for the whole circuit to enter boost mode, but because we could not recreate the test setup or have a significant reason for its occurrence, we could not affirm that the circuit was functional.

After the boost mode event, we found that the MPPT IC was limited in its functions due to more circuit design disagreements with the MPPT IC's datasheet. The MPPT IC was limited to only observe panel mode and buck mode waveforms. Figure 63 displays the set of PWM waveforms of the buck mode for the MPPT IC's pins LIA, HIA, LIB, HIB where buck leg of the DC-DC converter was driven by the LIA and HIA pins, and the boost leg was driven by LIB and HIB. Agreeing with our expected results, the actively switching waveforms had the same frequency of about 105 kHz, and the complementing waveforms have one switch ON and one switch OFF. In addition, we observed that the buck waveforms only appeared when the input voltage was above 5V and if we reduced the voltage after this threshold was reached, the waveform would become thinner until it reached around 2V where the waveform was at zero. Thus, the MPPT IC was also satisfying the criteria to buck the voltage. When we probed the driver IC, we found that the driver was either not producing the waveform at all or producing a waveform dissimilar to the MPPT IC waveforms. Thus, the DC-DC converter did not buck the input voltage and we saw about the same voltage values on the input and output.

(a) Pin LIA 100 kHz around 4.4 V

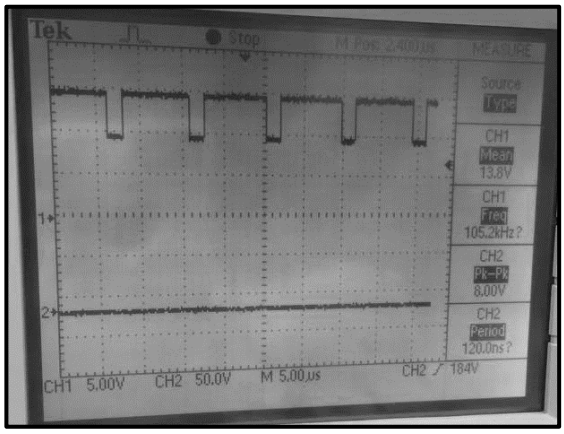

(b) Pin HIA 100Kz around 4.4 V

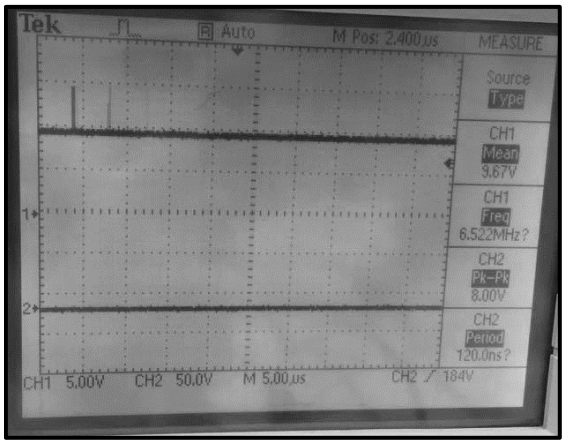

(c) Pin LIB ON

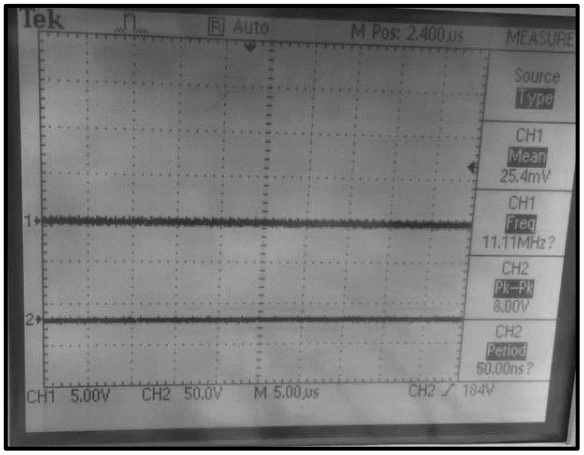

(d) Pin HIB OFF

Figure 63. Waveforms of Pins LIA, HIA, LIB, HIB on SM72445 IC

Before the last couple adjustments were made to the circuit (as noted in Appendix L), we determined that the MPPT IC was functional, but the driver IC was not producing the appropriate PWM waveforms. We determined that it was possible that the 10V rail and the 5V rail were not connected properly, potentially causing the boost mode event, and also preventing the boost mode to occur again. We found that to enter MPPT mode (not panel mode), there is an output current threshold that is supposed to be set but that the pin was not connected correctly for MPPT mode to occur. Thus, we assumed that due to the misconnections between components, we were able to enter MPPT mode. Also, we observed a "start-up" time when the circuit was first turned on, but we questioned if the soft start feature of the MPPT IC was truly working since we had no real measured data to prove our observation. Also from our log, we can see that there were many changes that were made to our circuit. The MPPT IC and driver IC datasheets did not clearly present information about to how to implement the driver and the IC

together in one circuit. The lack of clarity led to us questioning some of the connections that we soldered on the board between the two ICs. Although there was some soldering issues, we found that in general the IC was functional but the driver was not.

7.3 Findings and Conclusions

From our research, simulation, and testing, we found that implementing a portable MPPT solar charger is realizable and affordable. From our research we found that the Incremental Conductance algorithm would be the ideal algorithm for the solar charge controller system because INC performs more efficiently than Perturb and Observe from low (2V) to high (20V) voltages. For our implementation, we were limited to use an IC using a Perturb and Observe algorithm. Although this was not our recommendation for the algorithm, P&O was efficient and simple for our prototype implementation.

Also from our research, we found that in order to effectively use MPPT in the system, the system required using a DC-DC converter that would complement the MPPT algorithm. According to our research, a synchronous, non-inverting buck-boost converter was the DC-DC converter that is compatible with MPP and varying weather conditions on the panel. The synchronous, non-inverting buck-boost converter can provide the desire load voltage by taking in voltages above or below the load value. Thus, the buck-boost converter can handle dynamic input voltage variation due to fluctuating irradiance, temperature, and shading conditions seen by the PV panel. By simulating different DC-DC converter typologies as discussed Section 5, we confirmed our research finding that the non-inverting buck-boost converter was the most efficient converting power over most duty cycles. We suggest to design the DC-DC converter as a synchronous, non-inverting buck-boost converter for a successful MPPT implementation.

After designing and prototyping our proposed circuit design, we determined that an MPPT IC based circuit application was feasible, but we do not recommend using an MPPT IC unless the IC is researched in-depth. If provided more time for investigation and testing of our circuit, we should have been able to have the whole circuit functional. Still, we were able to show that the MPPT IC itself was functional. From our testing, we suggest that to integrate both the MPPT and driver IC requires extensive knowledge of how both the ICs should operate and how to connect them. Also, we suggest to build the application circuit on a PCB and with the recommended system design. We found that working with an MPPT IC would be more difficult to include INC algorithm and appropriate control system for the DC-DC converter. Nevertheless, the SM72445 IC and SM72295 IC were designed to work in the same circuit. Using the ICs is simpler than designing a whole MPPT solar charge controller because the driver and the control loop are already designed within the ICs.

In addition, from buying our components (including the two ICs), we estimated that for a PCB application of an MPPT charge controller would only cost around $5. The $5 implies manufacturing the PCB in large quantities, considering that most resistors and capacitors costs for PCBs are negligible and that most of the cost will come from the MPPT IC, the driver IC, inductors, and MOSFETs. For the MPPT solar charge controller to be sold with a PV panel, most companies would charge around $20 to $50 for the whole system. Comparatively, solar chargers without MPPT can cost $15-50, and usually MPPT solar charge controller without a PV panel is typically $50 or more. Thus, our MPPT solar charge controller for portable devices would be affordable compared to solar chargers lacking MPPT. Also, our MPPT solar charge controller design would be a returned investment because our design would provide more

efficient use of the PV panel, more time and power to charge a portable device, and less potential damage to the battery.

7.4 Summary

Although our proposed MPPT solar charge controller was not operational, we found that operating the Texas Instrument's SM72445 MPPT IC was at least possible under our time constraint. From our research and simulation results, we concluded that integrating MPPT with a synchronous non-inverting buck-boost converter would increase panel efficiency and power conversion efficiency. After testing our MPPT solar charge controller, we made the following suggestions:

- If using an MPPT IC in circuit design, contact the manufacturer to understand how the IC works and how it should be implemented with other IC's and components.
- Using a microcontroller instead of an MPPT IC is possible, but it would be more difficult to design the control and feedback circuitry and the MPPT algorithm.
- Employing an MPPT IC is a more convenient method to integrate MPPT into the solar charge controller system design.
- To effectively employ MPPT in solar charge controller for portable devices, a synchronous, non-inverting buck-boost converter is recommended because it can transfer power under dynamic input voltage conditions. However, the buck-boost converter is more difficult to control.

In considering our suggestions, an MPPT solar charge controller is feasible and affordable if implemented on a PCB board. Due to MPPT's affordability and increased efficiency under dynamic conditions, an MPPT solar charge controller for portable devices would be more effective than solar chargers currently sold without MPPT.

References

[1] *Analysis of Four DC-DC Converters in Equilibrium*. (2015, Jun 06). [Online]. Available: https://www.allaboutcircuits.com/technical-articles/analysis-of-four-dc-dc-converters-in-equilibrium/.

[2] *BU-409: Charging Lithium-ion*. (2017). [Online]. Available: http://batteryuniversity.com/learn/article/charging_lithium_ion_batteries.

[3] *BU-903: How to Measure State-of-charge*. (2016). [Online]. Available: http://batteryuniversity.com/learn/article/how_to_measure_state_of_charge.

[4] *Differences between Synchronous and Nonsynchronous Rectifying DC/DC Conversion*.(2015).[Online]. Available: http://micro.rohm.com/en/techweb/knowledge/dcdc/s-dcdc/02-s-dcdc/92.

[5] "The “MPPT vs. Non-MPPT” Graph," *Image,* 2017. Available: www.homepower.com.

[6] "The Right-Half-Plane Zero -- A Simplified Explanation," 2001.[Online]. Available: www.ti.com.

[7] *New Models for Photovoltaic Cells in Multisim*. (2014) [Online]. Available: https://forums.ni.com/t5/National-Instruments-Circuit/New-Models-for-Photovoltaic-Cells-in-Multisim/ba-p/3473652.

[8] SM72445 programmable maximum power point tracking controller with adjustable PWM frequency. [Online]. Available: http://www.ti.com/lit/ds/symlink/sm72445.pdf.

[9] J. Betten, "Benefits of a coupled-inductor SEPIC converter Balancing volt-microseconds," *Analog Applications Journal,* pp. 14- 17, 2011.

[10] B. Buckley. *MPPT - Maximum Power Point Tracking*. (2010). [Online]. Available: http://bryanwbuckley.com/projects/mppt.html.

[11] E. Coates. *Switched Mode Power Supplies*. (2016). [Online]. Available: http://www.learnabout-electronics.org/PSU/psu30.php.

[12] B. Conner, "LM3525,LM3622: A USB- Powered Lithium-Ion Battery Charger," *Application Brief,* 2001.

[13] B. Conner. A USB-powered lithium-ion battery charger. *Application Brief,* 2011. Available: http://www.ti.com/lit/an/snva520/snva520.pdf.

[14] R. A. Cullen, "What is Maximum Power Point Tracking (MPPT) and How does it Work," pp. 2, 2009.

[15] A. Durgadevi, S. Arulselvi and S. P. Natarajan. Photovoltaic modeling and its characteristics. 2011, Available: http://ieeexplore.ieee.org/document/5760162. DOI: 10.1109/ICETECT.2011.5760162.

[16] J. Falin, "Designing DC/DC converters based on SEPIC topology," *High- Performance Analog Products,* pp. 18-23, 2008.

[17] J. Falin and W. Li, "A solar-powered buck/boost battery charger," *High Performance Analog Products,* pp. 11, 2012.

[18] H. Fan. Design tips for an efficient non-inverting buck-boost converter. *Analog Applications Journal* pp. 20-25. 2014.

[19] V. J. Fesharaki *et al*, "The effect of temperature on photovoltaic cell efficiency " in *Proceedings of the 1stInternational Conference on Emerging Trends in Energy Conservation–ETEC, Tehran, Iran,* 2011, pp. 1-6.

[20] D. Freeman, "Introduction to Photovoltaic Systems Maximum Power Point Tracking," *Texas Instruments Application Report,* vol. 33, pp. 1508-1516, 2010.

[21] M. Green, "Design Calculations for Buck-Boost Converters," *Application Report,* 2012.

[22] A. Harish and M. V. D. Prasad. Microcontroller based photovoltaic MPPT charge controller. *Ijett 4(4),* pp. 1-4. 2013. Available: http://ijettjournal.org/volume-4/issue-4/IJETT-V4I4P304.pdf.

[23] C. Honsberg and S. Bowden. *Solar Cell Structure*. (2014). [Online]. Available: http://pveducation.org/pvcdrom/solar-cell-structure.

[24] C. Honsberg and S. Bowden. *Absorption of Light | PVEducation*. (2014). [Online]. Available: http://pveducation.org/pvcdrom/absorption-of-light.

[25] K. Ishaque, Z. Salam and G. Lauss. The performance of perturb and observe and incremental conductance maximum power point tracking method under dynamic weather conditions. *Applied Energy 119*pp. 228-236. 2014. Available: http://dx.doi.org/10.1016/j.apenergy.2013.12.054.

[26] Jaw-Kuen Shiau, Chun-Jen Cheng and Ching-En Tseng, "Stability analysis of a non-inverting synchronous buck-boost power converter for a solar power management system," in 2008, pp. 263-268.

[27] S. Keeping. *The SEPIC Option for Battery-Power Management | DigiKey*. (2014, Aug 19). [Online].Available: http://www.digikey.com/en/articles/techzone/2014/aug/the-sepic-option-for-battery-power-management.

[28] S. Keeping. *Voltage- and Current-Mode Control for PWM Signal Generation in DC-to-DC Switching Regulators*. (2014, Oct). Available: http://www.digikey.com/en/articles/techzone/2014/oct/voltage-and-current-mode-control-for-pwm-signal-generation-in-dc-to-dc-switching-regulators.

[29] S. Keeping. *Techniques to Limit Switching DC/DC Converter Inefficiency During Low Loads*. (2012, Jul 3). [Online]. Available: https://www.digikey.com/en/articles/techzone/2012/jul/techniques-to-limit-switching-dcdc-converter-inefficiency-during-low-loads.

[30] S. Keeping. *The Difference Between Switching Regulator Continuous and Discontinuous Modes and Why It's Important*. (2014, Dec 02). [Online]. Available: https://www.digikey.com/en/articles/techzone/2014/dec/the-difference-between-switching-regulator-continuous-and-discontinuous-modes-and-why-its-important.

[31] R. Mammano, "Switching Power Supply Topology Voltage Mode vs. Current Mode," *Design Note,* 1994.

[32] C. E. Mullett, "An Efficient Nonisolated DC-DC Converter and a Review of the More Common Topologies, 2003".

[33] M. Pomar *et al*. Integrated design and control applied to a buck boost converter. 2007, Available: http://ieeexplore.ieee.org/document/7068959.

[34] Ray Ridley, "Analyzing the Sepic Converter," pp. 14-18, November. 2006.

[35] E. Rogers, "Understanding Buck-Boost Power Stages in Switch Mode Power Supplies," *Application Note,* Nov, 2012.

[36] M. Rosu-Hamzescu and S. Oprea. Practical guide to implementing solar panel MPPT algorithms. *Application Report* 2013.
Available: http://ww1.microchip.com/downloads/en/AppNotes/00001521A.pdf.

[37] B. Sahu and G. A. Rincon-Mora. A low voltage, dynamic, noninverting, synchronous buck-boost converter for portable applications. *Tpel 19(2),* pp. 443-452. 2004.
Available: http://ieeexplore.ieee.org/document/1271328. DOI: 10.1109/TPEL.2003.823196.

[38] A. Scheurer *et al*, "Photovoltaic MPPT charge controller," 2012.

[39] D. Sera *et al*. Improved MPPT algorithms for rapidly changing environmental conditions. 2006,
Available: http://ieeexplore.ieee.org/document/4778635. DOI: 10.1109/EPEPEMC.2006.4778635.

[40] J. Shiau and C. Cheng. Design of a non-inverting synchronous buck-boost DC/DC power converter
with moderate power level. *Robotics and Computer-Integrated Manufacturing 26(3),* pp. 263–267. 2010. Available: http://www.sciencedirect.com/science/article/pii/S0736584509001148. DOI: 10.1016/j.rcim.2009.11.007.

[41] C. Simpson, "Battery Charging," *Application Report,* 2011.

[42] E. Torres, "State feedback control of a DC-DC converter for MPPT of a solar
PV module," Wordpress, Logan, UT, 2017.

[43] J. Tucker, "Understanding output voltage limitations of DC/DC buck converters," *Analog Applications Journal, 2017*.

[44] R. Vujanic, S. Mariethoz and M. Morari, "Design and Control of a Buck-Boost DC-DC Power Converter," 2008.

Appendix A: General Power Stage Component Calculations

To observe discrete differences in the component implementation for a buck-boost circuits and SEPIC converter, equations derived for determining component values for both typologies are presented in Table 21. The equations for buck-boost is to calculate the power stage of a non-inverting buck-boost, and the equations for SEPIC is to calculate the power stage of a SEPIC converter. These equations and further discussion of the equations can be found in Reference 21 and Reference 16.

Component Consideration	Buck-Boost Equation	SEPIC Equation
Duty Cycle	$D_{Buck} = \frac{(V_{out} * \eta)}{(V_{in\,min})}$ $D_{Boost} = \frac{(V_{in\,min} * \eta)}{(V_{out})}$	$D = \frac{(V_{out} + V_{diode})}{(V_{out} + V_{in} + V_{diode})}$
Inductor	$L_{Buck} = \frac{V_{out} * (V_{in\,max} - V_{out})}{I_{ripple} * f_{switching} * V_{in\,max} * I_{out}}$ $L_{Boost} = \frac{V_{in\,min}^2 * (V_{out} + V_{in\,max})}{I_{ripple} * f_{switching} * V_{out}^2 * I_{out}}$	$L_{1a\,min} = L_{1b\,min} = \frac{1}{2} \frac{V_{out} * (D_{max})}{I_{ripple} * f_{switching}}$
Input Capacitor	Based on data sheet, RMS Current rating, and ripple voltage : $I_{Cin(rms)} = \frac{L_{input}}{\sqrt{12}}$	Based on data sheet, RMS Current rating, and ripple voltage : $I_{Cin(rms)} = \frac{L_{input}}{\sqrt{12}}$
Output Capacitor	$C_{out\,\min\_buck} = \frac{I_{ripple} * I_{out}}{8 * f_{switching} * V_{out\,ripple}}$ $C_{out\,\text{overshoot}\_buck} = \frac{(I_{ripple} * I_{out})^2}{2 * V_{out} * V_{out\,ripple}}$ $C_{out\,\min\_boost} = \frac{I_{out} * D_{\max\,boost}}{f_{switching} * V_{out\,ripple}}$	$C_{out} \geq \frac{I_{out} * D_{max}}{V_{ripple} * f_{switching}}$

Table 21. Key Parameters that Characterize Buck-Boost Converters and SEPIC Converters [16, 21]

Where:

- $V_{in\,max}$ = maximum input voltage
- V_{out} = desired output voltage
- I_{out} = desired maximum output current
- $f_{switching}$ = switching frequency of converter
- L = value of inductor
- $L_{1a\,min}$ = minimum inductance of first inductor of coupled inductor
- $L_{1b\,min}$ = minimum inductance of second inductor of coupled inductor

- D = duty cycle: the maximum occurs at $V_{in\,min}$; minimum occurs at $V_{in\,max}$
- I_{ripple} = ripple current across inductor; value usually chosen between 20% to 40% of input current at worst case efficiency
- V_{ripple} = ripple voltage across capacitor, there is a ripple voltage across both the input and output capacitors
- C_{out} = output capacitor: $C_{out\,\min\_buck}$ is the minimum output capacitance required; $C_{out\,\text{overshoot}\_buck}$ is the minimum output capacitnce required for desired overshoot

Appendix B: Increasing Efficiencies at Low Loads

Battery-powered, portable devices tend to be in standby or sleep mode to save energy; however, at these low currents, the DC-DC converter is relatively inefficient and causes the power saving modes to be an insufficient application.

The efficiency of a DC-DC converter in relation to loads is illustrated in Figure 64. From Figure 64, the loads are divided into 3 parts: High load, Light Load, and Very Light Load. In High Load, the power losses are caused by high conduction losses from the load current. In Light Load, the power losses are caused by current-ripple conduction losses and switching losses from V-I overlap due to high frequency switching. In very light load, power losses are mainly due to current ripple.

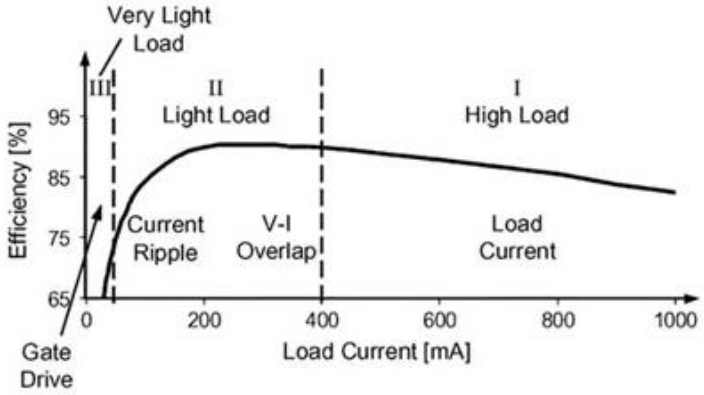

Figure 64. Efficiency Curve of a DC-DC Converter [28]

There are design techniques that can be implemented in converter modules that can extend battery life that efficiently address low load operation such as soft switching, and discontinuous operation. Techniques about limiting switching DC/DC converter inefficiencies from Reference 28 is discussed in Table 22.

Technique/ Feature	**Description**
Discontinuous Operation: Synchronous Rectification	Synchronous rectification is a MOSFET-based switching converter design. Synchronous rectifier switch opens when the main switch is closed and the other way around. To prevent cross conduction (both switches are ON simultaneously), only one switch must turn OFF before the other switch turns ON. A diode is still required to conduct during “dead time” or the interval when switching occurs. When used in synchronous operation, current flows from source to drain so that the diode can conduct during the dead time. When “dead time” interval is done, current flows through MOSFET. Since MOSFET has low channel resistance, the forward drop of the rectifying diode is reduced to millivolt; thus, the peak efficiency increases to 90%.
Soft Switching : Zero Voltage Switching	When the switch is turning On, the switch voltage is first dropped to zero before applying the gate voltage which creates a zero-loss transition. To turn OFF the switch, a parallel capacitor is used to suppress voltage spikes and enable low loss transition. Soft switching is a preferred application for high frequency switching MOSFETs. Soft switching limits inefficiency during low and very load lows because it prevents overlap losses by switching the MOSFET only when it is at zero voltage or current. Soft switching limiting improves efficiency and lowers EMI to allow high frequency operation.

Table 22. Descriptions of Two Techniques for Reducing DC-DC Converter Inefficiencies during Low Loads

Appendix C: Voltage Mode vs. Current Mode Checklist

The following checklist is used to help determine which method of control should be implemented in a design based on the characteristics of Voltage-Mode Control and Current-Mode Control. The list in Table 23 was modified from Reference 31.

Current Mode	Voltage Mode
➢ Power supply output will be used as current source or very high output voltage. ➢ Given a switching frequency, requires fastest dynamic response ➢ Application is for a DC/DC converter with relatively constrained input voltage ➢ Modular applications requiring parallel load sharing ➢ Push-pull circuits that require transformer flux balancing ➢ Low-cost applications using least amount of components	➢ Wide input line and/or output load variations ➢ Light load conditions where current ramp is insufficient to provide stable PWM operation. ➢ High power and/or noisy applications ➢ Multiple output voltages with cross-regulation ➢ Saturable reactor controllers used as auxiliary secondary-side regulators ➢ Applications that cannot afford the complexities of dual feedback loops and/or slope compensation.

Table 23. Checklist for Systems to Employ Current Mode or Voltage Mode 31.

Appendix D: Difference between Synchronous Rectification and Non-synchronous Rectification

Non-isolated buck-boost has two typologies: synchronous rectification and non-synchronous rectification.

- *Rectification*: driving the current in a specific direction (Alternate current is made usable for direct current requirement)
- Efficiency comparison:
  - Nonsynchronous: 80%
  - Synchronous: 95%
- Synchronous has higher efficiency which is better for battery-power applications

A detailed comparison of both typologies is provided in Table 24.

Nonsynchronous Rectification	**Synchronous Rectification**
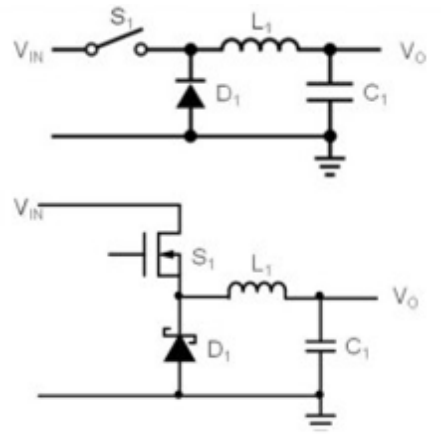 Figure 65a. Circuit Representation of Nonsynchronous Rectification [4]	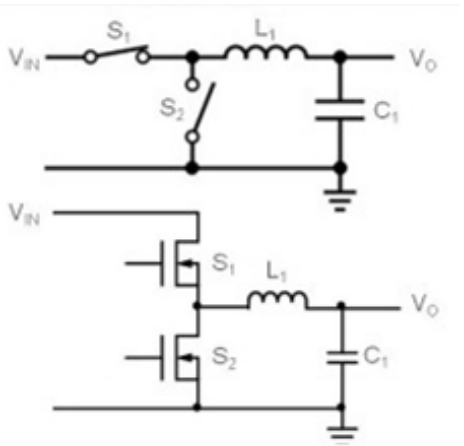 Figure 65b. Circuit Representation of Synchronous Rectification [4]
Operation: • S1 is transistor, D1 is Schottky diode • S1 =ON, no current in D1 (OFF) • S1 = OFF, forward current in D1 (ON)	Operation: • S1 and S2 are transistors • S1 = ON, S2 =OFF • S1 = OFF, S2 = ON
Advantages & Limitations • Current flow dictated by S1 • More simple circuit • Less efficiency	Advantages & Limitations • Current path same as nonsynchronous, but requires control circuit to dictate current flow • More complex circuit and control: requires dead time • Achieve higher efficiency because by using MOSFET for low side switch, can eliminate

	conduction losses from a diode and allows optimal timing control
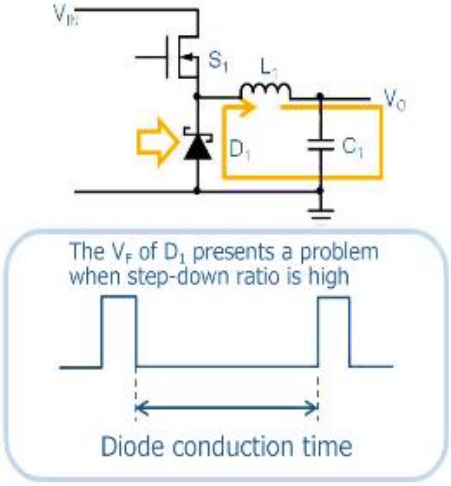 Figure 66a. Diode Conduction Operation [4]	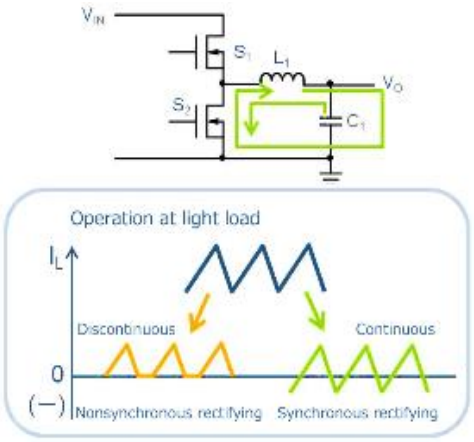 Figure 66b. Synchronous Rectification and Nonsynchronous Waveforms [4]

<u>Losses and Efficiencies</u>
• When Step-down ratio = high, D1 = long conduction time
• Diode losses due to forward voltage (V_F) which increases with current:
  ○ $I = Is * e\text{^}(V_F/nV_T)$
• During 90% period, operation produces loss = V_F (ex. 0.5V loss relative to 1.5V output)
• In light loads, enters discontinuous conduction mode, current goes to zero
	<u>Losses and Efficiencies</u>
	• Under light load, inductor current = 0A
	• Transistor losses due to saturation voltage (on-resistance) = 50mΩ
	  ○ 50mV at 1A, much lower than forward voltage of diode
	• For high step down ratio (ex. 12V to 1.5V), on-time for S2 is longer, about 90% of cycle
	• In light load, remains in continuous conduction mode because it can create reverse flows so that current in negative region still operates instead of going to zero
	• Continuous mode creates ringing in switching voltage, producing harmonic noise
	• Efficiency loss due to reserve current flow from output capacitor

Table 24. Differences Between Non-Synchronous Rectification and Synchronous Rectification [4]

Appendix E: Discontinuous Conduction Mode

Discontinuous operation typically occurs at low loads when the inductor current reaches zero. The point at which the inductor current reaches zero can be calculated. Once calculated, a condition is set when a discontinuous event occurs as seen in Figure 67a and Figure 67b, and in Equation 17 and Equation 18 for buck mode and boost mode, respectively. Buck and boost modes enter DCM similarly and experiences similar loss in efficiency:

- MOSFET =ON, inductor current increases
- MOSFET = OFF, inductor current decreases similarly to CCM, but since output current is low due to low load, inductor current approaches zero
- Ringing occurs due to inductor resonance from stray diode and switch capacitance reducing efficiency [30]

However, boost mode has a different threshold for entering DCM due to boost requiring a different duty cycle than buck. The Table 25 provides the condition to enter DCM for each operational mode and its corresponding waveform.

Buck (DCM)	**Boost (DCM)**
Condition to enter DCM: $I_{out} < V_{out}(1 - \left(\frac{V_{out}}{V_{IN}}\right))/2Lf$ (17)	Condition to enter DCM: $I_{out} < \frac{V_{in}^2(V_{out}-V_{IN})}{V_{in}^2} * 2Lf$ (18)
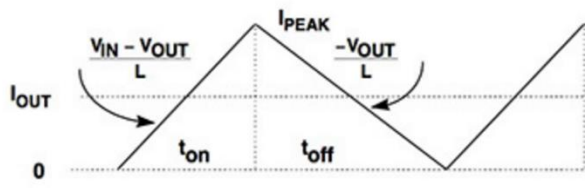 Figure 67a. Waveform of Buck when Inductor current Reaches Zero	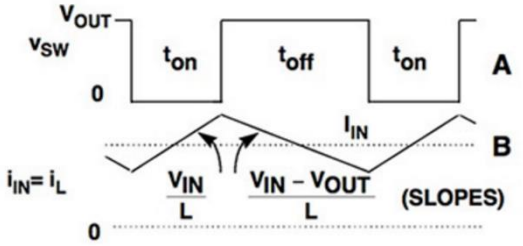 Figure 67b.Waveform of Boost when Inductor current Reaches Zero

Table 25. Characteristics of Buck and Boost during DCM [30]

Appendix F: MPPT IC Comparison Chart

After we established specific criteria for our ideal system, we applied the specifications to an IC (integrated circuit) application. In Table 26 is our research and comparison of different MPPT ICs. By using the comparison chart we determined an IC that was most compatible with our ideal system requirements. We both ranked all of the IC's with 1 being the most compatible and 6 being the worst compatible. We also had a set of questions as a ranking criteria which is also based on the system requirements:

- Within wide input voltage range (2V- 23V)?
- MPPT algorithm programmable?
- Switching Frequency Range (at least above 100kHz)?
- Synchronous Rectification (implies four switch buck boost)?
- Within output current in range (< 5A)?
- Current mode control?
- Handles over-current, over-voltage, and battery charging compatible?

The MPPT Design Name highlighted green is the selected IC we chose for our application.

MPPT Design Name	**Advantages**	**Concerns**	**Features**	**Link**
LT8490 - High Voltage, High Current Buck-Boost Battery Charge Controller with Maximum Power Point Tracking (MPPT) **Ranking:** **Nikki- Rank 2** **Joe- Rank 3**	• Buck boost typology • Synchronizable Fixed Frequency: 100kHz to 400kHz • Four Integrated Feedback Loops • Input and Output Current Monitor Pins	• Vin minimum is 6V, which is kinda high for what we need. • No Software or Firmware Development Required (fixed software) • Uses P&O	• V_{IN} Range: 6V to 80V • Single Inductor Allows V_{IN} Above, Below, or Equal to V_{BAT} • VBAT Range: 1.3V to 80V • Automatic MPPT for Solar Powered Charging • Automatic Temperature Compensation • Operation from Solar Panel or DC Supply • constant-current constant-voltage (CCCV) charging profile for lithium-ion • STATUS and FAULT pins containing charger information can be used to drive LED indicator lamps • device is available in a low profile (0.75mm) 7mm × 11mm 64-lead QFN package	http://www.linear.com/product/LT8490

LTC4020 - 55V Buck-Boost Multi-Chemistry Battery Charger **Ranking:** **Nikki- Rank 3** **Joe- Rank 2**	• 4.5V to 55V • Adjustable to different battery charging voltages based on reference voltage • Synchronous Buck-Boost DC/DC Controller • Input Voltage Regulation for High Impedance Input Supplies and Solar Panel Peak Power Operation • Maximum battery charge current is programmable • Power Path: VOUT powers both the linear battery charger and the system load with priority going to the system load • Program Switching Frequency: 50KHz to 500KHz.	• Needs at least 4.5V to turn on • MPPT based on Input Voltage Regulation Reference	• Li-Ion and Lead-Acid Charge Algorithms • ±0.5% Float Voltage Accuracy • ±5% Charge Current Accuracy • Instant-On for Heavily Discharged Batteries • Ideal Diode Controller Provides Low Loss PowerPath When Input Power is Limited • Onboard Timer for Protection and Termination • Bad Battery Detection with Auto-Reset • NTC Input for Temperature Qualified Charging • Binary Coded Open-Collector Status Pins • Low Profile (0.75mm) 38-Pin 5mm × 7mm QFN Package	http://www.linear.com/product/LTC4020
Ultra Low Power Harvester Power Management IC with Boost Charger, and Nanopower Buck Converter **Ranking:** **Nikki- Rank 6** **Joe- Rank 6**	• -0.3V to 5.5V is a good low end range for PV output voltage • Low power • Switching MOSFETs are internal. • Continuous Energy Harvesting From VIN as Thermoelectric Generator (TEG) Harvesting low as 100 mV • Programmable MPPT	• Not enough on the high range • Overall good if we had a way to accommodate voltages >5.5V.	• Battery Good Output Flag • Battery Charging and Protection • Energy can be Stored to Re-chargeable Li-ion Batteries, Thin-film Batteries, Supercapacitors, or Conventional Capacitors • Full Operating Quiescent Current of 488 nA • Cold-start Voltage: VIN ≥ 330 mV • designed to • efficiently extract microwatts (µW) to milliwatts (mW) generated from a variety of high output impedance DC sources like photovoltaic	http://www.ti.com/lit/ds/symlink/bq25570.pdf

Programmable Maximum Power Point Tracking Controller with Adjustable PWM Frequency **Ranking:** **Nikki- Rank 1** **Joe- Rank 1**	• programmable with I2C (the output voltage can be set) • Drives 4-switch PWM with single inductor • 110kHz,135kHz or 215kHz PWM operating frequency • Programmable maximum power point tracking	• Does require 5V source to run IC however. • We would have to somehow get 5V out of the PV at all times or have some other way to power it.	• Renewable Energy Grade • Panel Mode pin for optional bypass switch control • Photovoltaic solar panel voltage and current diagnostic • Output overvoltage protection • Over-current protection • efficiencies up to 99.5% • include maximum output voltage and current • programmable settings for slew rate, soft-start and Panel Mode	http://www.ti.com/product/sm72445?keyMatch=mppt%20controller&tisearch=Search-EN-Products
Ultra low power energy harvester and battery charger with embedded MPPT and LDOs **Ranking:** **Nikki- Rank 4** **Joe- Rank 5**	• Ideal voltage range of 0.5V to 18V • Programmable MPPT by external resistors • Fully integrated buck-boost DC-DC converter	• Limited output battery charging current to only 70mA • Not sure if synchronous typology	• High efficiency for any harvesting source • 2.2 V to 3.6 V trimmable battery discharge voltage level (± 1% accuracy) • Two fully independent LDOs (1.8 V and 3.3 V output) • 2.6 V to 5.3 V trimmable battery charge voltage level (± 1% accuracy) • Enable/disable LDO (low dropout regulator) control pins • Battery disconnect function for battery protection • Battery connected and ongoing charge logic open drain indication pins	http://www.st.com/en/power-management/spv1050.html
Semtech TS52001 Li-Ion Battery Chargers **Ranking:** **Nikki- Rank 5**	• Up to 1.5A of continuous output current in Constant Current (CC) mode • User programmable charging current • synchronous switching Li-ion Battery Charger	• Vin range: 4V to 8.1V • temperature independent photovoltaic (MPPT-Lite™) calculator to	• Utilizes a temperature-independent • PV MPPT-Lite™ regulation scheme • V_{OUT} reverse current blocking • Programmable temperature-compensated termination voltage with ±1% tolerance • High efficiency - up to 92% at typical load • Current mode PWM control in constant	http://www.mouser.com/new/semtech/semtech-ts52001/

Joe- Rank 4	• fully integrated power switches • Synchronous typology	optimize power output • switching frequency of 1MHz (facilitates low-cost LC filter combination)	voltage • Supervisor for V_{BAT} reported at the nFLT pin • Input supply under voltage lockout • Full protection for over-current, over-temp, V_{BAT} over-voltage, and charging timeout • Charge status indication • I^2C program interface with EEProm registers	Datasheet: http://www.mouser.com/ds/2/413/TS52001-1124.pdf

Table 26. Comprehensive Comparison between Different MPPT Integrated Circuits with Group Member's Ranking of Each Integrated Cirucit

Appendix G: Component Selection Calculation Sheet

Table 27 displays our calculation worksheet performed in excel. We determined the component values based on the equations and information provided by the SM72442 datasheet, and Texas Instrument Solar Magic Evaluation Board Application Note.

						Legend						
PV Characteristics		units		**Full Buck/ Boost Duty Cycles [1]**			Insert Value					
Pmax [2]	7	W		D buck min [3]	0.7122507123		Buy					
Voc min [4]	8	V		D buck max [5]	0.7286956522		important Calculated					
Vocmax [6]	9	V										
Vmppt min [7]	6.24	V		**Inductor L1 [8]**	0.000100589392	0.000100589392	**max inductor rip**	0.5318138651	0.5318138651	**Inductor Peak Current**	1.48413625	
Vmppt max [11]	7.02	V		L1 buck	0.000020150510	H	Ipp max buck	0.168272501	A	Ipk buck	1.48413625	1.48413625
Isc max [12]	0.96	A		L1 boost	0.000100589392	H	Ipp max boost	0.5318138651	A	Ipk boost	1.387701804	A
Impp min [13]	1.121794872	A		**Input Capacitor [14]**			**Capacitor Voltage rating [15]**					A
Impp max [16]	0.9971509972	A		Cin	9.608879225	uF	V_rating_cin	9	V			
Iout max [17]	1.4	A		**Output Capacitor [18]**			V_rating_cout	23	V			
Vin min	2	V		Cout	0.989838241	uF						
Vout max [19]	23	V										
Vout min [20]	5	V		**Power MOSFET Switches [21]**								
ΔVin p-p [22]	0.3	V			Voltage Rating [23]		Peak current [24]		RMS Current			
ΔVout p-p [25]	0.25	V		Q1 [26]	9	V	1.48413625	A		A		
Fsw min [27]	85000	Hz		Q2 [28]	9	V	1.48413625	A	0.750991747	A		
Fsw max	125000	Hz		Q3 [29]	23	V	1.48413625	A		A		
				Q4 [30]	23	V	1.48413625	A	0.5843079929	A		
					RMS Current [31]		**RMS Compared Values**					
				Q1 buck	1.181529262	A	1.181529262					
				Q1 boost	1.121794872	A						
				Q3 buck	1.4	A	1.4					
				Q3 bost	0.9576052965	A						
				Output Bypass Diode [32]			**PM Switch [33]**					
				V_rating_ D1 [34	23		*V rating [35]*	23	*Current Rating [36]*			
				I_rating_D1 [37]	1.4		Q5A		0.96			
							Q5B		0.96			
					Maximum output voltage (A0) [38]			**Maximum Output Current (A4) [39]**				
Configuring A0, A2, A4, A6					Vout_max	5	V		3.571428571			
RFB1	40000				Actual	1.68	V	Actual	3.6	V		
RFB2 [40]	20000	Ohms			**Condition to Enter Panel mode (A2) [41]**			**Output Voltage Slew Rate / PM c**		V		
RT1 [43]	10000	Ohms				3.448275862	V		4.697986577			
RB1	5000	Ohms			Actual	3.46	V	Actual	4.71	V		
RT2	4500	Ohms			**Built-In Current Sense Amplifier**			Vin	5	V		
RB2	10000	Ohms			I_max (A)	1.5	I_max (A)	1.5		V		
RT3	4000	Ohms			R_Sense	0.1	R_Sense	0.1				
RB3	10000	Ohms			R3 (Ohm)	500	R3 (Ohm)	500				
RT4	4500	Ohms			R6 (Ohm)	4700	R6 (Ohm)	4700				
RB4	70000	Ohms			Gain (V/V)	9.4	Gain (V/V)	9.4				

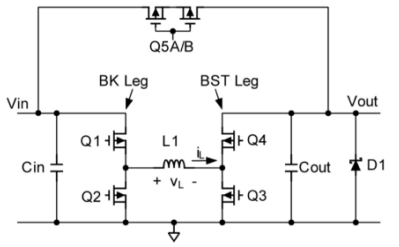

Figure 5. Buck-and-Boost Converter Topology With Panel Mode Switch

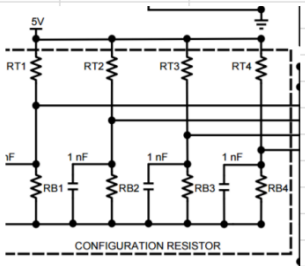

Table 27. Component Calculation Excel Sheet

Appendix H: Buck Converter Simulation Data

The simulated buck converter output voltage was measured at duty cycle (D1) increments of 0.1 from 0 to 1. The output voltage was compared to the input voltage to determine the gain of the converter. All gains were less than or equal to 1 indicating buck operation. Voltages were measured using the oscilloscope tool in NI Multisim 13.0 after a runtime of 5ms. Table 28 presents the data of the buck converter simulation.

D1	VIN (V)	VOUT (V)	Expected Gain (V/V)	Actual Gain (V/V)	Error
0	7	0	0	0	#DIV/0!
0.1	7	1.013	0.1	0.1447142857	44.71428571
0.2	7	2	0.2	0.2384285714	19.21428571
0.3	7	2.574	0.3	0.3677142857	22.57142857
0.4	7	3.305	0.4	0.4721428571	18.03571429
0.5	7	4.027	0.5	0.5752857143	15.05714286
0.6	7	4.752	0.6	0.6788571429	13.14285714
0.7	7	5.093	0.7	0.7275714286	3.93877551
0.8	7	5.817	0.8	0.831	3.875
0.9	7	6.248	0.9	0.8925714286	0.8253968254
1	7	7	1	1	0

Table 28. Buck Converter Simulation Expected Gain vs. Actual Gain

Appendix I: Boost Converter Simulation Data

The simulated boost converter output voltage was measured at duty cycle (D1) increments of 0.1 from 0 to 1. The output voltage was compared to the input voltage to determine the gain of the converter. All gains were greater than or equal to 1 indicating boost operation. Voltages were measured using the oscilloscope tool in NI Multisim 13.0 after a runtime of 5ms. Table 29 presents the data of the boost converter simulation.

D1	VIN (V)	VOUT (V)	Expected Gain (V/V)	Actual Gain (V/V)	Error
0	7	6.645	1	0.9492857143	5.071428571
0.1	7	7.089	1.111111111	1.012714286	8.855714286
0.2	7	8.549	1.25	1.221285714	2.297142857
0.3	7	9.705	1.428571429	1.386428571	2.95
0.4	7	11.436	1.666666667	1.633714286	1.977142857
0.5	7	13.525	2	1.932142857	3.392857143
0.6	7	17.021	2.5	2.431571429	2.737142857
0.7	7	20.402	3.333333333	2.914571429	12.56285714
0.8	7	30.88	5	4.411428571	11.77142857
0.9	7	30.945	10	4.420714286	55.79285714
1	7	0.406	#DIV/0!	0.058	#DIV/0!

Table 29. Boost Converter Simulation Expected Gain vs. Actual Gain

Appendix J: Cascaded Boost-Buck Converter Simulation Data

The simulation model of the cascaded boost-buck converter was tested in two different modes, boost and buck. For boost mode, duty cycle, D2, was held at 1 and D1 was varied by 0.1 increments between 0 and 1. For buck, D1 was held at 0 and D2 was incremented by 0.1 intervals between 0 and 1. The output voltage for each test was compared to the input voltage supplied by the Multisim Advanced PV Panel Model. The input and output power values were also measured using Multisim's wattmeter tool. All measurements were taken after a runtime of 5ms. Table 30 presents the data of the boost converter simulation.

D1	D2	Mode	Vin (V)	Vout (V)	Expected Gain (V/V)	Actual Gain (V/V)	Error	P_IN (W)	P_OUT (W)	Efficiency (%)
0	1	Boost	8.084	7.687	1	0.9509	4.911	2.08	1.97	94.71
0.1	1	Boost	7.901	8.61	1.111	1.0897	1.923807113	2.607	2.471	94.78
0.2	1	Boost	7.911	9.49	1.25	1.1996	4.032360005	3.166	3.002	94.82
0.3	1	Boost	7.722	10.473	1.429	1.3563	5.062160062	3.856	3.656	94.81
0.4	1	Boost	7.364	11.454	1.667	1.5554	6.675719718	4.623	4.373	94.59
0.5	1	Boost	5.264	10.8	2	2.0517	2.583586626	4.187	3.887	92.83
0.6	1	Boost	4.122	10.516	2.5	2.5512	2.047549733	3.999	3.712	92.82
0.7	1	Boost	1.268	5.804	3.333	4.5773	37.31861199	1.34	1.124	83.88
0.8	1	Boost	0.501	3.383	5	6.7525	35.0499002	0.547	0.381	69.65
0.9	1	Boost	0.214	1.279	10	5.9766	40.23364486	0.183	0.055	30.05
1	1	Boost	0.105	0.0025	#DIV/0!	0.0238	#DIV/0!	0.101	0	0
0	0	Buck	8.532	0	0	0	#DIV/0!	0	0	#DIV/0!
0	0.1	Buck	8.519	1.216	0.1	0.1427	42.73975819	0.068	0.054	79.41
0	0.2	Buck	8.499	2.122	0.2	0.2497	24.83821626	0.174	0.15	86.21
0	0.3	Buck	8.48	2.904	0.3	0.3425	14.1509434	0.301	0.269	89.37
0	0.4	Buck	8.464	3.432	0.4	0.4055	1.370510397	0.464	0.419	90.3
0	0.5	Buck	8.348	4.451	0.5	0.5332	6.636320077	0.678	0.636	93.81
0	0.6	Buck	8.338	5.227	0.6	0.6269	4.481490365	0.972	0.907	93.31
0	0.7	Buck	8.323	5.803	0.7	0.6972	0.39649165	1.24	1.148	92.58
0	0.8	Buck	8.219	6.557	0.8	0.7978	0.276797664	1.522	1.434	94.22
0	0.9	Buck	8.141	7.245	0.9	0.8899	1.117798796	1.851	1.749	94.49
0	1	Boost	8.084	7.687	1	0.9509	4.910935181	2.08	1.97	94.71

Table 30. Buck-Boost Converter Simulation Expected Gain vs. Actual Gain

Appendix K: Full-Bridge Converter Simulation Data

The simulated full-bridge converter circuit was tested at all combinations of duty cycles D1 and D2. The duty cycles were varied between 0 and 1 in 0.1 increments. Input and output power was measured using Multisim's wattmeter tool, and all measurements were taken after a runtime of 3ms. Table 31 presents the data of the full-bridge converter simulation.

D1	D2	Mode	V_IN (V)	V_OUT (V)	Meas. Gain (V/V)	Expected Gain (V/V)	Gain Error (%)	P_IN (W)	P_OUT (W)	Efficiency (%)
0	0	Boost	8.53	0	0	#DIV/0!	#DIV/0!	0	0	#DIV/0!
0.1	0	Boost	7.4	0	0	#DIV/0!	#DIV/0!	-4.188	0	0
0.2	0	Boost	1.439	0	0	#DIV/0!	#DIV/0!	-1.817	0	0
0.3	0	Boost	1.119	0	0	#DIV/0!	#DIV/0!	-1.295	0	0
0.4	0	Boost	0.645	0	0	#DIV/0!	#DIV/0!	-0.848	0	0
0.5	0	Boost	0.283	0	0	#DIV/0!	#DIV/0!	-0.411	0	0
0.6	0	Boost	0.308	0	0	#DIV/0!	#DIV/0!	-0.343	0	0
0.7	0	Boost	0.161	0	0	#DIV/0!	#DIV/0!	-0.228	0	0
0.8	0	Boost	0.161	0	0	#DIV/0!	#DIV/0!	-0.182	0	0
0.9	0	Boost	0.117	0	0	#DIV/0!	#DIV/0!	-0.132	0	0
1	0	Boost	0.115	0	0	#DIV/0!	#DIV/0!	-0.11	0	0
0	0.1	Buck	8.53	0	0	0	#DIV/0!	-0.145	0	0
0.1	0.1	Boost	8.229	5.698	0.69	1	30.76	1.538	1.087	70.68
0.2	0.1	Boost	6.864	9.918	1.44	2	27.75	4.699	3.247	69.1
0.3	0.1	Boost	3.135	7.751	2.47	3	17.59	2.883	2.02	70.07
0.4	0.1	Boost	2.361	7.033	2.98	4	25.53	2.405	1.649	68.57
0.5	0.1	Boost	1.537	5.802	3.77	5	24.5	1.755	1.104	62.91
0.6	0.1	Boost	1.198	4.914	4.1	6	31.64	1.28	0.803	62.73
0.7	0.1	Boost	0.689	4.143	6.01	7	14.1	0.854	0.571	66.86
0.8	0.1	Boost	0.616	3.207	5.21	8	34.92	0.593	0.343	57.84
0.9	0.1	Boost	0.498	3.164	6.35	9	29.41	0.476	0.334	70.17
1	0.1	Boost	0.422	2.954	7	10	30	0.403	0.294	72.95
0	0.2	Buck	8.53	0	0	0	#DIV/0!	0.145	0	0
0.1	0.2	Buck	8.442	3.654	0.43	0.5	13.43	0.488	0.441	90.37
0.2	0.2	Boost	8.112	7.541	0.93	1	7.04	2.027	1.899	93.69
0.3	0.2	Boost	7.996	8.348	1.04	1.5	30.4	2.496	2.336	93.59
0.4	0.2	Boost	7.21	11.02	1.53	2	23.58	4.332	4.043	93.33
0.5	0.2	Boost	6.374	11.822	1.85	2.5	25.81	5.024	4.686	93.27
0.6	0.2	Boost	5.199	11.531	2.22	3	26.07	4.777	4.458	93.32
0.7	0.2	Boost	3.806	10.05	2.64	3.5	24.56	3.641	3.406	93.55
0.8	0.2	Boost	2.453	7.896	3.22	4	19.53	2.41	2.097	87.01
0.9	0.2	Boost	2.507	8.167	3.26	4.5	27.61	2.364	2.234	94.5
1	0.2	Boost	2.277	7.924	3.48	5	30.4	2.227	2.1	94.3
0	0.3	Buck	8.53	0	0	0	#DIV/0!	0	0	#DIV/0!
0.1	0.3	Buck	8.501	2.215	0.26	0.33333333	21.83	0.169	0.163	96.45
0.2	0.3	Buck	8.205	6.819	0.83	0.66666666	-24.66	1.633	1.552	95.04
0.3	0.3	Boost	8.118	7.629	0.94	1	6.02	2.055	1.955	95.13
0.4	0.3	Boost	7.678	9.807	1.28	1.33333333	4.2	3.372	3.197	94.81
0.5	0.3	Boost	6.756	11.72	1.73	1.66666666	-4.09	4.903	4.648	94.8

D1	D2	Mode	V_IN (V)	V_OUT (V)	Meas. Gain (V/V)	Expected Gain (V/V)	Gain Error (%)	P_IN (W)	P_OUT (W)	Efficiency (%)
0.6	0.3	Boost	6.331	11.918	1.88	2	5.88	5.034	4.773	94.82
0.7	0.3	Boost	5.567	11.533	2.07	2.33333333	11.21	4.807	4.564	94.94
0.8	0.3	Boost	4.18	10.287	2.46	2.66666666	7.71	3.941	3.507	88.99
0.9	0.3	Boost	3.082	7.907	2.57	3	14.48	2.821	2.129	75.47
1	0.3	Boost	2.993	9.014	3.01	3.33333333	9.65	2.916	2.762	94.72
0	0.4	Buck	8.53	0	0	0	#DIV/0!	0	0	#DIV/0!
0.1	0.4	Buck	8.51	1.975	0.23	0.25	7.17	0.138	0.133	96.38
0.2	0.4	Buck	8.395	4.912	0.59	0.5	-17.02	0.842	0.821	97.51
0.3	0.4	Buck	8.327	5.894	0.71	0.75	5.62	1.218	1.184	97.21
0.4	0.4	Boost	8.144	7.71	0.95	1	5.33	2.094	2.029	96.9
0.5	0.4	Boost	7.863	9.418	1.2	1.25	4.18	3.13	3.028	96.74
0.6	0.4	Boost	7.197	11.342	1.58	1.5	-5.06	4.54	4.392	96.74
0.7	0.4	Boost	6.961	11.652	1.67	1.75	4.35	4.789	4.634	96.76
0.8	0.4	Boost	6.045	11.323	1.87	2	6.34	5.005	4.377	87.45
0.9	0.4	Boost	4.228	8.59	2.03	2.25	9.7	3.862	2.509	64.97
1	0.4	Boost	4.731	11.146	2.36	2.5	5.76	4.367	4.243	97.16
0	0.5	Buck	8.53	0	0	0	#DIV/0!	0	0	#DIV/0!
0.1	0.5	Buck	8.516	1.643	0.19	0.2	3.53	0.093	0.092	98.92
0.2	0.5	Buck	8.439	4.089	0.48	0.4	-21.13	0.577	0.569	98.61
0.3	0.5	Buck	8.424	4.388	0.52	0.6	13.18	0.662	0.652	98.49
0.4	0.5	Buck	8.294	6.293	0.76	0.8	5.16	1.373	1.346	98.03
0.5	0.5	Boost	8.125	7.846	0.97	1	3.43	2.124	2.089	98.35
0.6	0.5	Boost	8.017	8.591	1.07	1.2	10.7	2.557	2.508	98.08
0.7	0.5	Boost	7.414	10.947	1.48	1.4	-5.47	4.166	4.078	97.89
0.8	0.5	Boost	7.251	11.288	1.56	1.6	2.7	4.427	4.337	97.97
0.9	0.5	Boost	6.591	11.631	1.76	1.8	1.96	4.987	4.604	92.32
1	0.5	Boost	6.309	12.054	1.91	2	4.47	5.038	4.946	98.17
0	0.6	Buck	8.53	0	0	0	#DIV/0!	0	0	#DIV/0!
0.1	0.6	Buck	8.52	1.41	0	0.16666666	100	0.068	0.067	98.53
0.2	0.6	Buck	8.462	3.556	0.42	0.33333333	-26.07	0.434	0.428	98.62
0.3	0.6	Buck	8.438	4.114	0.49	0.5	2.49	0.58	0.573	98.79
0.4	0.6	Buck	8.394	4.901	0.58	0.66666666	12.42	0.821	0.811	98.78
0.5	0.6	Buck	8.23	6.951	0.84	0.83333333	-1.35	1.661	1.637	98.56
0.6	0.6	Boost	8.12	7.873	0.97	1	3.04	2.132	2.101	98.55
0.7	0.6	Boost	7.931	9.066	1.14	1.16666666	2.02	2.829	2.787	98.52
0.8	0.6	Boost	7.298	10.3	1.41	1.33333333	-5.85	4.363	3.599	82.49
0.9	0.6	Boost	7.227	10.896	1.51	1.5	-0.51	4.432	4.027	90.86
1	0.6	Boost	7.18	11.333	1.58	1.66666666	5.3	4.412	4.357	98.75
0	0.7	Buck	8.53	0	0	0	#DIV/0!	0.048	0.0479	99.79
0.1	0.7	Buck	8.523	1.191	0.14	0.14285714	2.18	0.048	0.0479	99.79
0.2	0.7	Buck	8.484	2.969	0.35	0.28571428	-22.48	0.3	0.297	99

D1	D2	Mode	V_IN (V)	V_OUT (V)	Meas. Gain (V/V)	Expected Gain (V/V)	Gain Error (%)	P_IN (W)	P_OUT (W)	Efficiency (%)
0.3	0.7	Buck	8.459	3.629	0.43	0.42857142	-0.1	0.448	0.444	99.11
0.4	0.7	Buck	8.41	4.635	0.55	0.57142857	3.55	0.732	0.725	99.04
0.5	0.7	Buck	8.309	6.08	0.73	0.71428571	-2.44	1.262	1.248	98.89
0.6	0.7	Buck	8.24	6.82	0.83	0.85714285	3.44	1.586	1.57	98.99
0.7	0.7	Boost	8.099	7.928	0.98	1	2.11	2.141	2.12	99.02
0.8	0.7	Boost	8.059	8.256	1.02	1.14285714	10.36	2.319	2.298	99.09
0.9	0.7	Boost	7.592	9.489	1.25	1.28571428	2.79	3.679	3.039	82.6
1	0.7	Boost	7.738	9.766	1.26	1.42857142	11.65	3.243	3.219	99.26
0	0.8	Buck	8.53	0	0	0	#DIV/0!	0	0	#DIV/0!
0.1	0.8	Buck	8.525	1.012	0.12	0.125	5.03	0.035	0.0347	99.14
0.2	0.8	Buck	8.474	2.636	0.31	0.25	-24.43	0.374	0.234	62.57
0.3	0.8	Buck	8.451	3.246	0.38	0.375	-2.43	0.5	0.351	70.2
0.4	0.8	Buck	8.396	4.136	0.49	0.5	1.48	0.812	0.57	70.2
0.5	0.8	Buck	8.356	5.633	0.67	0.625	-7.86	0.908	0.895	98.57
0.6	0.8	Buck	8.092	5.435	0.67	0.75	10.45	2.281	0.979	42.92
0.7	0.8	Buck	8.218	6.993	0.85	0.875	2.75	1.657	1.645	99.28
0.8	0.8	Boost	8.099	7.962	0.98	1	1.69	2.148	2.133	99.3
0.9	0.8	Boost	7.8	8.443	1.08	1.125	3.78	3.239	2.4	74.1
1	0.8	Boost	7.841	9.312	1.19	1.25	4.99	2.94	2.922	99.39
0	0.9	Buck	8.53	0	0	0	#DIV/0!	0	0	#DIV/0!
0.1	0.9	Buck	8.526	0.914	0.11	0.11111111	3.52	0.0286	0.0282	98.6
0.2	0.9	Buck	8.5	2.391	0.28	0.22222222	-26.58	0.194	0.192	98.97
0.3	0.9	Buck	8.489	2.787	0.33	0.33333333	1.51	0.263	0.261	99.24
0.4	0.9	Buck	8.295	3.622	0.44	0.44444444	1.75	1.38	0.44	31.88
0.5	0.9	Buck	8.331	4.903	0.59	0.55555555	-5.93	1.133	0.796	70.26
0.6	0.9	Buck	8.364	5.291	0.63	0.66666666	5.11	0.943	0.937	99.36
0.7	0.9	Buck	8.267	6.469	0.78	0.77777777	-0.61	1.41	1.402	99.43
0.8	0.9	Buck	8.212	7.004	0.85	0.88888888	4.05	1.653	1.644	99.46
0.9	0.9	Boost	7.939	7.937	1	1	0.03	2.64	2.068	78.33
1	0.9	Boost	7.983	8.257	1.03	1.11111111	6.91	2.511	2.307	91.88
0	1	Buck	8.53	0	0	0	#DIV/0!	0	0	#DIV/0!
0.1	1	Buck	8.526	0.864	0.1	0.1	-1.34	0.026	0.025	96.15
0.2	1	Buck	8.502	2.322	0.27	0.2	-36.56	0.182	0.181	99.45
0.3	1	Buck	8.492	2.677	0.32	0.3	-5.08	0.242	0.24	99.17
0.4	1	Buck	8.466	3.435	0.41	0.4	-1.44	0.397	0.394	99.24
0.5	1	Buck	8.402	4.717	0.56	0.5	-12.28	0.746	0.742	99.46
0.6	1	Buck	8.377	5.103	0.61	0.6	-1.53	0.872	0.867	99.43
0.7	1	Buck	8.299	6.118	0.74	0.7	-5.31	1.252	1.246	99.52
0.8	1	Buck	8.245	6.686	0.81	0.8	-1.36	1.495	1.488	99.53
0.9	1	Buck	8.154	7.502	0.92	0.9	-2.23	1.882	1.874	99.57
1	1	Boost	8.064	8.033	1	1	0.38	2.16	2.151	99.58

Table 31. Full-Bridge Converter Simulation Expected Gain vs. Actual Gain

Appendix L: Testing Results and Log

For our initial testing, we recognized that there were some components that were disconnected or not connected at all. Once we were able to get some of the expected waveforms from the SM72445 IC, we investigated our implementation for more building errors and reasons to why our circuit may or may not work. We present our initial results after major building errors were addressed seen in Table 32 , and our testing log that recorded a couple of significant testing results and findings for our conclusions.

SM72445 (Master)							
Pin Name	**Pin #**	**Desired Value**	**Result**	**Pin Name**	**Pin #**	**Desired Value**	**Result**
RST	1	5V	5.44V	PM	28	5V (Active low, PM off)	5.21V
NC1	2	GND	GND	LIA	27	110 kHz PWM	105k PWM (80%)
VDDD	3	5V	5.44V	HIA	26	110 kHz PWM	105k PWM (20%)
VSSD	4	GND	GND	HIB	25	110 kHz PWM	13k PWM (98%)
NC2	5	5V	5V	LIB	24	110 kHz PWM	13k PWM (2%)
I2C0	6	5V (1)	5V	NC4	23	5V	5.2V
I2C1	7	GND (0)	GND	I2C2	22	GND (0)	GND
SCL	8	I2C Clock Waveform	GND	AIOUT	21	Depends on IOUT	157Hz, falling sawtooth wave (2.5V - 4V)
SDA	9	I2C Data TX	GND	A6	20	4.69V (Max slew, no PM)	4.82V
NC3	10	GND	GND	AIIN	19	Depends on IIN	4.74V noisy DC
PM_OUT	11	GND	GND	A4	18	3.6V (Minimum Iout = ?)	3.68V
VDDA	12	5V	5.44V	AVOUT	17	~1.68V @ Vout = 5V	1.92V
VSSA	13	GND	GND	A2	16	3.44V (H-Bridge, low freq.)	3.54V
A0	14	1.68V	1.7V	AVIN	15	Depends on Vin	12k waveform, ~1.9V
SM72295 (Driver)							
Pin Name	**Pin #**	**Desired Value**	**Result**	**Pin Name**	**Pin #**	**Desired Value**	**Result**
SIA	1		4.3V DC	HSA	28	N/A	N/A
SOA	2		0V	HOA	27	N/A	N/A
IIN	3		0V	HBA	26	N/A	N/A
BIN	4		0V	VCCA	25	N/A	N/A
AGND	5		0V	LOA	24	N/A	N/A
LIA	6		Same as LIA above	PGND	23	N/A	N/A
HIA	7		Same as HIA above	LOB	22	N/A	N/A
HIB	8		Same as HIB above	VCCB	21	N/A	N/A
LIB	9		Same as LIB above	HBB	20	N/A	N/A
PGOOD	10		4.86V	HOB	19	N/A	N/A
BOUT	11		200Hz wave, 1.5-1.9V ripple	HSB	18	N/A	N/A
IOUT	12		N/A	VDD	17	N/A	N/A
SOB	13		N/A	OVS	16	N/A	N/A
SIB	14		N/A	OVP	15	N/A	N/A

Table 32. Initial Testing Results and Expected Values for Each Pin on SM72445 IC an SM72295 IC

Circuit Testing Log

Date: 4/23/2017

- Connected 12C0 to GND, NC2 to 5V, and pulled back in Arduino wires.
- Performed Test 1 as seen in Table 33.
- Changed the circuit to have a shared GND.
- Trying to isolate input voltage, saw that input voltage and PV+ were shorting each other. Found a tiny wire between the input voltage pin and the PV+ pin. Unsoldered the short.
- Showed PWM for HIA and LIA (210 kHz): "boosting"- from 0.29V to 1.29 V, gates HIB and LIB (26 kHz).
- Drawing 40mA at beginning and up to 200mA once IC fully powered "ON".
- Performed Test 2 as seen in Table 33 that showed a random occurrence of Boosting.
- When producing same output as input: IC is off, all four produce 50kHz PWM. Duty cycle on HIA and HIB are high (about 98%) and LIB and LIA are low. Perhaps in Panel mode?
- HIA and LIA are 105 kHz, HIB full ON and LIB full OFF.

Test 1		**Test 2**		
Input Voltage (V)	**Output Voltage (V)**	**Input Voltage (V)**	**Output Voltage (V)**	**Gain**
0.54	0.24	1.05	2.5	2.38
0.98	0.68	2.02	5.57	2.76
1.5	1.16	3.01	8.61	2.86
1.98	1.61	3.97	11.41	2.87
2.5	2.12	5	14.25	2.85
2.99	2.6	5.98	16.8	2.81
3.53	3.13	6.97	19.26	2.76
3.99	3.58	7.98	21.6	2.71
4.49	4.08	9.02	23.8	2.64
5.02	4.61			
5.51	5.27			
5.98	5.61			
6.55	6.19			

Table 33. Test 1 Results Showing PM Mode and Test 2 Results Showing Boost Mode

Date: 4/24/2017

- Attached four potentiometers onto the configurable resistor divider to get exact voltage values for the pins A0-A6. Attempted testing but no significant results.

Date: 4/25/2017

- Above 5V (about 5.3) 105.3 kHz waveform appeared on LIA , HIA, LIB full ON, LIB full OFF, once in MPPT, as you reduce it after entering MPPT mode, the waveform shrinks and when it hits 3.2 V the waveform shuts off.
- If you hit the RST pin, it enters panel mode, where all four are in 50 kHz.
- Connected current sense things the according to the SM7445 and SM72997 datasheet include AIOUT AIOUT, AIN to IIN, SOB and SIB to the driver where moved to be across current sense resistor.
- Took out the diode all together, connect the output of the MOSFET from the full bridge to go into the current sense R and have Current Sense to Vout, connect SOB anjd SIB to measure the voltage across the current sense resistor

Appendix M: Implementation Circuit Schematic

Figure 68 displays the schematic of our implemented circuit. All of the connections presented in the schematic are exactly the same in the physical implementation.

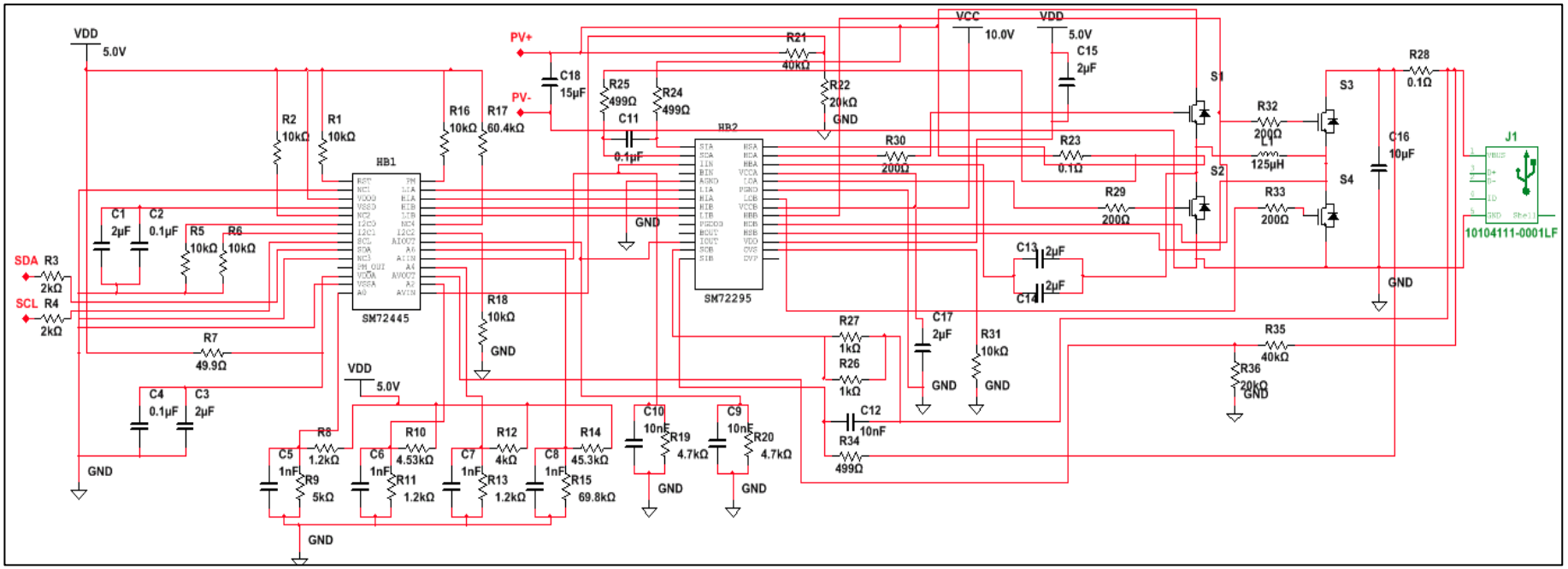

Figure 68. Circuit Schematic of Our Actualized Implementation